Bell inequalities with Orbital Angular Momentum of Light

Carolina Vannier dos Santos Borges

UNIVERSIDADE FEDERAL FLUMINENSE
INSTITUTO DE FÍSICA

UNIVERSITE PARIS-SUD

ÉCOLE DOCTORALE ONDES ET MATIÈRE
Institut des Sciences Moléculaires d'Orsay

DISCIPLINE : Physique

THÈSE DE DOCTORAT

soutenue le 08/10/2012

par

Carolina VANNIER DOS SANTOS BORGES

Bell inequalities with Orbital Angular Momentum of Light

Directeur de thèse :	Antonio ZELAQUETT KHOURY	Professeur à l'Universidade Federal Fluminense
Co-directeur de thèse :	Arne KELLER	Professeur à l'Université Paris-Sud

Composition du jury :

Président du jury :	Jean-Louis LEGOUËT	Directeur de recherche au CNRS
Rapporteurs :	Kaled DECHOUM	Professeur à l'Universidade Federal Fluminense
	Nicolas TREPS	Professeur à l'Université Pierre et Marie Curie
Examinateurs :	Jandir HICKMANN	Professeur à l'Universidade Federal de Alagoas
	Marcelo FRANÇA SANTOS	Professeur à l'Universidade Federal de Minas Gerais

Abstract

We shall present a theoretical description of paraxial beams, showing the propagation modes that arise from the solution of the paraxial equation in free space. We then discuss the angular momentum carried by light beams, with its decomposition in spin and orbital angular momentum and its quantization.

We present the polarization and transverse modes of a beam as potential degrees of freedom to encode information. We define the Spin-Orbit modes and explain the experimental methods to produce such modes. We then apply the Spin-Orbit modes to perform a BB84 quantum key distribution protocol without a shared reference frame.

We propose a Bell-like inequality criterion as a sufficient condition for the spin-orbit non-separability of a classical laser beam. We show that the notion of separable and non-separable spin-orbit modes in classical optics builds a useful analogy with entangled quantum states, allowing for the study of some of their important mathematical properties. We present a detailed quantum optical description of the experiment in which a comprehensive range of quantum states are considered.

Following the study of Bell's inequalities we consider bipartite quantum systems characterized by a continuous angular variable θ. We show how to reveal non-locality on this type of system using inequalities similar to CHSH ones, originally derived for bipartite spin 1/2 like systems. Such inequalities involve correlated measurement of continuous angular functions and are equivalent to the continuous superposition of CHSH inequalities acting on two-dimensional subspaces of the infinite dimensional Hilbert space. As an example, we discuss in detail one application of our results, which consists in measuring orientation correlations on the transverse profile of entangled photons.

Resumo

Apresentaremos uma descrição teórica dos feixes paraxiais, mostrando os modos de propagação que surgem da solução da equação paraxial no espaço livre. Em seguida discutiremos o momento angular contido nos feixes de luz, e sua decomposição em parte orbital e de spin, e também sua quantização.

Apresentaremos os modos de polarização e modos transversos de um feixe como graus de liberdade em potencial para codificar informação. Definiremos os modos Spin-Órbita e explicaremos os métodos experimentais utilizados para produzir estes modos. Aplicaremos então os modos Spin-Órbita à implementação de um protocolo BB84 de distribuição de chave quântica sem um referencial compartilhado.

Propomos um critério em forma de desigualdade tipo-Bell, como condição suficiente para a não-separabilidade dos modos Spin-Órbita em um laser clássico. Mostraremos que a noção de modos Spin-Órbita separáveis e não-separáveis em ótica clássica pode formar uma analogia útil com os estados quânticos emaranhados, e portanto permite o estudo de algumas de suas propriedades matemáticas. Apresentaremos uma descrição detalhada do nosso experimento, de acordo com a Ótica Quântica, onde uma larga gama de estados quânticos será considerada.

Continuando no estudo de desigualdades de Bell, consideraremos sistemas quânticos bipartidos caracterizados por uma variável angular θ. Mostraremos como revelar não-localidade nesse tipo de sistema usando desigualdades similares às CHSH, originalmente derivadas para sistemas bipartidos de spin 1/2. Tais desigualdades envolvem medidas correlacionadas de funções angulares contínuas e são equivalentes a uma superposição contínua de desigualdades CHSH atuando em subespaços 2-dimensionais do espaço de Hilbert infinito-dimensional. Como exemplo, discutiremos em detalhe uma aplicação dos nossos resultados que consiste em medir correlações em orientação no perfil transverso de fótons emaranhados.

Résumé

Dans une première partie introductive, nous rappelons la description théorique de la propagation de faisceaux optiques en terme des modes solutions de l'équation de propagation dans l'approximation paraxialle. Dans ce cadre, nous présentons les notions de moment cinétique transporté par les faisceaux lumineux, et de sa décomposition en moment cinétique intrinsèque (ou spin) et en moment angulaire.

La seconde partie est consacrée au codage de l'information dans les degrés de libertés de polarisation et de modes transverses des faisceaux optiques. Les modes spin-orbites sont définis et un dispositif expérimental optique pour produire ces modes est présenté. Les modes spin-orbites sont alors exploités pour implémenter un protocole de distribution de clés BB84 ne nécessitant pas le partage à priori d'une base de référence.

Dans une troisième partie, nous proposons un critère de type inégalité de Bell, qui constitue une condition suffisante pour caractériser la non-séparabilité en spin-orbite d'un faisceau optique classique. Nous montrons ensuite que la notion de modes spin-orbite séparable ou non-séparable constitue une analogie pertinente avec la notion d'intrication d'états quantiques et permet l'étude de certaines de ses propriétés fondamentales. Enfin, une implémentation expérimentale de cette simulation de tests de Bell avec des faisceaux optiques classiques est présentée, ainsi que sa description détaillée dans le cadre de l'optique quantique.

Dans une dernière partie, nous nous intéressons à des inégalités de Bell, pour des états quantiques de systèmes quantique à deux parties, qui sont caractérisées chacune par une variable continue de type angulaire (périodique). Nous montrons comment détecter la non-localité sur ce type de système, avec des inégalités qui sont similaires aux inégalités CHSH; inégalités qui avaient été développées originellement pour des systèmes de type spin 1/2. Nos inégalités, sont construites à partir de la mesure de la corrélation de fonctions angulaires. Nous montrons qu'elles sont en fait la superposition continue d'inégalités CHSH de type spin 1/2. Nous envisageons une possible implémentation expérimentale, où les corrélations mesurées sont les corrélations angulaires du profil transverse des photons intriqués.

Agradecimentos/*Remerciements*

Eu agradeço ao meu orientador Antonio Zelaquett Khoury, que sempre demonstrou grande confiança em mim e que, por possuir um admirável conhecimento no nosso ramo de pesquisa e também um grande talento didático, contribuiu substancialmente para o meu crescimento na Física.

Je remercie mon co-directeur de thèse Arne Keller et ma collaboratrice Pérola Milman, qui m'ont accueillie en France pendant mon stage, et qui m'ont aidée à m'initier à la recherche théorique. Ils sont deux exemples à suivre, et je suis heureuse de les avoir rencontrés.

Agradeço aos meus colegas de laboratório Carlos Eduardo de Souza, José Augusto Huguenin e Bernardo Coutinho, que dedicaram seu tempo a sanar minhas dúvidas no universo de equipamentos do lab e no universo da ótica experimental como um todo. Agradeço também aos professores do grupo de Ótica e Informação Quântica do IF-UFF, Daniel Jonathan, Kaled Dechoum e Ernesto Galvão que contribuíram para a minha formação com preciosas aulas e também comentários durante os seminários de grupo.

As muitas horas passadas no IF foram compartilhadas com colegas muito especiais, como Alê Lima, Wanessa Sarzêdas, Dayanne Fernandes, Raphael Dias, Daniel Brod, dentre outros. Agradeço a eles pela companhia nas horas de trabalho e também de descontração. Agradeço ao corpo de professores do IF-UFF que foram exemplos de profissionais capazes e apaixonados pelo que fazem, além de terem sido peças importantes do meu aprendizado.

Agradeço aos meus pais que me ensinaram pelo exemplo a ter senso crítico, e de quem sempre tive a liberdade de discordar. Agradeço todo o carinho e amor incondicional que recebi deles, dos meus irmãos e de todos os membros da minha família, e por sempre terem me dado a sensação de que faço parte de um todo. Agradeço em especial à minha tia Cristina, que sempre me fez praticar a difícil arte de explicar o porquê de tudo.

Agradeço aos meu amigos Nathalie, Danilo, Felipe e Caetano, que me acompanham desde os tempos de escola e que me ajudaram a definir meus objetivos e comemoraram comigo todas as etapas vencidas. Agradecimento especial à Nathalie que me ajudou a

ressuscitar o meu francês antes do meu estágio, e que sempre foi especialista em injetar ânimo e auto-confiança numa amiga por vezes esgotada.

Por fim agradeço ao Igor, companheiro de todas as horas, que me apóia nos momentos de crises e dúvidas, divide comigo os momentos alegres e planos para o futuro, e ainda serve de exemplo com seu espírito investigativo, raciocínio afiado e conhecimentos ecléticos. Agradeço também pelas leituras críticas do manuscrito, e por todas as discussões de física que pude ter sem sair de casa ;) E apesar de toda a ajuda, foi quem mais me ensinou a pensar por mim mesma e ser independente. <3

Contents

List of Figures

1

Introduction

The first descriptions of light phenomena date back to the ancient Greece, and the earliest known lenses were developed in ancient Mesopotamia [1] around the year 700 BC. Optics was first described in a geometrical form, with the concept of light rays, and despite it being the very first theoretical description of light, it is remarkable how much geometrical optics can explain. Starting with the basic examples of reflection and refraction, it is also possible to describe telescopes, microscopes, the human eye and so on.

The first important work to deviate from the geometrical view was Christiaan Huygens's *Treatise on light*, published in 1690, which founded the wave theory of light[2, 3]. In this treatise he presented what is known as Huygens principle, a fundamental concept in the analysis of waves, which states that each point in the wave front behaves as a punctual source for a spherical wave. The interference of all these secondary waves emitted by all the points in a wave front will give the propagation of the wave. Thomas Young and Augustin Fresnel, through their work on interference and diffraction, helped to consolidate the wave theory as the main theory of light.

In 1861, Maxwell was able to unify light and the electromagnetic theory when he deducted the existence of electromagnetic waves which propagated with the same velocity as light. This fact was experimentally confirmed by Hertz, who was able to produce electromagnetic waves in the radio frequency, and prove that these waves had the same properties as light. Ironically, it was in the experiments performed by Hertz that the first evidences of the photoelectric effect appeared, pointing again to a corpuscular theory of light.

In fact, it was the difficulty in explaining a radiation phenomenon, the black body radiation, with classical physics that lead Planck to the idea of *quanta*. Later Einstein explained the photoelectric effect applying Planck's idea of quanta to light, and the photon was born.

Quantum theory made it possible to explain several phenomena such as atomic structure and the process of light emission by an atom, and it reconciled the corpuscular and the wave natures of light as coexistent aspects. However some of the aspects of quantum theory were still doubtful from the point of view of great scientists such as Einstein. Together with Podolski and Rosen, Einstein proposed in 1935 a gedanken experiment to evidence what they thought was a clear sign that quantum mechanics was an incomplete theory [4]. They made evident that quantum mechanics predictions would not satisfy locality and realism conditions at the same time, so they concluded that the quantum mechanical description of a physical system should be supplemented by postulating the existence of "hidden variables". These hidden variables would allow one to predetermine the results of measurements made on any observable of the system.

It was only in 1964 that John Bell proposed a quantitative way to test whether any local realistic theory could account for the results seen and predicted by quantum mechanics. To test his theorem, Bell developed a set of inequalities [5], that were later generalized and put into a form more suitable to experiments by Clauser, Horne, Shimony and Holt (CHSH) [6].

The discovery of laser as a source of light in the 60's has brought Optics back as an important and very active field of research, due to its innumerable applications. The laser helped to develop the fields of non-linear and quantum optics, which investigate the interaction of light and matter. Quantum optics has been a very fruitful field to explore fundamental issues of quantum mechanics, and in 1982 a quantum optics experiment performed by Aspect *et al* finally measured the CHSH inequalities [7]. The field of Quantum Information has also profited from the optical experiments, specially the protocols requiring communication, such as the quantum key distribution protocols [8].

The work composing this thesis is based on optical implementations for quantum information protocols, and it is specially focused on Bell's inequalities. To properly introduce the theoretical background needed for the understanding of this work, we will discuss in this introductory chapter some fundamentals on paraxial optics, the angular

momentum of light, its decomposition and quantization. In Chapter 2 we present the polarization and transverse modes as carriers of qubits of information, and we discuss the combined 4 dimensional basis of Spin-Orbit modes, including a discussion of experimental methods to produce such modes, and their quantization. In Chapter 3 we present one application of the spin-orbit modes to implement a quantum key distribution protocol without a shared reference frame between the two parties. In Chapter 4 we introduce the concept of Bell's inequalities and present a Bell-like inequality criterion for the non-separability of the spin-orbit modes, with experimental results. In Chapter 5 we develop a continuous variable inequality using bounded spectrum operators and propose an experimental setup to measure the inequality using correlations on the transverse profile of entangled photons.

1.1 Paraxial Optics

The Maxwell equations are the laws which describe the dynamics of the electromagnetic field. From these basic laws we can derive a wave equation, suggesting the existence of electromagnetic waves. The small part of the electromagnetic spectrum which is visible to the human eye is what we call light. [9]

In homogeneous media and in the absence of charges or currents, the Maxwell equations can be written as [10]:

$$\boldsymbol{\nabla} \cdot \mathbf{E} = 0 \; ; \tag{1.1}$$

$$\boldsymbol{\nabla} \times \mathbf{E} = -\frac{\partial \mathbf{B}}{\partial t} \; ; \tag{1.2}$$

$$\boldsymbol{\nabla} \cdot \mathbf{B} = 0 \; ; \tag{1.3}$$

$$\boldsymbol{\nabla} \times \mathbf{B} = \mu_0 \epsilon_0 \frac{\partial \mathbf{E}}{\partial t} \; . \tag{1.4}$$

We can take the rotational of Eq. (1.2) and using Eq. (1.4) we get:

$$\nabla^2 \mathbf{E} - \mu_0 \epsilon_0 \frac{\partial^2 \mathbf{E}}{\partial t^2} = 0 \; , \tag{1.5}$$

which constitutes a wave equation for the field $\mathbf{E}$, with propagation speed $c = \frac{1}{\sqrt{\mu_0 \epsilon_0}}$, which is the speed of light. We can perform similar calculations to obtain an identical wave equation for the field $\mathbf{B}$.

In this work we are interested in monochromatic waves, very concentrated along the direction of propagation, because this is the type of radiation emitted by a laser

source, as the one used in our experiments. In this case we can make some useful approximations. First we describe the electric field as a sum of two complex quantities, such that:

$$\mathbf{E}(\mathbf{r},t) = \mathbf{E}^{(+)}(\mathbf{r},t) + (\mathbf{E}^{(+)}(\mathbf{r},t))^* \ , \tag{1.6}$$

where

$$\mathbf{E}^{(+)}(\mathbf{r},t) = e^{-i(\omega t - kz)}\boldsymbol{\epsilon} u(\mathbf{r})\mathcal{E}(z,t). \tag{1.7}$$

In this notation $\boldsymbol{\epsilon}$ is the polarization vector, $u(\mathbf{r})$ is the transverse beam structure, normalized upon integration of its modulus over the transverse plane and $\mathcal{E}(z,t)$ is the field envelope that gives the 'slow' variations in amplitude (on the scale of the wavelength) over the direction of propagation and over time.

In a homogenious medium, for a free-propagating monochromatic beam, $\mathcal{E}(z,t)$ is a constant. In this case, substituting (1.7) in the wave equation (1.5) we get [11]:

$$\nabla^2[u(\mathbf{r})e^{ikz}] + k^2[u(\mathbf{r})e^{ikz}] = 0 \ , \tag{1.8}$$

where $k = \omega/c$.

For a plane wave, $u(\mathbf{r})$ will be constant. However, for physically realizable beams $u(\mathbf{r})$ will vary with x, y and z, but if the diffraction of the beam is sufficiently small, it may vary slowly with z. In this case, we can assume that $|\partial^2 u/\partial z^2| \ll 2k|\partial u/\partial z|$. Neglecting the term $\partial^2 u/\partial z^2$ in the Helmholtz equation (1.8) we find that $u(\mathbf{r})$ satisfies the paraxial equation:

$$\nabla_t^2 u(\mathbf{s},z) + 2ik\frac{\partial u(\mathbf{s},z)}{\partial z} = 0, \tag{1.9}$$

where $\mathbf{s}$ refers to the transverse coordinates $\mathbf{s} \equiv (x,y)$ or $\mathbf{s} \equiv (\rho,\phi)$ we choose, and ∇_t^2 is the corresponding laplacian operator associated with the transverse coordinates.

The simplest solution for this equation, in cartesian coordinates, is the fundamental gaussian mode, given by [12]:

$$u_0(x,y,z) = \sqrt{\frac{2}{\pi}}\frac{1}{w(z)}\exp\left[-\frac{x^2+y^2}{w^2(z)} + ik\frac{x^2+y^2}{2R(z)} - i\arctan\left(\frac{z}{z_R}\right)\right] \ , \tag{1.10}$$

where $R(z)$ is the curvature radius of the beam given by

$$R(z) = z\left(1 + \frac{z_R^2}{z^2}\right), \tag{1.11}$$

$w(z)$ is the beam waist given by

$$w(z) = w_0\sqrt{\left(1 + \frac{z^2}{z_R^2}\right)}, \tag{1.12}$$

w_0 is the minimum waist of the beam, defined at the plane $z = 0$, and the last parameter z_R is the Rayleigh length, given by

$$z_R = \frac{\pi w_0}{\lambda}. \tag{1.13}$$

The fundamental mode can be regarded as a paraxial-spherical wave, and it is the best approximation to the mode generated by a laser source. However, (1.10) is only the lowest order solution among an infinite family of solutions to Eq. (1.9).

1.1.1 Paraxial Modes: Hermite-Gauss and Laguerre-Gauss families

The ensemble of all possible solutions of Eq. (1.9) constitute a basis for the transverse modes of a paraxial beam in free space. The expression in cartesian coordinates for a mode of arbitrary order is given below, and these are called Hermite-Gaussian (HG) modes:

$$\begin{aligned} u_{m,n}(x,y,z) &= \frac{A_{nm}}{w(z)} H_m\left[\frac{\sqrt{2}x}{w(z)}\right] H_n\left[\frac{\sqrt{2}y}{w(z)}\right] \exp\left\{-\frac{x^2+y^2}{w^2(z)}\right\} \times \\ &\times \exp\left\{ik\frac{x^2+y^2}{2R(z)}\right\} e^{-i\phi_{mn}(z)}\ , \end{aligned} \tag{1.14}$$

where A_{mn} is a normalization factor and H_k is the Hermite polynomial of order k. The order of the HG mode is defined as $m + n$ and $\phi_{mn}(z)$ is the Gouy phase given by

$$\phi_{mn}(z) = i(m + n + 1)\arctan\left(\frac{z}{z_R}\right). \tag{1.15}$$

In cylindrical coordinates we can obtain a different family of solutions, called the Laguerre-Gaussian (LG) modes:

$$\begin{aligned} u_p^l(\rho,\phi,z) &= \frac{A_p^l}{w(z)}\left(\frac{\sqrt{2}\rho}{w(z)}\right)^{|l|} L_p^{|l|}\left[\frac{2\rho^2}{w^2(z)}\right] \exp\left\{-\frac{\rho^2}{w^2(z)}\right\} \times \\ &\times \exp\left\{ik\frac{\rho^2}{2R(z)}\right\} e^{il\phi} e^{-i\phi_{pl}(z)}\ , \end{aligned} \tag{1.16}$$

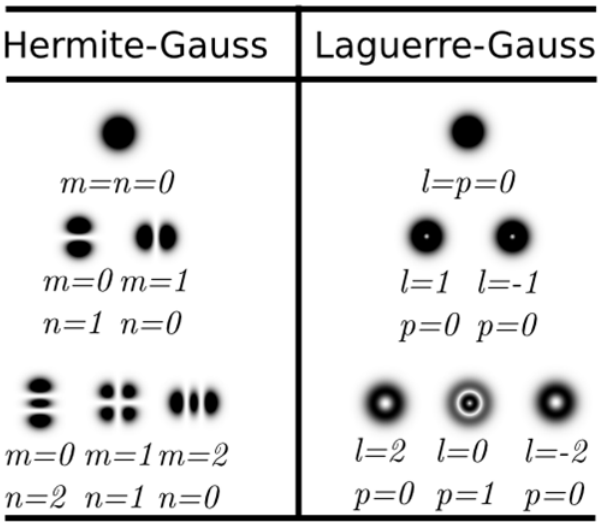

Figure 1.1: Intensity transverse profiles for HG and LG modes

where the integer $p \geq 0$ is the radial index and the integer l is the azimuthal index. A_p^l is a normalization factor and $L_p^{|l|}$ are the generalized Laguerre polynomials [13]. The order of the LG mode is defined as $2p + |l|$ and the Gouy phase is given by

$$\phi_{pl}(z) = (2p + |l| + 1) \arctan\left(\frac{z}{z_R}\right). \tag{1.17}$$

When $l \neq 0$, because of the factor $e^{il\phi}$ the LG modes present a helicoidal wavefront around the z axis. This suggests, as we shall see in detail in Section 1.2, that they carry orbital angular momentum proportional to l.

The intensity transverse profile for these two families of modes are shown in Fig. 1.1, from zero to second order.

It is interesting to note the analogy between the Hermite-Gaussian modes and the two-dimensional harmonic oscillator eigenstates [14, 15]. Let us rewrite eq. (1.14):

$$\begin{aligned} u_{m,n}(x,y,z) &= \exp\left\{ik\frac{x^2+y^2}{2R(z)} - i(m+n+1)\arctan\left(\frac{z}{z_R}\right)\right\} \times \\ &\quad \frac{1}{w(z)}\psi_m\left[\frac{\sqrt{2}x}{w(z)}\right]\psi_n\left[\frac{\sqrt{2}y}{w(z)}\right], \end{aligned} \tag{1.18}$$

where

$$\psi_m(\xi) = (2^m m!\sqrt{\pi})^{-1/2} e^{-\xi^2/2} H_m(\xi). \tag{1.19}$$

The function $\psi_m(\xi)$ is the eigenstate of the harmonic oscillator, defined by the Hamiltonian

$$H = \frac{1}{2}\left(-\frac{\partial^2}{\partial\xi^2} + \xi^2\right) , \tag{1.20}$$

and it is straightforward to generalize it to the two-dimensional case. The mode expression in (1.18) has three parameters that depend on the z coordinate, the beam radius $R(z)$, the Gouy phase and the beam waist $w(z)$. We can see that the difference between the beam propagation and the evolution of the harmonic oscillator are in these terms, as they describe the effect of diffraction of the beam, absent in the harmonic oscillator eigenfunctions, due to the confining harmonic potential. However, the variation of the term $\arctan\left(\frac{z}{z_R}\right)$, which multiplies the equivalent of the energy level $(m + 1/2) + (n + 1/2)$, is analogous to the phase Ωt gained by the oscillator of frequency Ω with time. Since the Gouy phase goes from $-\pi/2$ to $\pi/2$ during a free propagation from $-\infty$ to ∞, this evolution is equivalent to half a cycle of the oscillator.

This analogy offers the possibility of applying the operator algebra of the harmonic oscillator to the paraxial beam optics. In this context, the LG_p^l modes are the eigenstates of the orbital angular momentum operator and each photon in this mode carries an orbital angular momentum of $l\hbar$. The index p represents the energy of the oscillator, and l represents the difference between the right-hand and the left-hand excitations, so it goes from $-p$ to p.

In a quadratic index medium with the form $n^2 = n_0^2[1-g^2(x^2+y^2)]$ we obtain steady-state solutions [16], i.e., without the diffraction terms. In this case the quadratic index acts as the quadratic potential of the two-dimensional harmonic oscillator, spatially containing the states.

1.2 Angular Momentum of light

The rotational characteristics of a light beam are generally expressed by the angular momentum of the optical field. In order to discuss the angular momentum of a light beam, we must examine some of its general properties. In classical electromagnetic theory, the time averaged linear momentum density and angular momentum density

are given by [17]:

$$\mathbf{p} = \epsilon_0 \langle \mathbf{E} \times \mathbf{B} \rangle \ , \tag{1.21}$$

$$\mathbf{j} = \epsilon_0 (\mathbf{r} \times \langle \mathbf{E} \times \mathbf{B} \rangle) = \mathbf{r} \times \mathbf{p} \ , \tag{1.22}$$

and the total linear and angular momenta are obtained by the integration of these quantities over all space:

$$\mathbf{P} = \int d^3 r \mathbf{p} \ , \tag{1.23}$$

$$\mathbf{J} = \int d^3 r \mathbf{j} \ . \tag{1.24}$$

Making use of the complex notation of Eq. (1.7), and using Maxwell's equation $i\omega \mathbf{B}^{(+)} = \boldsymbol{\nabla} \times \mathbf{E}^{(+)}$, we can write the linear and angular momenta as

$$\mathbf{P} = \mathrm{Re} \, \frac{\epsilon_0}{2i\omega} \int d^3 r \ \mathbf{E}^{(+)*} \times \left(\boldsymbol{\nabla} \times \mathbf{E}^{(+)} \right) \ , \tag{1.25}$$

$$\mathbf{J} = \mathrm{Re} \, \frac{\epsilon_0}{2i\omega} \int d^3 r \ \mathbf{r} \times \left[\mathbf{E}^{(+)*} \times \left(\boldsymbol{\nabla} \times \mathbf{E}^{(+)} \right) \right] \ . \tag{1.26}$$

Using partial integration and the fact that $\mathbf{E}$ is a transverse field, and considering that the fields vanish as $|\mathbf{r}| \to \infty$ we obtain [11, 18]

$$\mathbf{P} = \mathrm{Re} \, \frac{\epsilon_0}{2i\omega} \int d^3 r \sum_{j=x,y,z} E_j^{(+)*} \, \boldsymbol{\nabla} E_j^{(+)} \ , \tag{1.27}$$

$$\begin{aligned} \mathbf{J} &= \mathrm{Re} \, \frac{\epsilon_0}{2i\omega} \int d^3 r \sum_{j=x,y,z} E_j^{(+)*} \, (\mathbf{r} \times \boldsymbol{\nabla}) \, E_j^{(+)} \\ &+ \mathrm{Re} \, \frac{\epsilon_0}{2i\omega} \int d^3 r \ \mathbf{E}^{(+)*} \times \mathbf{E}^{(+)} \ . \end{aligned} \tag{1.28}$$

It is clear from the expression above the separation between the orbital angular momentum (OAM) represented by the first term of $\mathbf{J}$, and the spin angular momentum, represented by the second term. The OAM is related to the macroscopic energy circulation caused by the beam's spatial configuration, and depends on the phase gradient. The spin term is clearly independent of the choice of reference point or origin of coordinates, so it is considered an intrinsic property of the beam and it is associated with light beams that carry circular or elliptic polarization.

The distinction between spin and orbital angular momentum is sometimes mistaken for the distinction between intrinsic and extrinsic angular momentum. To explain the

latter, we shall look at the total angular momentum with respect to a different reference point, denoted $\mathbf{r_0}$. From Eq. (1.26) we have

$$\begin{aligned}\mathbf{J}(\mathbf{r_0}) &= \mathrm{Re}\,\frac{\epsilon_0}{2i\omega}\int d^3r\,(\mathbf{r}-\mathbf{r_0})\times\left[\mathbf{E}^{(+)*}\times\left(\boldsymbol{\nabla}\times\mathbf{E}^{(+)}\right)\right]\\ &= \mathrm{Re}\,\frac{\epsilon_0}{2i\omega}\int d^3r\,\mathbf{r}\times\left[\mathbf{E}^{(+)*}\times\left(\boldsymbol{\nabla}\times\mathbf{E}^{(+)}\right)\right]\\ &- \mathbf{r_0}\times\mathrm{Re}\,\frac{\epsilon_0}{2i\omega}\int d^3r\,\mathbf{E}^{(+)*}\times\left(\boldsymbol{\nabla}\times\mathbf{E}^{(+)}\right)\\ &= \mathbf{J}(0)-\mathbf{r_0}\times\mathbf{P}\,. \end{aligned} \tag{1.29}$$

As we can see, the first term of this equation is the angular momentum $\mathbf{J}$ from Eq. (1.28), which encompasses the OAM and the spin term. However there is also a new orbital term, which depends explicitly on $\mathbf{r_0}$. We can express the OAM and spin components as:

$$\mathbf{L_o}(\mathbf{r_0}) = \mathrm{Re}\,\frac{\epsilon_0}{2i\omega}\int d^3r\sum_{j=x,y,z}E_j^{(+)*}\,(\mathbf{r}\times\boldsymbol{\nabla})\,E_j^{(+)}-\mathbf{r_0}\times\mathbf{P}\,, \tag{1.30}$$

$$\mathbf{L_s} = \mathrm{Re}\,\frac{\epsilon_0}{2i\omega}\int d^3r\,\mathbf{E}^{(+)*}\times\mathbf{E}^{(+)}\,. \tag{1.31}$$

Now we can write the OAM with respect to another reference point $\mathbf{r_0'}$ as $\mathbf{L_o}(\mathbf{r_0'})$, and look at the difference $\Delta\mathbf{L_o}$

$$\Delta\mathbf{L_o}=\mathbf{L_o}(\mathbf{r_0'})-\mathbf{L_o}(\mathbf{r_0})=(\mathbf{r_0'}-\mathbf{r_0})\times\mathbf{P} \tag{1.32}$$

We can define the z direction as the direction of the total linear momentum $\mathbf{P}$, i.e., $\mathbf{P}=P\boldsymbol{\epsilon}_z$. In this case, $\Delta L_{oz}=[(\mathbf{r_0'}-\mathbf{r_0})\times\mathbf{P}]\cdot\boldsymbol{\epsilon}_z=0$, which means that the variation over the OAM due to a shift in the reference point only has transverse components with respect to the total linear momentum direction. In this sense we can consider the L_{oz} component of the OAM as intrinsic [19]. In that way, a decomposition of the total angular momentum in intrinsic and extrinsic components would be

$$\mathbf{J}=\mathbf{J}_I+\mathbf{J}_E\,, \tag{1.33}$$

where

$$\begin{aligned}\mathbf{J}_I &= \mathbf{L_s}+L_{oz}\boldsymbol{\epsilon}_z\,;\\ \mathbf{J}_E &= \mathbf{L_{o\perp}}\equiv\mathbf{L_o}-L_{oz}\boldsymbol{\epsilon}_z\,. \end{aligned} \tag{1.34}$$

The OAM is associated with the helical structure of the wavefront and also to the existence of a vortex over the axis [20, 21], i.e., a phase singularity where the intensity of the field is zero. A detailed calculation of the spin-orbit decomposition is found in [11].

1.3 Quantization of the Angular Momentum

Performing the canonical quantization of the electromagnetic field, we can represent the fields **E**, **B** and **A** as operators. We will work in the Coulomb gauge, therefore the vector field **A** satisfies the wave equation

$$\boldsymbol{\nabla}^2\mathbf{A}(\mathbf{r},t) - \frac{1}{c^2}\frac{\partial^2\mathbf{A}(\mathbf{r},t)}{\partial t^2}(\mathbf{r},t) = 0 \tag{1.35}$$

and

$$\boldsymbol{\nabla}\cdot\mathbf{A}(\mathbf{r},t) = 0, \tag{1.36}$$

and the electric and magnetic fields are given by

$$\mathbf{E}(\mathbf{r},t) = -\frac{\partial\mathbf{A}}{\partial t}(\mathbf{r},t), \tag{1.37}$$

$$\mathbf{B}(\mathbf{r},t) = \boldsymbol{\nabla}\times\mathbf{A}(\mathbf{r},t). \tag{1.38}$$

The expansion for the field operators $\hat{\mathbf{E}}(\mathbf{r},t)$, $\hat{\mathbf{B}}(\mathbf{r},t)$ and $\hat{\mathbf{A}}(\mathbf{r},t)$ can be written as [11]:

$$\hat{\mathbf{E}}(\mathbf{r},t) = \frac{1}{L^{3/2}}\sum_{\mathbf{k}}\sum_{s}\left(\frac{\hbar\omega}{2\epsilon_0}\right)^{1/2}[i\hat{a}_{\mathbf{k}s}(0)\boldsymbol{\epsilon}_{\mathbf{k}s}e^{i(\mathbf{k}\cdot\mathbf{r}-\omega t)} + h.c.]; \tag{1.39}$$

$$\hat{\mathbf{B}}(\mathbf{r},t) = \frac{1}{L^{3/2}}\sum_{\mathbf{k}}\sum_{s}\left(\frac{\hbar}{2\omega\epsilon_0}\right)^{1/2}[i\hat{a}_{\mathbf{k}s}(0)(\mathbf{k}\times\boldsymbol{\epsilon}_{\mathbf{k}s})e^{i(\mathbf{k}\cdot\mathbf{r}-\omega t)} + h.c.]; \tag{1.40}$$

$$\hat{\mathbf{A}}(\mathbf{r},t) = \frac{1}{L^{3/2}}\sum_{\mathbf{k}}\sum_{s}\left(\frac{\hbar}{2\omega\epsilon_0}\right)^{1/2}[\hat{a}_{\mathbf{k}s}(0)\boldsymbol{\epsilon}_{\mathbf{k}s}e^{i(\mathbf{k}\cdot\mathbf{r}-\omega t)} + h.c.], \tag{1.41}$$

where L is the size of the quantization box, $\hat{a}_{\mathbf{k}s}(t)$ and $\hat{a}^{\dagger}_{\mathbf{k}s}(t)$ are the annihilation and creation operators and *h.c.* stands for hermitian conjugate.

Now we can find a quantized form for the orbital and spin parts of the angular momentum using the expressions above. The classical form of $\mathbf{L_o}$ and $\mathbf{L_s}$ given by Eqs.

(1.30) and (1.31) can also be written as [11]:

$$\mathbf{L_o}(\mathbf{r_0}) = \epsilon_0 \sum_{i=x,y,z} \int E_i(\mathbf{r} \times \nabla) A_i d^3r - \mathbf{r_0} \times \mathbf{P} \ , \tag{1.42}$$

$$\mathbf{L_s} = \epsilon_0 \int \mathbf{E} \times \mathbf{A} d^3r \ . \tag{1.43}$$

Performing the symmetrization we can define the Hermitian spin angular momentum operator as:

$$\hat{\mathbf{L}}_\mathbf{s} = \frac{1}{2}\epsilon_0 \int_{L^3} (\hat{\mathbf{E}} \times \hat{\mathbf{A}} - \hat{\mathbf{A}} \times \hat{\mathbf{E}}) d^3r \ . \tag{1.44}$$

For the orbital part we have

$$\hat{\mathbf{L}}_\mathbf{o}(\mathbf{r_0}) = \hat{\mathbf{L}}_\mathbf{o}(0) - \mathbf{r_0} \times \hat{\mathbf{P}} \ , \tag{1.45}$$

with

$$\hat{\mathbf{L}}_\mathbf{o}(0) = \frac{1}{2}\epsilon_0 \int_{L^3} \{\hat{E}_i(\mathbf{r} \times \nabla)\hat{A}_i + [(\mathbf{r} \times \nabla)\hat{A}_i]\hat{E}_i\} d^3r \ . \tag{1.46}$$

1.3.1 Spin Angular Momentum Operator

Using the mode expansions of Eq. (1.39) we can rewrite Eq. (1.44) as:

$$\begin{aligned} \hat{\mathbf{L}}_\mathbf{s} &= \frac{1}{2L^3} \sum_{\mathbf{k},\mathbf{k}'} \sum_{s,s'} \left(\frac{\hbar\omega}{2}\right)^{1/2} \left(\frac{\hbar}{2\omega'}\right)^{1/2} \int_{L^3} [i\hat{a}_{\mathbf{k}s}(0)\boldsymbol{\epsilon}_{\mathbf{k}s} e^{i(\mathbf{k}\cdot\mathbf{r}-\omega t)} + h.c.] \\ &\times [\hat{a}_{\mathbf{k}'s'}(0)\boldsymbol{\epsilon}_{\mathbf{k}'s'} e^{i(\mathbf{k}\cdot\mathbf{r}-\omega t)} + h.c.] d^3r + h.c. \ . \end{aligned} \tag{1.47}$$

Performing the volume integral and using the commutation relations between $\hat{a}_{\mathbf{k}'s'}$ and $\hat{a}^\dagger_{\mathbf{k}'s'}$ we have

$$\hat{\mathbf{L}}_\mathbf{s} = i\hbar \sum_{\mathbf{k},s} \sum_{s'} (\hat{a}^\dagger_{\mathbf{k}s'} \hat{a}_{\mathbf{k}s} + \frac{1}{2}\delta_{ss'})(\boldsymbol{\epsilon}_{\mathbf{k}s} \times \boldsymbol{\epsilon}^*_{\mathbf{k}s'}) \ . \tag{1.48}$$

In order to simplify the expression of $\hat{\mathbf{L}}_\mathbf{s}$ we can choose to examine two special cases of polarization basis. If $\boldsymbol{\epsilon}_{\mathbf{k}1}$ and $\boldsymbol{\epsilon}_{\mathbf{k}2}$ are real, orthogonal unit vectors, corresponding to two orthogonal linear polarizations, then

$$\boldsymbol{\epsilon}_{\mathbf{k}s} \times \boldsymbol{\epsilon}^*_{\mathbf{k}s'} = \pm\boldsymbol{\kappa}(1 - \delta_{ss'}) \ , \tag{1.49}$$

where $\boldsymbol{\kappa}$ is the unit vector in the direction of the wave vector $\mathbf{k}$. Substituting this result in Eq. (1.48) we obtain

$$\hat{\mathbf{L}}_\mathbf{s} = i\hbar \sum_{\mathbf{k}} \boldsymbol{\kappa}(\hat{a}^\dagger_{\mathbf{k}2}\hat{a}_{\mathbf{k}1} - \hat{a}^\dagger_{\mathbf{k}1}\hat{a}_{\mathbf{k}2}) \ , \tag{1.50}$$

which shows that each component of the $\hat{\mathbf{L}}_\mathbf{s}$ operator is in the wave vector direction.

Now it is interesting to look for a polarization basis in which the $\hat{\mathbf{L}}_\mathbf{s}$ operator is diagonal in terms of Fock states. To achieve that, we must find the polarization vectors such that $\boldsymbol{\epsilon}_{\mathbf{k}s} \times \boldsymbol{\epsilon}^*_{\mathbf{k}s'} \propto \delta_{ss'}$. It turns out that the circular polarization vectors $\boldsymbol{\epsilon}_{\mathbf{k}\lambda}(\lambda = \pm 1)$ defined below fulfill this condition:

$$\boldsymbol{\epsilon}_{\mathbf{k},+1} = \frac{1}{\sqrt{2}}(\boldsymbol{\epsilon}_{\mathbf{k}1} + i\boldsymbol{\epsilon}_{\mathbf{k}2}) \tag{1.51}$$

$$\boldsymbol{\epsilon}_{\mathbf{k},-1} = \frac{1}{\sqrt{2}}(i\boldsymbol{\epsilon}_{\mathbf{k}1} + \boldsymbol{\epsilon}_{\mathbf{k}2}) \ . \tag{1.52}$$

These vectors represent right-hand and left-hand circularly polarized light and they satisfy the condition

$$\boldsymbol{\epsilon}_{\mathbf{k}\lambda} \times \boldsymbol{\epsilon}^*_{\mathbf{k}\lambda'} = -i\lambda\boldsymbol{\kappa}\delta_{\lambda\lambda'} \ , \tag{1.53}$$

which, substituted into Eq. (1.48), leads to

$$\begin{aligned} \hat{\mathbf{L}}_\mathbf{s} &= \sum_{\mathbf{k},\lambda} \hbar\boldsymbol{\kappa}\lambda(\hat{a}^\dagger_{\mathbf{k}\lambda}\hat{a}_{\mathbf{k}\lambda} + \frac{1}{2}) \\ &= \sum_{\mathbf{k}} \hbar\boldsymbol{\kappa}(\hat{n}_{\mathbf{k},+1} - \hat{n}_{\mathbf{k},-1}) \ , \end{aligned} \tag{1.54}$$

where $\hat{n}_{\mathbf{k}\lambda} = \hat{a}^\dagger_{\mathbf{k}\lambda}\hat{a}_{\mathbf{k}\lambda}$ is the number operator. We can interpret the above equation and observe that each photon with right-hand(left-hand) circular polarization contributes with $+(-)\hbar\boldsymbol{\kappa}$ to the total spin angular momentum. The projection of the spin angular momentum on the direction of propagation is the *helicity* and the parameter $\lambda = \pm 1$ is the spin of the photon. The spin angular momentum per photon can be $\pm\hbar$. Since $\hat{\mathbf{L}}_\mathbf{s}$ can be written as a function of the number operators $\hat{n}_{\mathbf{k}\lambda}$, it commutes with the Hamiltonian operator $\hat{H}$ for the free electromagnetic field, and therefore is a constant of the motion.

1.3.2 Orbital Angular Momentum Operator

For the orbital part of the angular momentum operator the expansion in plane waves is not as suitable as for the spin part. The fact that the quantization was made with a box with a discrete set of modes breaks the symmetry of the directions of propagation. Since the OAM depends on the space functions of the modes, we have to resort to a

continuous mode decomposition of the field operators. In a continuous Fock space we have:

$$\hat{\mathcal{A}}(\mathbf{k},t) = \sum_{s} \hat{a}(\mathbf{k},s)\boldsymbol{\epsilon}(\mathbf{k},s)e^{-i\omega t} \ , \tag{1.55}$$

where $\mathbf{k}$ is a continuous variable. With this expansion the OAM operator can be expressed as [22]:

$$\hat{\mathbf{L}}_{\mathbf{o}}(0) = -\frac{i\hbar}{2}\int \left[\hat{\mathcal{A}}_i^{\dagger}(\mathbf{k},t)(\mathbf{k}\times\nabla_{\mathbf{k}})\hat{\mathcal{A}}_i(\mathbf{k},t) - h.c.\right] d^3k \ , \tag{1.56}$$

where $\nabla_{\mathbf{k}}$ is the gradient operator with respect to $\mathbf{k}$.

2

Spin-Orbit Entanglement in Paraxial Modes

In the field of Quantum Information, photonic systems are frequently used to perform experiments. There are many degrees of freedom of a photon that can be useful such as polarization, transverse mode, frequency, path of propagation and so on. In our work we exploit the polarization state of light and the transverse profile modes. In the first section of the chapter we will show how these two properties can be described as a qubit, making way to Quantum Information applications.

2.1 Polarization and Transverse Mode Qubits

The qubit is a fundamental concept for Quantum Information and Quantum Computation [23]. It is a mathematical object defined as an arbitrary superposition, with weights that are complex numbers, of two possible orthogonal states. The interest of such an object is that in Quantum Physics, several systems allow the definition of a subspace of this type, such as two energy levels of an atom, the alignment of a nuclear spin in a uniform magnetic field, and also the polarization of a photon. The qubit has a geometrical representation called the Bloch sphere. If we write the arbitrary state of one qubit as

$$|\psi\rangle = \cos\left(\frac{\theta}{2}\right)|0\rangle + e^{i\phi}\sin\left(\frac{\theta}{2}\right)|1\rangle \ , \tag{2.1}$$

then the numbers θ and ϕ define a point in the surface of the sphere shown in Fig. 2.1.

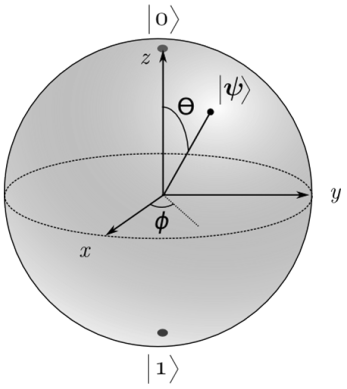

Figure 2.1: Bloch Sphere

The arbitrary state of Eq. (2.1) is expressed in terms of the computational basis $\{|0\rangle, |1\rangle\}$, also called the Z basis, because it is formed by the eigenvectors of the Pauli operator σ_z. Another possible choice of basis is the set $\{|+\rangle, |-\rangle\}$ where $|+\rangle = \frac{|0\rangle+|1\rangle}{\sqrt{2}}$ and $|-\rangle = \frac{|0\rangle-|1\rangle}{\sqrt{2}}$. This is known as the X basis, composed by the eigenvectors of σ_x.

The polarization state of a photon presents the same mathematical structure of a qubit, and has its own geometrical representation, called the Poincaré sphere [9]. In this representation, the cartesian coordinates of a point in the sphere correspond to the Stokes parameters that describe the polarization state.

In [24] Padgett and co-workers develop an analog of the Poincaré sphere to represent the first order transverse modes, presented in Section 1.1. To build this representation, they defined new Stokes parameters where the LG modes play the role of the circular polarization, and each HG mode substitutes the linear polarization presenting the same orientation. The definition follows:

$$\begin{aligned} o_1 &= \frac{I_{HG_{10}^{0^\circ}} - I_{HG_{10}^{90^\circ}}}{I_{HG_{10}^{0^\circ}} + I_{HG_{10}^{90^\circ}}}, \\ o_2 &= \frac{I_{HG_{10}^{45^\circ}} - I_{HG_{10}^{135^\circ}}}{I_{HG_{10}^{45^\circ}} + I_{HG_{10}^{135^\circ}}}, \\ o_3 &= \frac{I_{LG_0^1} - I_{LG_0^{-1}}}{I_{LG_0^1} + I_{LG_0^{-1}}}, \end{aligned} \tag{2.2}$$

where I_{HG} and I_{LG} are the intensities associated with the mode indicated in the subscript. The two Poincaré spheres are shown in Figure 2.2.

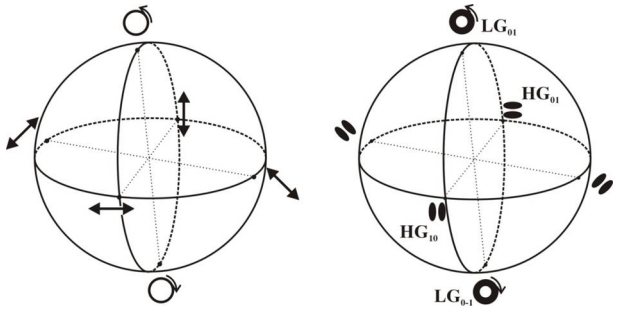

Figure 2.2: Poincaré Sphere and Transverse modes Sphere

2.2 Spin-Orbit Modes

We can label the polarization unit vectors according to their orientation, denoting the horizontally oriented unit vector as $\boldsymbol{\epsilon}_H$ and the vertical one as $\boldsymbol{\epsilon}_V$. Similarly, we can denote the HG_{10} mode as ψ_h and HG_{01} mode as ψ_v, also evidencing their natural orientation. The pair of modes $\{\psi_h, \psi_v\}$ forms a basis for the first-order subspace of transverse modes. In Fig. 2.3 we can see how to decompose different modes in the $\{\psi_h, \psi_v\}$ basis. Combining the spin-orbit degrees of freedom we can define an arbitrary spin-orbit mode $\mathbf{E}(\mathbf{r})$ for the electromagnetic field [25] as

$$\mathbf{E}(\mathbf{r}) = \alpha\psi_h(\mathbf{r})\boldsymbol{\epsilon}_H + \beta\psi_h(\mathbf{r})\boldsymbol{\epsilon}_V + \gamma\psi_v(\mathbf{r})\boldsymbol{\epsilon}_H + \delta\psi_v(\mathbf{r})\boldsymbol{\epsilon}_V. \tag{2.3}$$

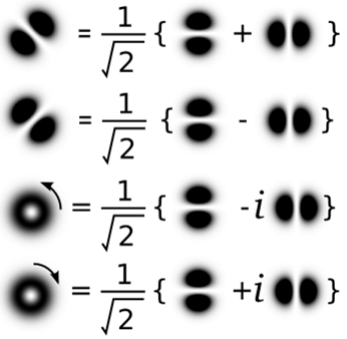

Figure 2.3: Decomposition of the $\psi_{45^\circ}, \psi_{135^\circ}, \psi_{+1}$ and ψ_{-1} transverse modes in the $\{\psi_h, \psi_v\}$ basis

We can also define two types of spin-orbit modes, the separable (S) and non-separable (NS) ones. If the polarization part and the orbital part can be described

separately, then the mode is called separable. It means that one single state of polarization is attributed to the entire wave front, in contrast with the NS case, where the modes exhibit a polarization gradient leading to a polarization-vortex behavior [26]. An arbitrary separable mode is of the form:

$$\mathbf{E}_S(\mathbf{r}) = [\alpha_h \psi_h(\mathbf{r}) + \alpha_v \psi_v(\mathbf{r})](\beta_H \boldsymbol{\epsilon}_H + \beta_V \boldsymbol{\epsilon}_V). \tag{2.4}$$

The criteria to distinguish between separable and non-separable is analogous to the concurrence [27]. For the mode in Eq. (2.3), the quantity C is defined as

$$C = 2|\alpha\delta - \beta\gamma| \ . \tag{2.5}$$

It is important to note that, even for maximally non-separable (MNS) modes, with $C = 1$, the concept of entanglement does not apply. The modes described here represent classical amplitudes. The quantum aspect will only arise if we excite these modes with single photons, as will be discussed in Section 2.4.

The MNS modes have a mathematical structure analog to the one of maximally entangled states. One example of MNS mode is

$$\mathbf{E}_{MNS}(\mathbf{r}) = \frac{1}{\sqrt{2}}[\psi_h(\mathbf{r})\boldsymbol{\epsilon}_H + \psi_v(\mathbf{r})\boldsymbol{\epsilon}_V]. \tag{2.6}$$

There is an SO(3) representation of the MNS modes, developed in [28, 29] where each point in the volume of the SO(3) sphere corresponds to a MNS mode and two points diametrically opposite are identified. This representation in terms of optical modes allowed the experimental demonstration of the double connected nature of the SO(3) rotation group and the investigation of the topological phase acquired by a laser beam passing through a cycle of spin-orbit transformations [25].

Due to the similarity with the mathematical structure of the Bell states [23], we can define a set of four MNS modes as Bell modes, as follows:

$$\begin{aligned}
\mathbf{E}_{\Phi^+}(\mathbf{r}) &= \frac{1}{\sqrt{2}}[\psi_h(\mathbf{r})\boldsymbol{\epsilon}_H + \psi_v(\mathbf{r})\boldsymbol{\epsilon}_V] \ , \\
\mathbf{E}_{\Phi^-}(\mathbf{r}) &= \frac{1}{\sqrt{2}}[\psi_h(\mathbf{r})\boldsymbol{\epsilon}_H - \psi_v(\mathbf{r})\boldsymbol{\epsilon}_V] \ , \\
\mathbf{E}_{\Psi^+}(\mathbf{r}) &= \frac{1}{\sqrt{2}}[\psi_h(\mathbf{r})\boldsymbol{\epsilon}_V + \psi_v(\mathbf{r})\boldsymbol{\epsilon}_H] \ , \\
\mathbf{E}_{\Psi^-}(\mathbf{r}) &= \frac{1}{\sqrt{2}}[\psi_h(\mathbf{r})\boldsymbol{\epsilon}_V - \psi_v(\mathbf{r})\boldsymbol{\epsilon}_H] \ .
\end{aligned} \tag{2.7}$$

These modes form an alternative basis for the subspace of first order spin-orbit modes.

2.3 Experimental Production of Spin-Orbit Modes

Now that we have presented the kind of modes of the electromagnetic field we are interested in, it is important to describe their production in the laboratory. For the polarization degree of freedom, the techniques applied are quite simple. We have a laser source which already provides us with a fairly well polarized beam. Even if it is not the case, we can separate two polarized components of a beam using a polarizing beam splitter (PBS). Starting from a well known linearly polarized beam, it is possible to manipulate its polarization with half-wave plates (HWP) and quarter-wave plates (QWP). In fact, with a set of two QWP and one HWP it is possible to perform any unitary operation over the polarization state [30].

2.3.1 Holographic masks to generate LG and HG modes

In this subsection we briefly describe the techniques to access the orbital degree of freedom necessary to our experiments. First of all, we must be able to generate the modes we will work with, that is, the first order HG and LG modes. One of many possible ways to accomplish that is to build holographic masks that, once in the path of the beam, generate the desired mode. There are many types of masks, which can be produced with different techniques [31, 32]. The general idea is to create an interference pattern of the desired beam profile with a reference beam, usually a plane wave. The pattern is computationally generated using the analytic description of the desired mode. The final result is a density plot of the squared modulus of the sum of the amplitudes of the interfering beams. The calculated interference can be normal or tilted, if the beams are incident with a relative angle. In the second case, the generated beam will propagate in a different direction from the incident beam, reconstructing the geometry of the generation of the hologram. Two examples of interference patterns, one normal and one tilted, are shown in Figure 2.4.

The interference pattern can be miniaturized and printed in a microfilm, which constitutes an amplitude mask. The transmission coefficient in each point of the mask depends on the amplitude of the interference. It is simpler to make a binary transmission coefficient, so the mask is black where the normalized amplitude is bigger than 0.5, and transparent everywhere else. This binary pattern can also be engraved into a phase mask, substituting the black and white areas with thicker and thiner areas,

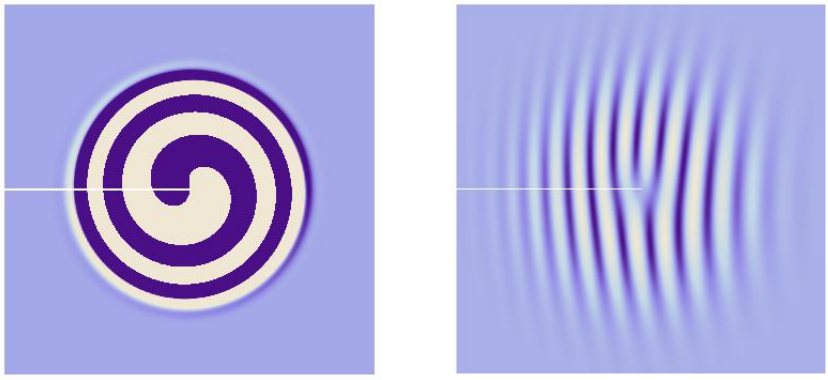

(a) Normal interference pattern between a plane wave and an LG_0^1 mode

(b) Tilted interference pattern between a plane wave and an LG_0^1 mode

Figure 2.4: Interference patterns for holographic masks

forming a relief. The propagation through the thicker parts gives the beam a phase of π relative to the thinner ones.

A peculiar aspect of the binary masks is the generation of a multiplicity of modes, as a diffraction grating. This aspect can be undesirable if we are interested in just one of the modes, as we end up loosing a significant part of the initial intensity of the beam. However in some experiments this multiple generation of modes can be an advantage, if we are interested in more than one of them [25]. One possible way to reduce the loss of intensity to the higher order diffraction modes is to use a blazed mask. It represents a compromise between the simpler binary mask and the full hologram generated by the interference pattern.

In our experiments we have used phase masks produced by a member of the laboratory, Carlos Eduardo R. de Souza, and the detailed description of the process can be found in [33]. It is possible to produce masks to generate both LG and HG modes, and their profile is shown in Figs. 2.5(a) and 2.5(b).

Once we have a starter mode, we can obtain other modes through some manipulations. One way to transform the transverse mode of a beam is to use a Dove prism [34]. Inside the prism, the beam suffers a refraction, then a total internal reflection, and finally another refraction as it exits the prism. The net effect is to invert the image with respect to the plane of reflection. So if the prism is rotated at an angle θ with

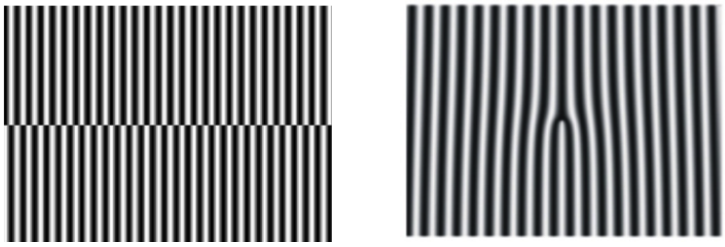

(a) HG mask (b) LG mask

Figure 2.5: Masks

respect to the vertical it will reflect the image in an apparent rotation of 2θ.

It is interesting to note that, for an LG mode, even though it presents rotational symmetry, it can still be affected by the Dove prism. Two Dove prisms, rotated with respect to each other by an angle θ rotate the passing beam by an angle 2θ. If the beam has a term $e^{il\phi}$ it becomes $e^{il(\phi+2\theta)}$, so the two Dove prisms give the LG beam an l dependent phase [35].

To create a mode such as the one in Eq. (2.3) we must be able to superpose coherently each of the four components, and also we must be able to choose the parameters α, β, γ and δ. We can see an example of setup in Fig. 2.6. In this setup an HG_{10} mode is produced by a holographic mask and then a Mach-Zender interferometer manipulates this mode in two different ways: in one arm, the polarization is rotated with a HWP, going from horizontal to vertical, and in the other arm the transverse mode is rotated, going from HG_{10} to HG_{01}. The two resulting modified modes are superimposed in the last beam splitter (BS), and the final mode is

$$\mathbf{E}(\mathbf{r}) = \frac{1}{\sqrt{2}}[\psi_h(\mathbf{r})\boldsymbol{\epsilon}_V + \psi_v(\mathbf{r})\boldsymbol{\epsilon}_H], \tag{2.8}$$

which is one example of maximally non-separable mode.

2.3.2 Q-plates and other experimental methods

Other devices for manipulating the OAM degree of freedom include cylindrical lenses [21], spiral phase plates [36] and q-plates [37]. The q-plates are a very interesting and successful example of these methods since they are meant not only to generate OAM modes, but also to couple the orbital and spin degrees of freedom of a photon. It enables in one device a kind of process that was only possible through interferometric

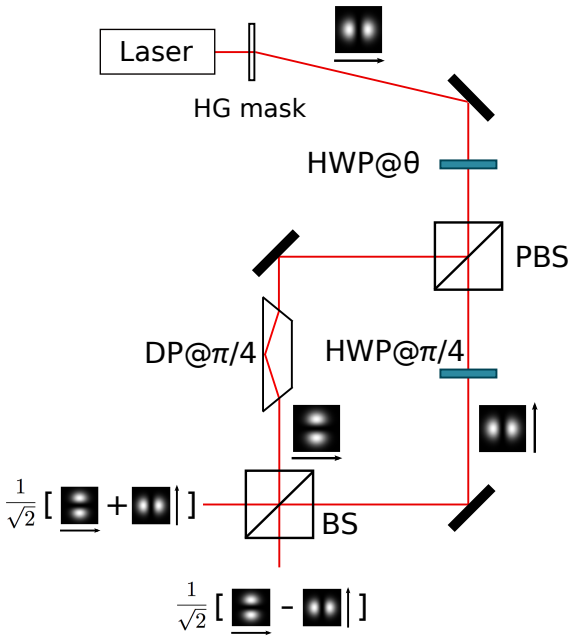

Figure 2.6: Mach-Zender interferometer with a half wave plate (HWP) oriented at $\pi/4$ radians and a Dove prism (DP) also oriented at $\pi/4$ radians. The arrows close to the transverse profile pictures represent the polarization orientation.

techniques before. The q-plate is made from a birefringent material inducing a phase retardation of δ. It presents an optical pattern characterized by two indices, q and α_0. q is the number of rotations that the optical axis exhibits in a path circling once around the center of the plate, and α_0 is the initial optical axis orientation with respect to some reference orientation, i.e., α_0 is the angle that the optical axis forms at a reference angular position.

The plate has its optimal tuning when $\delta = \pi$. In this situation, an incoming beam carrying circular polarization has its OAM state changed. The azimuthal index l will change by an amount $\Delta l = \pm 2q$, where the sign is positive for left-circular and negative for right-circular polarization. The handedness of the output circular polarization is also inverted.

2.4 Quantization of the Spin-Orbit Modes

In a quantum mechanical description of light, the electromagnetic field is quantized so we must define the spin-orbit modes described in Section 2.2 in this context. We remind here the expression given in Section 1.1 for the classical electric field:

$$\mathbf{E}(\mathbf{r},t) = \mathbf{E}^{(+)}(\mathbf{r},t) + (\mathbf{E}^{(+)}(\mathbf{r},t))^* \ , \tag{2.9}$$

where

$$\mathbf{E}^{(+)}(\mathbf{r},t) = e^{-i(\omega t - kz)}\boldsymbol{\epsilon} u(\mathbf{r})\mathcal{E}(z,t). \tag{2.10}$$

The quantum field operator $\hat{\mathbf{E}}^{(+)}(\mathbf{r},t)$ is analog to the complex field $\mathbf{E}^{(+)}(\mathbf{r},t)$ with the classical amplitude $\mathcal{E}(z,t)$ being substituted by an amplitude operator $\hat{a}$ for each mode. The expansion of $\hat{\mathbf{E}}^{(+)}(\mathbf{r},t)$ in plane wave modes is given by:

$$\hat{\mathbf{E}}^{(+)}(\mathbf{r},t) = i\sum_i \sqrt{\frac{\hbar\omega_i}{2\epsilon_0}}\mathbf{f}_i(\mathbf{r})\hat{a}_i e^{-i\omega_i t} \ , \tag{2.11}$$

where

$$\mathbf{f}_i(\mathbf{r}) = L^{-\frac{3}{2}}\boldsymbol{\epsilon}_i e^{i\mathbf{k}_i\cdot\mathbf{r}} \tag{2.12}$$

is the spatial function, normalized inside the quantization box.

The plane wave expansion is the most simple, but it is not very physical, since the wave front in these modes is infinite. As we work with laser beams, we are interested in expanding the field operator in terms of either the LG modes or the HG modes,

that obey the paraxial equation, and were introduced in Section 1.1. We can restrict ourselves to a monochromatic field for the purpose of all the experiments described here. In this case we can rewrite the field operator of a given frequency ω as:

$$\hat{\mathbf{E}}^{(+)}(\mathbf{r},t) = i\sum_{\lambda,\sigma}\sqrt{\frac{\hbar\omega}{2\epsilon_0 L}}\boldsymbol{\epsilon}_\sigma u_\lambda(\mathbf{r})\hat{a}_{\lambda\sigma}e^{-i\omega(t-z/c)} \tag{2.13}$$

The mode amplitudes carry the indices σ for the polarization and λ for the transverse distribution. λ can represent a set of indices, depending on the choice of transverse basis. If we choose the HG modes, $\lambda = \{m,n\}$ with $m,n = 0,1,2,...,\infty$, and alternatively, if we choose the LG basis, $\lambda = \{p,l\}$ with $p = 0,1,2,...,\infty$ and l can be any integer from $-p$ to p.

In this work we restrict ourselves to the first order transverse modes subspace. Adding the polarization, we have a 4 dimensional complex space, for which we can chose several different basis. The first and perhaps most simple one is the one used in Eq. (2.3). In this basis, the electric field operator is expressed as:

$$\hat{\mathbf{E}}(\mathbf{r}) = \psi_h(\mathbf{r})\boldsymbol{\epsilon}_H\hat{a}_{hH} + \psi_h(\mathbf{r})\boldsymbol{\epsilon}_V\hat{a}_{hV} + \psi_v(\mathbf{r})\boldsymbol{\epsilon}_H\hat{a}_{vH} + \psi_v(\mathbf{r})\boldsymbol{\epsilon}_V\hat{a}_{vV}. \tag{2.14}$$

We can also choose the rotated basis $\{\boldsymbol{\epsilon}_{\alpha+},\boldsymbol{\epsilon}_{\alpha-}\}$ and $\{\psi_{\beta+},\psi_{\beta-}\}$ combined, to express the field operator. With the relations

$$\begin{aligned}
\boldsymbol{\epsilon}_{\alpha+} &= \boldsymbol{\epsilon}_H\cos\alpha + \boldsymbol{\epsilon}_V\sin\alpha\ ,\\
\boldsymbol{\epsilon}_{\alpha-} &= -\boldsymbol{\epsilon}_H\sin\alpha + \boldsymbol{\epsilon}_V\cos\alpha\ ,\\
\psi_{\beta+}(\mathbf{r}) &= \psi_h(\mathbf{r})\cos\beta + \psi_v(\mathbf{r})\sin\beta\ ,\\
\psi_{\beta-}(\mathbf{r}) &= -\psi_h(\mathbf{r})\sin\beta + \psi_v(\mathbf{r})\cos\beta\ ,
\end{aligned} \tag{2.15}$$

we can derive the relations between the amplitude operators in the two basis:

$$\begin{aligned}
\hat{\mathbf{E}}(\mathbf{r}) &= \psi_{\beta+}(\mathbf{r})\boldsymbol{\epsilon}_{\alpha+}\hat{a}_{\beta+\alpha+} + \psi_{\beta+}(\mathbf{r})\boldsymbol{\epsilon}_{\alpha-}\hat{a}_{\beta+\alpha-} \\
&\quad + \psi_{\beta-}(\mathbf{r})\boldsymbol{\epsilon}_{\alpha+}\hat{a}_{\beta-\alpha+} + \psi_{\beta-}(\mathbf{r})\boldsymbol{\epsilon}_{\alpha-}\hat{a}_{\beta-\alpha-} \\
&= \psi_h(\mathbf{r})\boldsymbol{\epsilon}_H[\cos\alpha\cos\beta\ \hat{a}_{\beta+\alpha+} - \sin\alpha\cos\beta\ \hat{a}_{\beta+\alpha-} \\
&\quad - \cos\alpha\sin\beta\ \hat{a}_{\beta-\alpha+} + \sin\alpha\sin\beta\ \hat{a}_{\beta-\alpha-}] \\
&\quad + \psi_v(\mathbf{r})\boldsymbol{\epsilon}_H[\cos\alpha\sin\beta\ \hat{a}_{\beta+\alpha+} - \sin\alpha\sin\beta\ \hat{a}_{\beta+\alpha-} \\
&\quad + \cos\alpha\cos\beta\ \hat{a}_{\beta-\alpha+} - \sin\alpha\cos\beta\ \hat{a}_{\beta-\alpha-}] \\
&\quad + \psi_h(\mathbf{r})\boldsymbol{\epsilon}_V[\sin\alpha\cos\beta\ \hat{a}_{\beta+\alpha+} + \cos\alpha\cos\beta\ \hat{a}_{\beta+\alpha-} \\
&\quad - \sin\alpha\sin\beta\ \hat{a}_{\beta-\alpha+} - \cos\alpha\sin\beta\ \hat{a}_{\beta-\alpha-}] \\
&\quad + \psi_v(\mathbf{r})\boldsymbol{\epsilon}_V[\sin\alpha\sin\beta\ \hat{a}_{\beta+\alpha+} + \cos\alpha\sin\beta\ \hat{a}_{\beta+\alpha-} \\
&\quad + \sin\alpha\cos\beta\ \hat{a}_{\beta-\alpha+} + \cos\alpha\cos\beta\ \hat{a}_{\beta-\alpha-}]\ .
\end{aligned} \tag{2.16}$$

Looking at Eq. (2.14) we can identify the terms in brakets with the operators $\hat{a}_{hH}$, $\hat{a}_{vH}$, $\hat{a}_{hV}$ and $\hat{a}_{vV}$.

One important alternative basis is the Bell basis, presented in Eq. (2.7), which is formed by four different maximally non-separable modes. The field operator in this basis is:

$$\begin{aligned}
\hat{\mathbf{E}}(\mathbf{r}) &= \frac{1}{\sqrt{2}}[\psi_h(\mathbf{r})\boldsymbol{\epsilon}_H + \psi_v(\mathbf{r})\boldsymbol{\epsilon}_V]\hat{a}_{\Phi^+} + \frac{1}{\sqrt{2}}[\psi_h(\mathbf{r})\boldsymbol{\epsilon}_H - \psi_v(\mathbf{r})\boldsymbol{\epsilon}_V]\hat{a}_{\Phi^-} \\
&+ \frac{1}{\sqrt{2}}[\psi_h(\mathbf{r})\boldsymbol{\epsilon}_V + \psi_v(\mathbf{r})\boldsymbol{\epsilon}_H]\hat{a}_{\Psi^+} + \frac{1}{\sqrt{2}}[\psi_h(\mathbf{r})\boldsymbol{\epsilon}_V - \psi_v(\mathbf{r})\boldsymbol{\epsilon}_H]\hat{a}_{\Psi^-}\ .
\end{aligned} \tag{2.17}$$

If we again isolate the terms $\psi_h(\mathbf{r})\boldsymbol{\epsilon}_H$, $\psi_v(\mathbf{r})\boldsymbol{\epsilon}_H$, $\psi_h(\mathbf{r})\boldsymbol{\epsilon}_V$ and $\psi_v(\mathbf{r})\boldsymbol{\epsilon}_V$ as in Eq. (2.16), we can find the relations:

$$\begin{aligned}
\hat{a}_{hH} &= \frac{1}{\sqrt{2}}(\hat{a}_{\Phi^+} + \hat{a}_{\Phi^-})\ ; \\
\hat{a}_{vV} &= \frac{1}{\sqrt{2}}(\hat{a}_{\Phi^+} - \hat{a}_{\Phi^-})\ ; \\
\hat{a}_{hV} &= \frac{1}{\sqrt{2}}(\hat{a}_{\Psi^+} + \hat{a}_{\Psi^-})\ ; \\
\hat{a}_{vH} &= \frac{1}{\sqrt{2}}(\hat{a}_{\Psi^+} - \hat{a}_{\Psi^-})\ .
\end{aligned} \tag{2.18}$$

Note that there is no choice of values for the angles α and β in Eq. (2.16) that leads to this Bell basis. It is reminiscent of the fact that there are no local rotations that can transform a separable 2-qubit state into an entangled state.

Now that we have defined the annihilation operators $\hat{a}_{\lambda\sigma}$ for each of the modes of our 4-dimensional basis, we can also define their hermitian conjugates $\hat{a}^\dagger_{\lambda\sigma}$, and the number operators $\hat{n}_{\lambda\sigma} = \hat{a}^\dagger_{\lambda\sigma}\hat{a}_{\lambda\sigma}$. The tensor product of the eigenstates of the number operator $|n_{\lambda\sigma}\rangle$ over the four modes of the basis forms a Fock state:

$$|\{n\}\rangle = \bigotimes_{\lambda,\sigma} |n_{\lambda\sigma}\rangle \ , \tag{2.19}$$

where $\{n\}$ is the set of occupation numbers $n_{\sigma_1\lambda_1}, n_{\sigma_2\lambda_1}, ...$ for all four modes. We can build a Fock state by applying repeatedly the creation operators $\hat{a}^\dagger_{\lambda\sigma}$ over the vacuum state $|\{0\}\rangle$, with the proper normalization:

$$|\{n\}\rangle = \bigotimes_{\lambda,\sigma} \left[\frac{(\hat{a}^\dagger_{\lambda\sigma})^{n_{\lambda\sigma}}}{\sqrt{(n_{\lambda\sigma})!}} \right] |\{0\}\rangle \ . \tag{2.20}$$

We can also build a coherent state on one of the possible modes, which written in the Fock basis has the form:

$$|\nu_{\lambda\sigma}\rangle = e^{-|\nu|^2/2} \sum_{n_{\lambda\sigma}=0}^{\infty} \frac{(\nu\hat{a}^\dagger_{\lambda\sigma})^{n_{\lambda\sigma}}}{\sqrt{(n_{\lambda\sigma})!}} |0\rangle \ . \tag{2.21}$$

Let us now analyze which states can be generated by the experimental setup of Figure 2.6. If we pump the apparatus with a single photon source, the state generated will be the Fock state:

$$|1_{\Psi^+}\rangle = \hat{a}^\dagger_{\Psi^+}|0\rangle \ . \tag{2.22}$$

This is an entangled state if we make the partition between polarization and transverse mode, as we can see by rewriting it in the $\{hH, hV, vH, vV\}$ basis:

$$|1_{\Psi^+}\rangle = \frac{1}{\sqrt{2}}(\hat{a}^\dagger_{hV} + \hat{a}^\dagger_{vH})|0\rangle = \frac{1}{\sqrt{2}}[|0_{hH}, 1_{hV}, 0_{vH}, 0_{vV}\rangle + |0_{hH}, 0_{hV}, 1_{vH}, 0_{vV}\rangle] \ . \tag{2.23}$$

We can also pump the apparatus with a gaussian beam at the fundamental mode of the laser, which can be approximated by a coherent state. After the mask and the MZ interferometer, this fundamental mode has been transformed into the MNS mode (2.8), so the final state is

$$|\nu_{\Psi^+}\rangle = e^{-|\nu|^2/2} \sum_{n_{\Psi^+}=0}^{\infty} \frac{(\nu\hat{a}^\dagger_{\Psi^+})^{n_{\Psi^+}}}{\sqrt{(n_{\Psi^+})!}} |0\rangle \ . \tag{2.24}$$

We can look at the first terms of the sum, and write the $\hat{a}^\dagger_{\Psi^+}$ operator in terms of the set $\{\hat{a}^\dagger_{hH}, \hat{a}^\dagger_{vH}, \hat{a}^\dagger_{hV}, \hat{a}^\dagger_{vV}\}$:

$$\begin{aligned} |\nu_{\Psi^+}\rangle &= e^{-|\nu|^2/2}\left[1+\nu\hat{a}^\dagger_{\Psi^+}+\frac{(\nu\hat{a}^\dagger_{\Psi^+})^2}{2}+...\right]|0\rangle \\ &= e^{-|\nu|^2/2}\left[1+\nu\left(\frac{\hat{a}^\dagger_{hV}+\hat{a}^\dagger_{vH}}{\sqrt{2}}\right)+\frac{\nu^2}{2}\left(\frac{\hat{a}^\dagger_{hV}+\hat{a}^\dagger_{vH}}{\sqrt{2}}\right)^2+...\right]|0\rangle \\ &= e^{-|\nu|^2/2}\left[|0\rangle+\nu\left(\frac{|0_{hH},1_{hV},0_{vH},0_{vV}\rangle+|0_{hH},0_{hV},1_{vH},0_{vV}\rangle}{\sqrt{2}}\right)+...\right]. \end{aligned} \tag{2.25}$$

From this derivation we can see that the 1 photon term is the same entangled state that we obtained in Eq. (2.23).

We can also write the full coherent state $|\nu_{\Psi^+}\rangle$ in terms of the modes $\psi_h\boldsymbol{\epsilon}_V$ and $\psi_v\boldsymbol{\epsilon}_H$. Using again the relation between $\hat{a}^\dagger_{\Psi^+}$, $\hat{a}^\dagger_{hV}$ and $\hat{a}^\dagger_{vH}$, we have:

$$\begin{aligned} |\nu_{\Psi^+}\rangle &= e^{-|\nu|^2/2}\left[1+\nu\left(\frac{\hat{a}^\dagger_{hV}+\hat{a}^\dagger_{vH}}{\sqrt{2}}\right)+\frac{\nu^2}{2}\left(\frac{\hat{a}^\dagger_{hV}+\hat{a}^\dagger_{vH}}{\sqrt{2}}\right)^2+...\right]|0\rangle \\ &= e^{-|\nu|^2/2}\sum_{N=0}^{\infty}\sum_{k=0}^{N}\frac{(\nu/\sqrt{2})^N}{\sqrt{k!(N-k)!}}|k_{hV},(N-k)_{vH}\rangle \\ &= e^{-|\nu|^2/2}\sum_{k=0}^{\infty}\sum_{l=0}^{\infty}\frac{(\nu/\sqrt{2})^{k+l}}{\sqrt{k!l!}}|k_{hV},l_{vH}\rangle \\ &= |(\nu/\sqrt{2})_{hV},(\nu/\sqrt{2})_{vH}\rangle\ . \end{aligned} \tag{2.26}$$

So, even if the 1 photon part of this state is maximally entangled in the $\{hV, vH\}$ subspace, the complete state is a product state.

3

Quantum Cryptography with Spin-Orbit Modes

The problem of secure communication exists long before quantum information theory. With the advent of quantum information algorithms, the problem of cryptography was touched twice: in one hand, the modern cryptography schemes based on the difficulty to factorize big numbers was threatened by the possibility of a much faster quantum factorization algorithm. On the other hand, quantum information provided a new solution to the problem, with the fundamentally secure quantum key distribution protocol. An introduction to the problem of quantum cryptography can be found in [23].

In this chapter we describe the BB84 quantum key distribution protocol in its original form, and afterwards we present the proposal to perform such a protocol without a shared reference frame between the two parties. This implementation follows the idea of decoherence-free subspaces and was done in collaboration with Dr. Leandro Aolita and Dr. Stephen Walborn from the UFRJ Quantum Optics group, who first proposed the logical encoding allowing the communication without a shared reference frame [38]. We will describe the experimental setup, exploring the polarization and transverse modes of laser beams, and finally show our results. The work present in this chapter is published in [39].

3.1 BB84 Protocol

A Quantum Key Distribution protocol is based in the private key cryptography system. A simple and effective private key cryptosystem is the Vernam cipher. The idea is that if two parties, Alice and Bob, share a secret key in the form of a random string of bits, they can add this string to any message they want to communicate using a public channel. Since the other party also knows the key, it can subtract the key from the encrypted message to get the original message. If Alice and Bob are the only ones who have the key, the protocol is secure.

The question that arises is then how to produce and share such a key. Of course, if Alice and Bob can meet, they can produce two copies of a key and share it. But if they need to do the same thing being apart, then they need a secure way to share this information. If they have a public quantum channel through which they can send qubits with an error rate lower then a certain threshold, then the security is guaranteed by the properties of quantum information. The two properties that guarantee the security of the protocol are the no-cloning theorem and the fact that attempts to intercept the information made by a third party (Eve) introduce disturbance to the signal, and are eventually noticed [23].

Let us now describe the BB84 protocol, proposed by Bennett and Brassard [40] in more detail. Alice wants to send a string of n bits to Bob. She can encode these bits in n qubits, choosing randomly between two basis, X and Z for example. The encoding follows Table 3.1 below:

	0	1
X basis	$\|+\rangle = \frac{\|0\rangle+\|1\rangle}{\sqrt{2}}$	$\|-\rangle = \frac{\|0\rangle-\|1\rangle}{\sqrt{2}}$
Z basis	$\|0\rangle$	$\|1\rangle$

Table 3.1: Encoding table

Since the four possible states that Alice can send are not all mutually orthogonal, no measurement can distinguish between them with complete certainty. When Bob receives the qubits, he has to choose in which of the two possible basis he will measure. Every time he chooses the same basis that Alice used in the encoding, his result will be accurate, i.e., will correspond to the bit Alice wanted to encode. When he chooses the

wrong basis, the result is right with only 50% probability, i.e., he has no real information about the bit encoded.

After the communication of the sequence of n qubits, Alice and Bob compare their choice of basis for each qubit sent/measured. They discard all the bits of the sequence where there was no coincidence of basis, and keep the ones encoded and measured in the same basis. For the latter, they can be sure that the information was transmitted correctly. Note that the public announcement of the basis chosen, made *after* the transmission of the qubits is complete, gives Eve no information.

To guarantee that there has been no eavesdropping, Alice and Bob have to sacrifice some of the successful bits. They publicly announce a sequence of randomly chosen bits and compare the results. If the number of disagreements is bigger than a given boundary they must abort the protocol and start over. The boundary is determined by the information reconciliation and privacy amplification algorithms that they can perform.

3.2 Spaces Free of Decoherence

A very common way to implement the cryptography protocol described above is to use the transmission of polarized single photons. This implementation requires that Alice and Bob have aligned their reference frames, so that they can agree on the orientation of a given state of polarization. The lack of alignment between the two parties is equivalent to a collective random rotation over the qubits in the channel, a kind of global decoherence.

The idea of decoherence-free subspaces was developed to circumvent this kind of problem. One can envisage a logical qubit, encoded in a multi-qubit system, with the appropriate symmetry properties so that the state is invariant under the decoherence process. In the case of rotation-noise or lack of alignment it is interesting to find a logical qubit that is rotationally invariant.

The proposal in [38] makes use of two degrees of freedom (polarization and transverse spatial mode) of the same photon, so that a single photon carries two qubits. The logical qubit states will be in fact two-qubit states. It is assumed that Alice and Bob have established a common propagation direction through which they will send photons. This is important because in the paraxial approximation both the polarization

and the transverse spatial mode of the photons are defined in the plane transverse to the propagation direction. For example, the state of linear polarization of a photon can be described by an observer as:

$$|\Psi\rangle = \cos\theta|H\rangle + \sin\theta|V\rangle \tag{3.1}$$

where θ is the polarization orientation. In a different reference frame, rotated by an angle δ from the first, the angle used to describe the same polarized photon would be $\theta + \delta$ instead of θ.

The transverse spatial mode can also be used to encode a qubit. We can use the first order HG modes as a basis that spans all the first order modes, as discussed in Section 2.2. These modes are also defined relative to their reference frame, and we can define as $|h\rangle$ the HG_{10} mode and as $|v\rangle$ the HG_{01}, which is equivalent to the HG_{10} after a 90° rotation. The state of a photon in a HG mode oriented at an angle θ is given by:

$$|\psi\rangle = \cos\theta|h\rangle + \sin\theta|v\rangle \tag{3.2}$$

and similarly to the polarization, the angle used to describe this state will change if the observer is in a rotated reference frame. In our notation, the upper case letters designate polarization states and lower case letters designate transverse mode states.

Now we can define the logical qubit, combining the two degrees of freedom described above. We have seen that a rotated reference frame will have the same effect over both physical qubits. This is further guaranteed by the the fact that these two qubits can be encoded in the same photon, so there is no distance between them. The computational logical basis is defined as:

$$\left\{|0_L\rangle = \frac{|0\rangle|1\rangle - |1\rangle|0\rangle}{\sqrt{2}}, |1_L\rangle = \frac{|0\rangle|0\rangle + |1\rangle|1\rangle}{\sqrt{2}}\right\} \tag{3.3}$$

If we identify the horizontal states $|H\rangle$ and $|h\rangle$ with the $|0\rangle$ state in the Bloch sphere, and consequently the states $|V\rangle$ and $|v\rangle$ with the $|1\rangle$, then a rotation around the propagation direction by an angle θ would be equivalent to a rotation $R^y(2\theta)$ around the y axis on the Bloch sphere:

$$\begin{aligned} R^y(2\theta)|0\rangle &= \cos\theta|0\rangle + \sin\theta|1\rangle \\ R^y(2\theta)|1\rangle &= \cos\theta|1\rangle - \sin\theta|0\rangle \end{aligned} \tag{3.4}$$

All states in the subspace generated by the basis in (3.3) are invariant under arbitrary bilateral rotations of the type $R^y(2\theta) \otimes R^y(2\theta)$.

3.3 Alignment-free BB84

In order to establish a perfect shared reference frame it is necessary to exchange an infinite amount of information [41, 42]. It is clear that a protocol which does not depend on this would be valuable.

Our scheme uses the logical states defined in (3.3), with the two qubits being the polarization and the transverse spatial mode of the same photon. We also need another logical basis, $\{|+_L\rangle, |-_L\rangle\}$, to complete the protocol, analogously to what was outlined in Section 3.1. These states are also eigenstates of $R^y(\theta) \otimes R^y(\theta)$, so the entire protocol is fault tolerant, since it occurs within the logical subspace. The protocol is implemented in a "plug-and-play" configuration: Bob prepares $|0_L\rangle$ as the initial state, sends it to Alice, who encodes the information by transforming it into one of the four possible states and then returns it to Bob. We chose this kind of setup because it is technically simpler and it also makes the no-reference aspect more clear.

In Figure 3.1(a) we show a logical quantum circuit that describes the implementation of the protocol. The upper wire of the circuit represents the polarization qubit and the lower represents the transverse mode. In the first box, Bob prepares the logical state $|0_L\rangle$ by performing a controlled-not (CNOT) over the product state $|-\rangle|v\rangle$. It is shown in [38] that a rotation over the logical space $R^y_L(\theta)$ is equivalent to perform a rotation $R^y(\theta)$ over the first qubit and do nothing with the second. So, in the second box, Alice performs a rotation over the polarization qubit, thus rotating the logical qubit. The angle θ of this rotation determines which logical qubit she encodes. Finally, Bob chooses in which basis he will perform the measurement. This is done by choosing the angle ϕ of a rotation over the polarization qubit, then performing a CNOT gate and a Hadamard rotation on the polarization. The final measurement is always in the H/V basis, hence the rotation before the measurement to select the basis.

Figure 3.1(b) shows the experimental setup. We used a He-Ne laser with a wavelength of 632,8 nm and a holographic mask described in Section 2.3 to produce the first order HG mode $|v\rangle$. To complete the preparation of the initial state of the quantum circuit, we use a polarizing beam splitter (PBS) oriented at $-45°$, so the polarization transmitted is $|-\rangle$. The next step is the CNOT gate, which is implemented by a Mach-Zender (MZ) interferometer. The control qubit is the polarization, so each path of the interferometer corresponds to a different polarization, $|H\rangle$ or $|V\rangle$. In the V-path,

there is a Dove prism (DP), always oriented at 45°, that transforms the HG-mode of the photons as $|v\rangle \rightarrow |h\rangle$ and $|h\rangle \rightarrow |v\rangle$. In the H-path, nothing happens, as expected from a CNOT gate. After the recombination of the two polarization components in the last PBS, the state that exits the MZ is the $|0_L\rangle$. The relative phase between the two components is controlled by the piezoelectric translator (PZT) attached to one of the mirrors, and is kept at zero. A nonzero phase changes the effect of the CNOT, generating a state outside the logical subspace. The phase can be monitored at an auxiliary detector M, before the beam is attenuated to the single photon regime, without affecting the protocol.

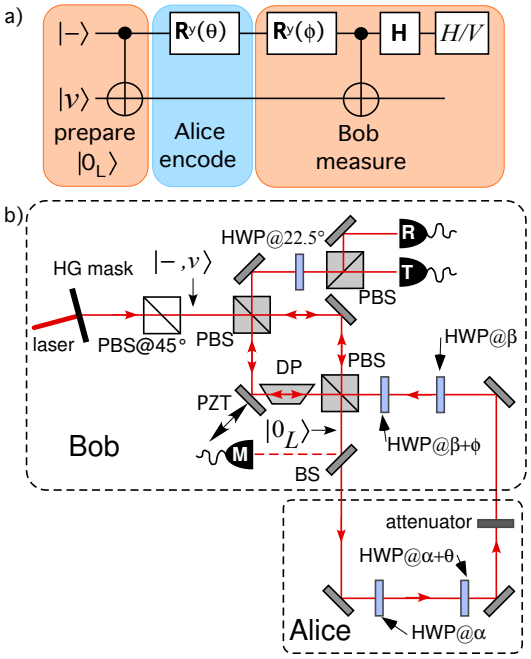

Figure 3.1: (a) Quantum circuit illustration of the BB84 protocol with logical states. The upper wire represents the polarization and the lower wire the transverse mode of the same photon. (b) Setup of the experiment. α and β are the angles of Alice's and Bob's reference frames. M is a detector used for monitoring the phase of Bob's interferometer.

After this preparation, Bob can send the photon in state $|0_L\rangle$ to Alice. Alice's "encoding-station" consist of only two half wave plates (HWP), one oriented at an angle α and the other at $\alpha + \theta$. Even though one wave plate can change the polarization of the photon, it requires two to make a real rotation operator. We can describe in matrix

notation the action of a single HWP oriented at angle α. In this notation we have

$$|H\rangle = \begin{pmatrix} 1 \\ 0 \end{pmatrix}, \; |V\rangle = \begin{pmatrix} 0 \\ 1 \end{pmatrix} \tag{3.5}$$

and

$$HWP(\alpha) = \begin{pmatrix} \cos 2\alpha & \sin 2\alpha \\ \sin 2\alpha & -\cos 2\alpha \end{pmatrix}. \tag{3.6}$$

Two consecutive HWPs at angles α and $\alpha + \theta$ give

$$HWP(\alpha + \theta)HWP(\alpha) = \begin{pmatrix} \cos 2\theta & -\sin 2\theta \\ \sin 2\theta & \cos 2\theta \end{pmatrix} \tag{3.7}$$

which is equivalent to the rotation $R^y(4\theta)$ over the polarization qubit, and equivalently a $R^y_L(4\theta)$ rotation on the logical subspace. So, the two HWPs can transform the state $|0_L\rangle$ into $|0_L\rangle$, $|1_L\rangle$, $|+_L\rangle = (|0_L\rangle + |1_L\rangle)/\sqrt{2}$ or $|-_L\rangle = (|0_L\rangle - |1_L\rangle)/\sqrt{2}$ if the relative angle between them is $\theta = 0°, 45°, 22.5°$ or $-22.5°$. Note that since the rotation depends only on the angle θ, the angle α is free to vary. In fact, if we change the angle α we are rotating the two HWPs together, simulating a change in the reference frame of Alice's laboratory. This will be useful in the final discussion.

After the encoding stage it is imperative to maintain the security of the transmission, so at this point there should be an attenuator to guarantee that each bit will be carried by single photons. After the transmission, Bob receives the state and must choose either the $0_L/1_L$ or the $+_L/-_L$ basis to perform the measurement. The choice is represented by the angle ϕ, which is the relative angle between two HWPs in Bob's laboratory. If $\phi = 0°$ the measurement is performed in the $0_L/1_L$ basis, which is the standard basis of the setup. In order to change basis Bob must make $\phi = 22.5°$, thus performing the logical rotation $R^y_L(4\phi)$, and mapping the $+_L/-_L$ states into the $0_L/1_L$ ones. Again, there is a free angle parameter β that determines the orientation of Bob's HWPs, and can thus be used to rotate Bob's reference frame.

The measure itself consists of a CNOT gate with the polarization qubit being the control, and a Hadamard rotation. The CNOT gate is the same as the one used in the preparation, so Bob can in fact use the same setup going in the opposite sense through the unused entrance and exit ports of the MZ interferometer. However, in this sense, the DP is in the H-path, so the effect of the MZ is equivalent to a $X_p\text{CNOT}X_p$

logical operation, where X_p is the first Pauli operator acting on the polarization qubit. Applying the $X_p\text{CNOT}X_p$ transforms the states as

$$|0_L\rangle \rightarrow \frac{(|H\rangle - |V\rangle)}{\sqrt{2}}|h\rangle = |-\rangle|h\rangle, \tag{3.8}$$

$$|1_L\rangle \rightarrow \frac{(|H\rangle + |V\rangle)}{\sqrt{2}}|v\rangle = |+\rangle|v\rangle. \tag{3.9}$$

These two states can be distinguished by polarization measurements performed using a HWP oriented at 22.5° and a PBS. The HWP acts as the Hadamard rotation in the logical circuit. With this mapping, detector R will register $|0_L\rangle$ and detector T will register $|1_L\rangle$.

First we look at the results assuming that Alice's and Bob's laboratory angles are the same ($\alpha = \beta = 0°$) and then we show that the results do not depend on the laboratory orientation. We have always used an intense laser, but attenuation to the single-photon regime is straightforward and was already mentioned in the setup description.

Figure 3.2 shows the images taken with a charge-coupled-device (CCD) camera of the intensity profiles that appear at positions R and T. In Figure 3.2(a) are the results for $\beta = 0°$ and $\phi = 0°$, which means that Bob is measuring in the $0_L/1_L$ basis. We can see that when Alice sends either states $|0_L\rangle$ or $|1_L\rangle$, Bob detects light in just one detector, with good visibility. When Alice sends the $|\pm_L\rangle$ states, then both detectors are illuminated with similar intensities. This split between the two detectors is necessary for the security of the BB84 protocol. Similarly, when Bob chooses $\phi = 22,5°$, he is measuring in the $+_L/-_L$ basis, so he can distinguish the $|\pm_L\rangle$ states and no longer the $|0_L\rangle$ and $|1_L\rangle$ states, as we can see in Figure 3.2(b). In both Figure 3.2(a) and Figure 3.2(b) the measurement is repeated while the angle of Alice's station is rotated by $\alpha = \{0°, 30°, 60°, 90°\}$, changing the relative orientation between the two laboratories. The images show that the measurement results are independent of this rotation.

To achieve a more quantitative proof of the independency on the relative angle, we measured the intensities at positions R and T with an optical power meter. In Figure 3.3 we can see the intensities in detectors R and T as a function of the angle α when Alice sends the state $|0_L\rangle$, for the two measurement basis. In all cases, the intensity remains nearly constant while α is varied. We can also see that there is a small probability (~ 0.068) that Bob gets the wrong result even if he chooses the right basis. This is mostly due to errors in the alignment of the interferometer.

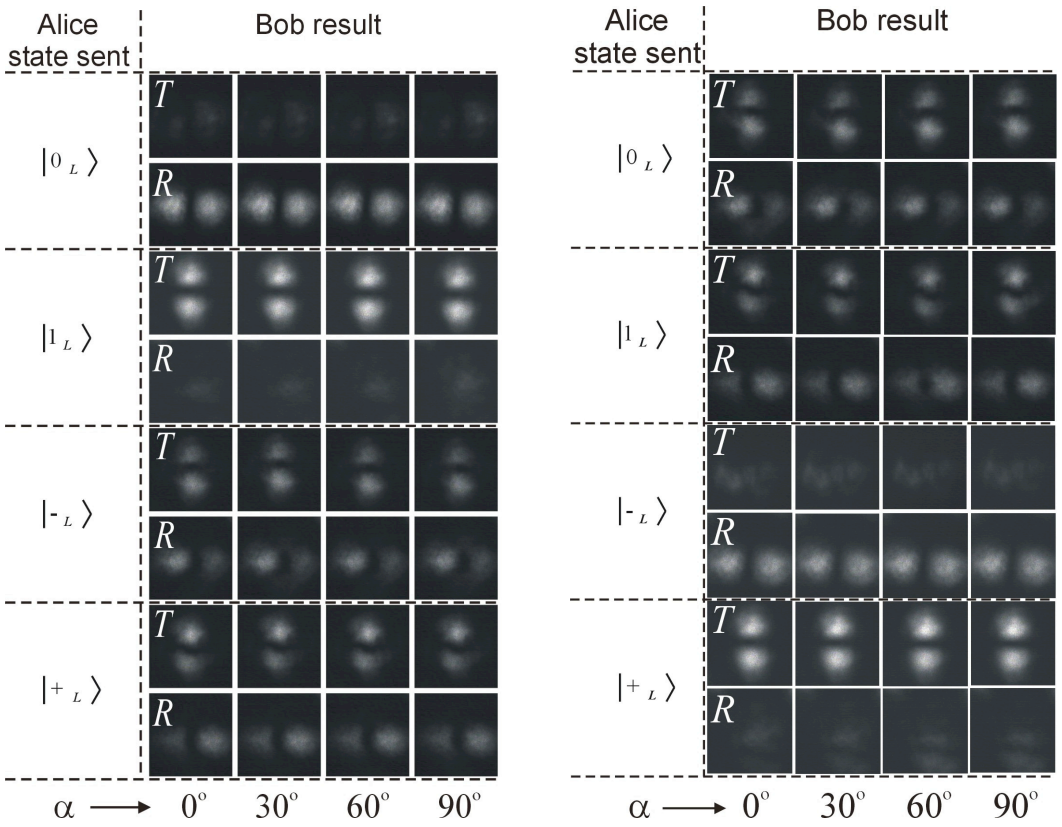

(a) Images from a CCD camera at detection positions R and T when Bob measures in the $0_L/1_L$ logical basis and Alice's laboratory frame is rotated by $\alpha = 0°, 30°, 60°$, and $90°$.

(b) Images from a CCD camera at detection positions R and T when Bob measures in the $+_L/-_L$ logical basis and Alice's laboratory frame is rotated by $\alpha = 0°, 30°, 60°$, and $90°$.

Figure 3.2: Image results

Alice's participation on the protocol consists only of a $R^y(\theta)$ operator, which depends only on the relative angle θ between her two half wave plates and is thus independent of the orientation angle α of Alice's station. However, the equivalence between the physical $R^y(\theta)$ operator on the first qubit and the logical operator $R_L^y(\theta)$ is a trait of the logical basis defined in Eq. 3.3. Thus, the "alignment-free" aspect of the experiment relies in the logical encoding. It is interesting to note that a similar plug-and-play experiment (where Bob takes care of the preparation and measurement, and Alice just rotates the state) using only photon polarization would allow the implementation of a reference-free BB84 scheme, provided that Bob prepares and measures the photons relative to the same reference frame. The logical states defined in Eq. 3.3, on the other

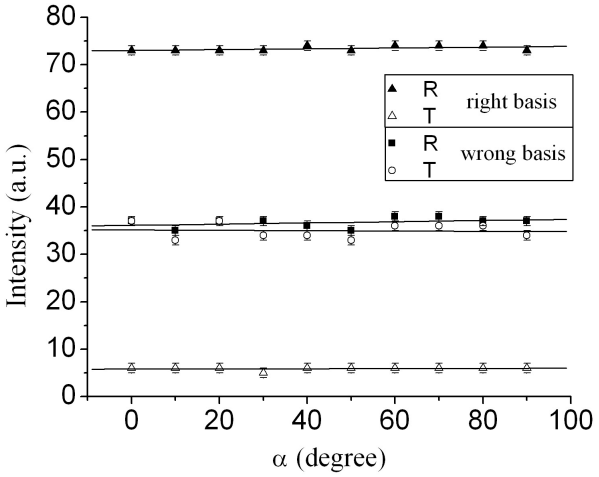

Figure 3.3: Intensity measured with a power meter as a function of Alice's laboratory angle α. Solid lines are linear curve fits.

hand, are invariant even for different preparation and measurement reference frames, and even if the state suffers undesired rotations during propagation.

As in the usual BB84 protocol, an eavesdropper Eve can attempt many different types of attacks. Considering some of the possible eavesdropping strategies particular to our protocol we see that, since each photon is in a polarization-mode entangled state, no information is available if Eve measures only the polarization or transverse mode of the photons. Also, any operation which removes the state from the logical subspace defined by $|0\rangle_L$ and $|1\rangle_L$ will produce errors in the key string and will be detected by Alice and Bob in the error-check procedure. The only advantageous strategies available to Eve are those that are analogous to the usual BB84 attacks, such as intercept-resend or cloning, for which the allowable quantum bit error rates for secure communication are well-known [43].

4

Spin-Orbit Bell Inequality

In this chapter we will first introduce and make a brief review on Bell inequalities. Later we discuss the analogy between the usual quantum mechanical context of Bell inequalities and our classical spin-orbit counterpart. Our spin-orbit inequality can show the non-separability of the spin-orbit degrees of freedom of a *classical* laser beam. We make use of the definition of separable and non-separable spin-orbit modes presented in Section 2.2. Afterwards we discuss our experimental setup and results for the measurement of such an inequality [44].

4.1 Introduction to Bell's inequalities

The concept of Bell's inequalities has its roots in the famous Einstein-Podolsky-Rosen (EPR) Gedanken experiment [4, 45]. In this paper, the authors point out a "spooky action at a distance" in Einstein words, that would arise according to the predictions of Quantum Mechanics (QM). They were in fact evidencing for the first time the strange properties of entangled states. At the time of the EPR paper QM was still being questioned, and the possibility of a different theory obeying local realism had to be tested. Since then there have been several experiments that confirm QM's predictions, and they do so through the violation of Bell's inequalities [7, 46, 47]. Currently, the interest in this subject is no longer to confirm QM (although there are still loopholes to close [48]), but to use Bell's inequalities as a tool to investigate new physical systems and establish their possibilities in the realm of Quantum Information.

In the following we will draw an outline of the derivation of Bell's theorem, and consequently of Bell's inequalities in the CHSH form [5, 6, 49]. We must start with EPR-Bohm's gedankenexperiment [50], that will be presented here in an optical form: we have a source that emits two photons in different directions. Each photon will go through a polarization analyzer followed by two detectors. The measurement for each photon has then two possible outcomes, $+1$ or -1, representing two orthogonal polarizations. Suppose that the polarizations state of the two photons is:

$$|\Psi\rangle = \frac{1}{\sqrt{2}}(|HH\rangle + |VV\rangle) \tag{4.1}$$

and we will denote by a and b the orientations of the two analyzers.

It is a simple matter to derive QM's predictions for the probabilities of single detections $P_{\pm}(a)$ and $P_{\pm}(b)$ and for the joint detections $P_{\pm\pm}(a,b)$ in any set of analyzer orientations a and b. We have:

$$\begin{aligned} P_{+}(a) = P_{-}(a) = \frac{1}{2} \\ P_{+}(b) = P_{-}(b) = \frac{1}{2} \end{aligned} \tag{4.2}$$

and

$$\begin{aligned} P_{++}(a,b) = P_{--}(a,b) = \frac{1}{2}\cos^2(b-a) \\ P_{+-}(a,b) = P_{-+}(a,b) = \frac{1}{2}\cos^2(b-a) \end{aligned} \tag{4.3}$$

Now we can build a correlation coefficient using these probabilities:

$$M(a,b) = P_{++}(a,b) + P_{--}(a,b) - P_{+-}(a,b) - P_{-+}(a,b) \tag{4.4}$$

and using QM's predictions we have

$$M_{QM}(a,b) = \cos[2(b-a)] \tag{4.5}$$

So we can see that even though the single detection probabilities give us a completely random set of results, the two measurements can be very correlated, depending on the relative orientation. For the case where $a = b$, the correlation is perfect and $M_{QM} = 1$. Einstein believed that the probabilistic nature of QM was in fact a lack of information in the theory. So he proposed that there should be a Local Supplementary Parameters

Theory that could predict with 100% of certainty the result of a measurement, if all the variables of the problem are known. Bell's inequalities were designed to test if such a Local Supplementary Parameters Theory was possible. Bell explicitly introduced supplementary parameters and with the locality assumption he derived results from such a theory.

We can represent the result of each measurement by a bi-valued function:

$$\begin{aligned} A(\lambda, a) &= \pm 1 \\ B(\lambda, b) &= \pm 1 \end{aligned} \tag{4.6}$$

that depend on the analyzer orientation and the supplementary parameter λ. We assume that the variable λ has a probability distribution over the emitted photons given by $\rho(\lambda)$. The correlation function has then the form:

$$M(a, b) = \int d\lambda \rho(\lambda) A(\lambda, a) B(\lambda, b). \tag{4.7}$$

Now consider the quantity

$$\begin{aligned} s(\lambda, a, a', b, b') &= A(\lambda, a)B(\lambda, b) - A(\lambda, a)B(\lambda, b') \\ &+ A(\lambda, a')B(\lambda, b) + A(\lambda, a')B(\lambda, b') \\ &= A(\lambda, a)[B(\lambda, b) - B(\lambda, b')] + A(\lambda, a')[B(\lambda, b) + B(\lambda, b')]. \end{aligned} \tag{4.8}$$

Considering all the sixteen possible combinations of values for $A(\lambda, a)$, $A(\lambda, a')$, $B(\lambda, b)$ and $B(\lambda, b')$, we can see that

$$s(\lambda, a, a', b, b') = \pm 2. \tag{4.9}$$

so, taking the average of $s(\lambda, a, a', b, b')$ over all the values of λ, we get

$$\begin{aligned} S(a, a', b, b') &= \int d\lambda \rho(\lambda) s(\lambda, a, a', b, b') \\ &= M(a, b) - M(a, b') + M(a', b) + M(a', b') \end{aligned} \tag{4.10}$$

and

$$-2 \leq S(a, a', b, b') \leq 2 \tag{4.11}$$

We can conclude that, if there is a variable (or set of variables) λ, unknown to QM, that can determine the results of all the measurements, then the quantity $S(a, a', b, b')$

is limited by (4.11). This form of inequality is the generalization of Bell's inequalities made by Clauser, Horne, Shimony and Holt [6].

For some sets of the orientation parameters a, a', b, b', QM's predictions violate the inequality above, thus conflicting with the Local Supplementary Parameters Theory. We are left to conclude that QM is a nonlocal theory.

The next step is to test the inequality experimentally. The first experiment to faithfully reproduce the proposal of EPR and successfully obtain a violation was done by Aspect *et al* [7] using the correlations in polarization of pairs of photons emitted in a radiative cascade. It is interesting to look for the set of orientations a, a', b, b' that allows for the maximal violation of the inequality. It can be shown that to obtain the extreme values of S_{QM}:

$$b - a = a' - b = b' - a' = \theta \tag{4.12}$$

and

$$\begin{aligned} \theta &= \pm\frac{\pi}{8} \quad \text{for} \quad S_{QM} = 2\sqrt{2} \\ \theta &= \pm\frac{3\pi}{8} \quad \text{for} \quad S_{QM} = -2\sqrt{2} \end{aligned} \tag{4.13}$$

The important quantities here are the relative angles, which are depicted in Figure 4.1.

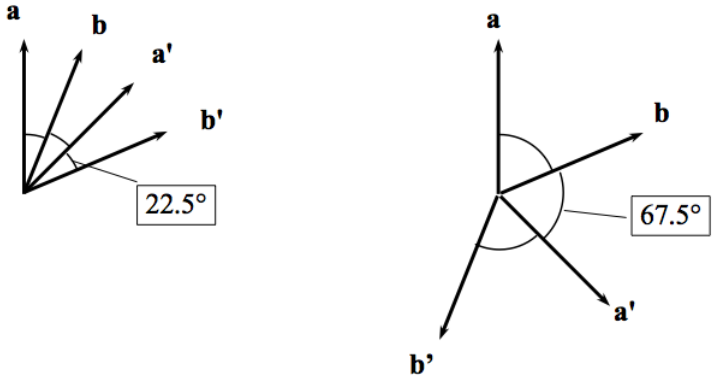

Figure 4.1: Relative orientations to maximize the value of S_{QM} and obtain maximum violation of Bell's inequalities

Once the violation is obtained there are some points to discuss. First we should interpret this result, and we can do that by looking at the assumptions necessary to derive the inequality:

- distant correlations can be understood with the introduction of the parameter λ that carries information necessary to the outcome of measurements.
- the functions $A(\lambda)$, $B(\lambda)$, and $\rho(\lambda)$ obey the locality condition, i.e. the function that decides the outcome of the detector of one of the parties cannot depend on the choice of orientation of the polarizer of the other party, since they are spatially separated.

So we can conclude that QM presents a kind of non-locality. One could think that this means that QM allows for faster than light communication, but in fact it doesn't, and causality is maintained [51].

4.2 The Spin-Orbit Inequality

The majority of proposed experiments to violate Bell's inequalities relies on a *pair* of entangled quantum particles, so the particles can be sent far away from each other, and the violation becomes a genuine non-locality test [52].

Entanglement in *single* particle degrees of freedom has already been investigated in [53], where a Bell-like inequality was violated by entangling the spin and the beam path of single neutrons in an interferometer. The same kind of single particle scheme has been proposed for photonic setups using the polarization and transverse (spin-orbit) modes [54]. Simulations of Bell-inequalities in classical optics have also been discussed in waveguides [55] and imaging systems [56]. The ability to produce and transform beams carrying orbital angular momentum has allowed for the development of important techniques with potential applications to quantum information [39, 57]. We have proposed and experimentally tested a setup to investigate the spin-orbit separability of a laser beam [44], which will be presented in this Chapter.

Following ref. [25] and Section 2.2, we make use of the definition of separable and non-separable modes. The separable modes are those that can be written in the form $\mathbf{E}_S(\mathbf{r}) = \psi(\mathbf{r})\boldsymbol{\epsilon}$, where $\psi(\mathbf{r})$ is a normalized c-number function of the transverse spatial coordinates (transverse mode) and $\boldsymbol{\epsilon}$ is a normalized polarization vector.

A criteria for the separability of the spin-orbit modes was also defined in Section 2.2. Let us take the arbitrary spin-orbit mode:

$$\mathbf{E}(\mathbf{r}) \;=\; A_1\psi_v(\mathbf{r})\boldsymbol{\epsilon}_V + A_2\psi_v(\mathbf{r})\boldsymbol{\epsilon}_H + A_3\psi_h(\mathbf{r})\boldsymbol{\epsilon}_V + A_4\psi_h(\mathbf{r})\boldsymbol{\epsilon}_H, \qquad (4.14)$$

for which $C = 2|A_2A_3 - A_1A_4|$, where A_i $(i = 1 \ ... \ 4)$ are complex numbers satisfying $\sum_{i=1}^{4} |A_i|^2 = 1$. For non-separable modes $0 < C \leq 1$, $C = 1$ corresponds to a maximally non-separable mode and $C = 0$ corresponds to a separable mode.

To develop the spin-orbit inequality we will use the rotated basis defined in (2.15):

$$\begin{aligned} \boldsymbol{\epsilon}_{\alpha+} &= \boldsymbol{\epsilon}_H \cos\alpha + \boldsymbol{\epsilon}_V \sin\alpha \ , \\ \boldsymbol{\epsilon}_{\alpha-} &= -\boldsymbol{\epsilon}_H \sin\alpha + \boldsymbol{\epsilon}_V \cos\alpha \ , \\ \psi_{\beta+}(\mathbf{r}) &= \psi_h(\mathbf{r}) \cos\beta + \psi_v(\mathbf{r}) \sin\beta \ , \\ \psi_{\beta-}(\mathbf{r}) &= -\psi_h(\mathbf{r}) \sin\beta + \psi_v(\mathbf{r}) \cos\beta \ , \end{aligned} \tag{4.15}$$

Consider the following normalized mode

$$\mathbf{E}_{MNS}(\mathbf{r}) = \frac{1}{\sqrt{2}} \left[\psi_v(\mathbf{r})\boldsymbol{\epsilon}_V + \psi_h(\mathbf{r})\boldsymbol{\epsilon}_H\right] . \tag{4.16}$$

Re-writing this maximally non-separable mode in the rotated basis we get:

$$\begin{aligned} \mathbf{E}_{MNS}(\mathbf{r}) &= \frac{1}{\sqrt{2}} \{\cos[(\beta-\alpha)](\psi_{\beta+}(\mathbf{r})\boldsymbol{\epsilon}_{\alpha+} + \psi_{\beta-}(\mathbf{r})\boldsymbol{\epsilon}_{\alpha-}) \\ &+ \sin[(\beta-\alpha)](\psi_{\beta-}(\mathbf{r})\boldsymbol{\epsilon}_{\alpha+} - \psi_{\beta+}(\mathbf{r})\boldsymbol{\epsilon}_{\alpha-})\} \ . \end{aligned} \tag{4.17}$$

Let $I_{(\pm)(\pm)}(\alpha,\beta)$ be the squared amplitude of the $\psi_{\beta(\pm)}(\mathbf{r})\boldsymbol{\epsilon}_{\alpha(\pm)}$ component in the expansion of $\mathbf{E}_{MNS}(\mathbf{r})$ in the rotated basis. They play the same role as the detection probabilities (4.3) in the quantum mechanical context. Due to the orthonormality of $\{\psi_{\beta+}, \psi_{\beta-}\}$ and $\{\boldsymbol{\epsilon}_{\alpha+}, \boldsymbol{\epsilon}_{\alpha-}\}$ it can be easily shown that:

$$I_{++}(\alpha,\beta) + I_{+-}(\alpha,\beta) + I_{-+}(\alpha,\beta) + I_{--}(\alpha,\beta) = 1 \ . \tag{4.18}$$

Following the analogy with the usual quantum mechanical CHSH [6] inequality for spin 1/2 particles, we can define

$$M(\alpha,\beta) = I_{++}(\alpha,\beta) + I_{--}(\alpha,\beta) - I_{+-}(\alpha,\beta) - I_{-+}(\alpha,\beta) = \cos[2(\beta-\alpha)] \ , \tag{4.19}$$

and derive a Bell-type inequality for the quantity

$$S = M(\alpha_1,\beta_1) + M(\alpha_1,\beta_2) - M(\alpha_2,\beta_1) + M(\alpha_2,\beta_2) \ . \tag{4.20}$$

For any separable mode, the quantity S is limited as $-2 \leqslant S \leqslant 2$. This is to be expected because having well defined states of polarization and transverse mode is

equivalent to the Local Realism condition over quantum variables, since the results of the measurements are pre-determined even if you don't know them, and the choice of basis for one variable will never interfere with the other. However this condition can be violated for non-separable modes. A maximal violation of the previous inequality, corresponding to $S = 2\sqrt{2}$, can be obtained for the set $\alpha_1 = \pi/8\,,\ \alpha_2 = 3\pi/8\,,\ \beta_1 = 0\,,\ \beta_2 = \pi/4$ as discussed in Section 4.1.

4.3 The MZIM

In the two-photon experiment outlined in Section 4.1 there are two measurements of the same kind of physical property, i.e., polarization of two different photons. In our case the two degrees of freedom are of different nature, requiring a different apparatus. So, in order to measure the proposed quantity S (4.20) we needed a "transverse mode polarizing beam splitter (PBS)" and a "transverse mode half wave plate (HWP)". The second is quite easily achieved, consisting of a Dove prism (DP), but the first is less simple.

We achieved our goal with the apparatus proposed in [58], which consists of a Mach-Zender interferometer with an additional mirror (MZIM), as depicted in Figure 4.2.

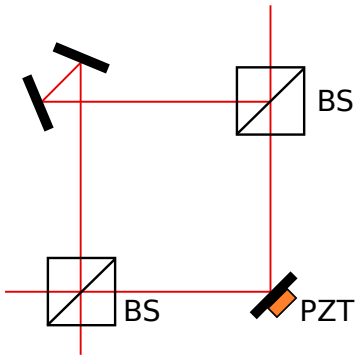

Figure 4.2: Mach-Zender interferometer with an additional mirror (MZIM) and a piezo-electric transducer (PZT) in one mirror to control the relative phase.

The MZIM functioning is based on the parity of the modes. Parity is evaluated according to the eigenvalue of the respective mode under reflection over the horizontal plane. Each reflection gives a π phase to the odd modes and no phase to the even

modes, thus decomposing the incident beam into even and odd components. In our case of interest, the odd modes of the basis are $\psi_h(\mathbf{r})\boldsymbol{\epsilon}_V$ and $\psi_v(\mathbf{r})\boldsymbol{\epsilon}_H$ and the even are $\psi_h(\mathbf{r})\boldsymbol{\epsilon}_H$ and $\psi_v(\mathbf{r})\boldsymbol{\epsilon}_V$. If we place a PBS at each exit of the MZIM, we can sort all four modes of the basis and measure their intensities separately.

4.4 The Bell Measurement

The experimental setup to observe maximal violation of the non-separability inequality (4.20) is shown in Figure 4.3 and is composed by two stages: preparation of the

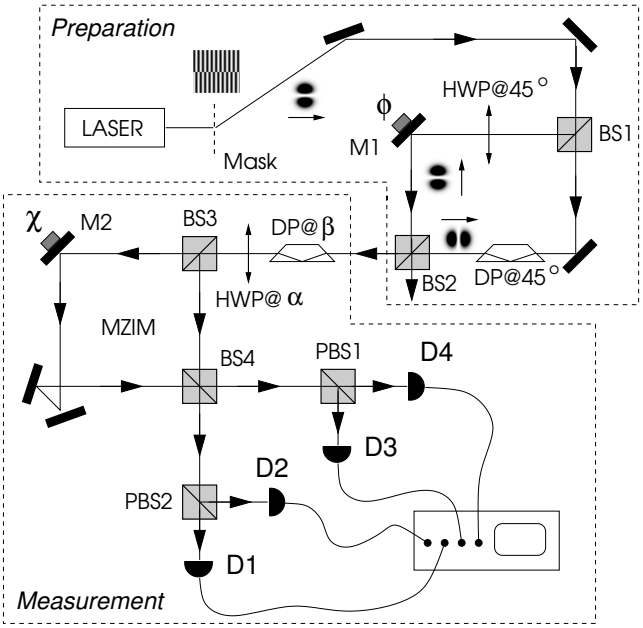

Figure 4.3: Experimental setup for the Bell-type inequality violation using a non-separable classical beam. HWP - half-wave plate, DP - Dove prism, (P)BS - (polarizing) beam splitter, D1, D2, D3, and D4 - photo-current detectors.

maximally non-separable mode and measurement of the intensities $I_{(\pm)(\pm)}(\alpha, \beta)$.

4.4.1 Preparation of the MNS mode

The preparation stage consists of a Mach-Zender (MZ) interferometer with a half-wave plate (HWP@45°) oriented at 45° with respect to the horizontal plane in one arm and a Dove prism (DP@45°) also oriented at 45° with respect to the horizontal plane in

the other arm. Before the MZ interferometer, the horizontally polarized TEM_{00} beam from a high stability laser (Lightwave 142H-532-400SF) at 532nm passes through a holographic mask [31, 59, 60] and produces mode $\mathbf{E}(\mathbf{r}) = \psi_v(\mathbf{r})\boldsymbol{\epsilon}_H$ at the first diffraction order. In the MZ interferometer, the half-wave plate converts $\boldsymbol{\epsilon}_H$ into $\boldsymbol{\epsilon}_V$ and the Dove prism changes $\psi_v(\mathbf{r})$ into $\psi_h(\mathbf{r})$ so the resulting mode at the output BS2 is:

$$\mathbf{E}(\mathbf{r}) = \frac{1}{\sqrt{2}}\left[\psi_h(\mathbf{r})\boldsymbol{\epsilon}_H + e^{i\phi}\psi_v(\mathbf{r})\boldsymbol{\epsilon}_V\right] , \tag{4.21}$$

where ϕ is the phase difference between the two arms of the MZ interferometer. Mirror M1 is mounted on a piezoelectric transducer (PZT) to allow fine control of the phase difference ϕ. The other output of BS2 is used to check the alignment between the two components of the mode prepared.

4.4.2 Measurement

The measurement stage is composed by a Dove prism oriented at a variable angle $\beta/2$ (DP@$\beta/2$), a half-wave plate oriented at a variable angle $\alpha/2$ (HWP@$\alpha/2$), a Mach-Zender interferometer with an additional mirror (MZIM) [58], and one polarizing beam splitter (PBS) after each of the MZIM outputs. Four photo-current detectors (D1, D2, D3 and D4) are used to measure the intensities at the PBS outputs. HWP@$\alpha/2$ combined with DP@$\beta/2$ define in which basis we are going to measure our initial mode.

We want MZIM to work as a parity selector delivering odd modes $\psi_v(\mathbf{r})\boldsymbol{\epsilon}_H$ and $\psi_h(\mathbf{r})\boldsymbol{\epsilon}_V$ in one port and even modes $\psi_v(\mathbf{r})\boldsymbol{\epsilon}_V$ and $\psi_h(\mathbf{r})\boldsymbol{\epsilon}_H$ in the other port. Let χ be the optical phase difference between the two arms of the MZIM. Note that proper functioning of the MZIM as a parity selector occurs only when $\chi = 2n\pi$ ($n = 0, 1, 2,...$). For $\chi = (2n+1)\pi$, the even and odd outputs are interchanged.

After propagating through DP@$\beta/2$ and through HWP@$\alpha/2$, the maximally non-separable mode given by Eq. (4.16) transforms to:

$$\mathbf{E}'(\mathbf{r}) = A_e^+(\phi)\psi_v(\mathbf{r})\boldsymbol{\epsilon}_V + A_o^-(\phi)\psi_v(\mathbf{r})\boldsymbol{\epsilon}_H + A_o^+(\phi)\psi_h(\mathbf{r})\boldsymbol{\epsilon}_V + A_e^-(\phi)\psi_h(\mathbf{r})\boldsymbol{\epsilon}_H, \tag{4.22}$$

where

$$\begin{aligned} A_e^{\pm}(\phi) &= e^{i\phi/2}\{\cos(\phi/2)\cos[(\beta-\alpha)] \pm i\sin(\phi/2)\cos[(\beta+\alpha)]\} , \\ A_o^{\pm}(\phi) &= e^{i\phi/2}\{\pm\cos(\phi/2)\sin[(\beta-\alpha)] + i\sin(\phi/2)\sin[(\beta+\alpha)]\} . \end{aligned} \tag{4.23}$$

If MZIM phase $\chi = 0$, then the four amplitudes above would be the ones measured by the detectors since MZIM interferometer together with PBS1 and PBS2 would separate the modes $\psi_v(\mathbf{r})\boldsymbol{\epsilon}_V$, $\psi_v(\mathbf{r})\boldsymbol{\epsilon}_H$, $\psi_h(\mathbf{r})\boldsymbol{\epsilon}_V$ and $\psi_h(\mathbf{r})\boldsymbol{\epsilon}_H$. But we will still consider the case in which χ may differ from zero, and then the corresponding intensities normalized to the total intensity are given by:

$$\begin{aligned} I_1 = I_2 &= \cos^2\left(\frac{\chi}{2}\right)|A_e^{\pm}(\phi)|^2 + \sin^2\left(\frac{\chi}{2}\right)|A_o^{\pm}(\phi)|^2, \\ I_3 = I_4 &= \sin^2\left(\frac{\chi}{2}\right)|A_e^{\pm}(\phi)|^2 + \cos^2\left(\frac{\chi}{2}\right)|A_o^{\pm}(\phi)|^2. \end{aligned} \tag{4.24}$$

We can test the violation of the non-separability inequality by making measurements in the bases (α_1, β_1), (α_1, β_2), (α_2, β_1) and (α_2, β_2) and obtaining the values of $M(\alpha, \beta)$ and subsequently S. The value of S for arbitrary ϕ and χ is given by:

$$S(\chi, \phi) = 2\sqrt{2}\,\cos\chi\cos^2(\phi/2)\,. \tag{4.25}$$

Thus maximal violation of the non-separability inequality is accomplished for $\phi = \chi = 0$. This is a key result because it shows that experimental errors in the phases will only diminish the violation, not increase it.

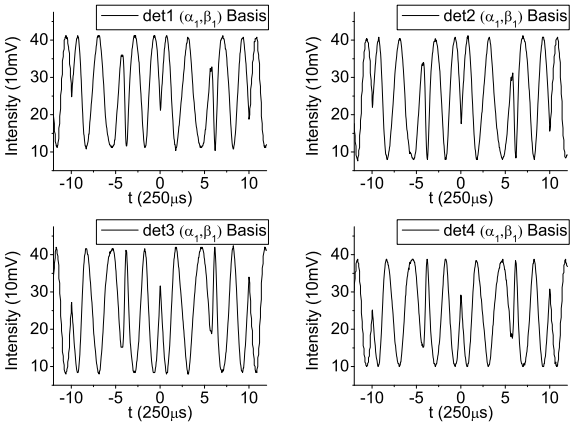

Figure 4.4: Experimental results for the maximally non-separable initial mode, measured in the (α_1, β_1) basis. Time parameterizes the MZIM phase χ.

In our experiment the MZIM phase χ is continuously varied by applying a voltage ramp to the PZT on M2 while intensities I_1 through I_4 are monitored at the oscilloscope.

Table 4.1: Mean values for M and S for maximally non-separable and separable modes.

	Maximally Non Separable	Separable
$\overline{M}(\alpha_1, \beta_1)$	0.609 ± 0.006	0.490 ± 0.008
$\overline{M}(\alpha_1, \beta_2)$	0.486 ± 0.009	0.000 ± 0.005
$\overline{M}(\alpha_2, \beta_1)$	-0.522 ± 0.004	-0.56 ± 0.01
$\overline{M}(\alpha_2, \beta_2)$	0.482 ± 0.009	0.000 ± 0.004
$\overline{S}$	2.10 ± 0.03	1.05 ± 0.03

An example of our experimental results is presented in Fig. 4.4, showing the oscillations caused by the variation of χ. We know from the intensities dependence on ϕ and χ that $\chi = 0$ corresponds to the peaks in the graphics, and $\phi = 0$ corresponds to a maximal visibility of these oscillations. Since we have repetitions of these peaks, we obtain an ensemble of intensities which allows us to calculate the averages and standard deviations of $M(\alpha, \beta)$ and S. For this end, we take thirty points distributed over the ten peaks measured. This procedure is repeated for all four bases and the results are shown in Table 4.1. The value of S obtained for the MNS mode is 2.10 ± 0.03, which violates the inequality by 3.3 standard deviations. In this table we also show our experimental results for a separable mode $\psi_V(\mathbf{r})\boldsymbol{\epsilon}_V$, which is easily obtained by blocking the Dove Prism arm of the preparation MZ interferometer.

4.5 The Inequality for the Quantized Modes

To describe our experiment in a complete quantum mechanical frame, we must take into account all possible inputs, and describe the evolution of the field operators inside the apparatus. In our notation, the mode amplitudes that enter the interferometer are $\hat{a}^i_{\sigma\lambda}$ where the index i represents the input, σ stands for polarization and λ for transverse mode. In Fig. 4.5 the input and output modes are indicated in the sketch of the measurement setup.

The output mode amplitude $\hat{b}^j_{\mu\nu}$ is a combination of the input amplitudes with coefficients $u^{i\sigma\lambda}_{j\mu\nu}$. Therefore, the field amplitude $\hat{\mathbf{E}}_j$ at output j is

$$\hat{\mathbf{E}}_j = \sum_{\mu,\nu} \hat{b}^j_{\mu\nu} \boldsymbol{\epsilon}_\mu \psi_\nu e^{i\vec{k_j}\cdot\vec{r}}, \tag{4.26}$$

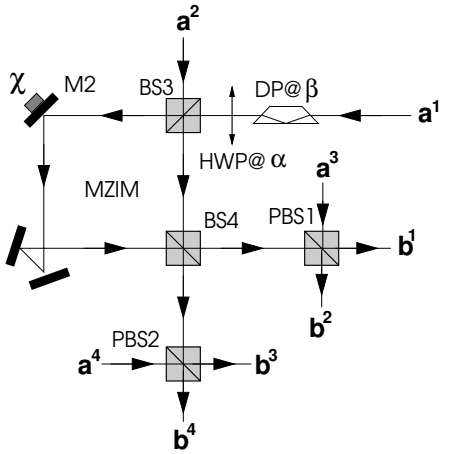

Figure 4.5: Input and output modes of the measurement apparatus.

where

$$\hat{b}^j_{\mu\nu} = \sum_{i,\sigma,\lambda} u^{i\sigma\lambda}_{j\mu\nu} \hat{a}^i_{\sigma\lambda}. \tag{4.27}$$

Since the intensities are expectation values calculated in normal ordering, all input modes in the vacuum state ($\hat{a}^1_{hV}$, $\hat{a}^1_{vH}$, $\hat{a}^2_{\sigma\lambda}$, $\hat{a}^3_{\sigma\lambda}$, and $\hat{a}^4_{\sigma\lambda}$) will not contribute. Assuming that MZIM is set for proper functioning ($\chi = 0$), the only occupied output modes are:

$$\begin{aligned}
\hat{b}^1_{hH} &= \cos\alpha \cos\beta \, \hat{a}^1_{hH} + \sin\alpha \sin\beta \, \hat{a}^1_{vV} \, , \\
\hat{b}^2_{vV} &= \sin\alpha \sin\beta \, \hat{a}^1_{hH} + \cos\alpha \cos\beta \, \hat{a}^1_{vV} \, , \\
\hat{b}^3_{vH} &= \sin\alpha \cos\beta \, \hat{a}^1_{hH} - \cos\alpha \sin\beta \, \hat{a}^1_{vV} \, , \\
\hat{b}^4_{hV} &= \cos\alpha \sin\beta \, \hat{a}^1_{hH} - \sin\alpha \cos\beta \, \hat{a}^1_{vV} \, .
\end{aligned} \tag{4.28}$$

The only nonzero contributions to the normalized detected intensities $I_j = \langle \hat{\mathbf{E}}^\dagger_j \cdot \hat{\mathbf{E}}_j \rangle / I_0$ are:

$$\begin{aligned}
I_1 &= \langle \hat{b}^{1\dagger}_{hH} \hat{b}^1_{hH} \rangle / I_0 \, , \\
I_2 &= \langle \hat{b}^{2\dagger}_{vV} \hat{b}^2_{vV} \rangle / I_0 \, , \\
I_3 &= \langle \hat{b}^{3\dagger}_{vH} \hat{b}^3_{vH} \rangle / I_0 \, , \\
I_4 &= \langle \hat{b}^{4\dagger}_{hV} \hat{b}^4_{hV} \rangle / I_0 \, ,
\end{aligned} \tag{4.29}$$

where $I_0 = \sum_{j=1}^4 \langle \hat{\mathbf{E}}^\dagger_j \cdot \hat{\mathbf{E}}_j \rangle$.

To evaluate the inequality, according to the CHSH prescription, we calculate $M(\alpha,\beta) = I_1 + I_2 - I_3 - I_4$ for the four bases and S as given by Eq. (4.20). With the description of the inequality above, we can calculate the theoretical value of S for different input quantum states.

4.5.1 Coherent state

For measurements made within its coherence length, the laser source can be described by a coherent state, so we use a coherent state to represent the intense laser beam prepared in the maximally non-separable mode

$$|\nu\rangle_{MNS} = e^{\frac{-|\nu|^2}{2}} \sum_{n=0}^{\infty} \frac{\nu^n (a^\dagger_{MNS})^n}{n!} |0\rangle \ , \tag{4.30}$$

where $a^\dagger_{MNS}$ is the creation operator associated with the MNS mode. Using the Bell basis notation (2.18), this particular MNS mode can be represented by the Φ^+ mode, so $a^\dagger_{MNS} \equiv a^\dagger_{\Phi^+}$. Its action on the vacuum state $|0\rangle$ produces a one-photon Fock state in the Φ^+ mode. Since this mode is decomposed as in Eq. (4.16), its corresponding creation operator can be written as $a^\dagger_{\Phi^+} = (a^\dagger_{vV} + a^\dagger_{hH})/\sqrt{2}$, where the first index corresponds to the transverse mode and the second to the polarization mode. Following the calculations of Eq. (2.26) we can show that

$$|\nu\rangle_{MNS} = |\nu/\sqrt{2}\rangle_{vV} |\nu/\sqrt{2}\rangle_{hH} \ , \tag{4.31}$$

which is the product of coherent states at modes $\psi_h(\mathbf{r})\boldsymbol{\epsilon}_H$ and $\psi_v(\mathbf{r})\boldsymbol{\epsilon}_V$ with complex amplitude $\nu/\sqrt{2}$. We can use this state to calculate the mean values of Eq. (4.29), knowing that the complex amplitude $\nu = \sqrt{I_0}$, where I_0 is the total initial intensity of the laser. The results are in the equations below:

$$\begin{aligned} I_1 = I_2 &= \frac{1}{2}\cos^2(\beta - \alpha) \, , \\ I_3 = I_4 &= \frac{1}{2}\sin^2(\beta - \alpha) \, . \end{aligned} \tag{4.32}$$

They give $S = 2\sqrt{2}$ for the same choice of bases used in the experiment, showing maximal violation for the two-mode coherent state. Since this state is a tensor product, this violation cannot be attributed to entanglement. In fact, we will see that this violation is closely related to optical coherence when we investigate the statistical mixture case.

Performing the Fock state decomposition of $|\nu\rangle_{MNS}$, analogous to what is done in Eq. (2.26), we have:

$$|\nu\rangle_{MNS} = e^{\frac{-|\nu|^2}{2}}[|0\rangle + \frac{\nu}{\sqrt{2}}(|1_{hH}0_{vV}\rangle + |0_{hH}1_{vV}\rangle) + ...] \tag{4.33}$$

As expected, we find that the single photon component is maximally entangled. Therefore, post-selection of single photon states from $|\nu\rangle_{MNS}$ followed by the experimental setup used here allows one to investigate the usual Bell inequality from probability measurements.

4.5.2 Single photon Fock state

Let us now assume the input mode prepared in a single photon state $\hat{a}^{\dagger}_{MNS}|0\rangle = \frac{1}{\sqrt{2}}(|1_{hH}0_{vV}\rangle + |0_{hH}1_{vV}\rangle)$. As we already mentioned, this state is clearly entangled. In this regime, the intensity measurements translate to photocounts associated with the detection probabilities in each output port of the measurement device. These probabilities violate the CHSH inequality and one is left in the traditional framework of Bell's experiments, in this case for the spin-orbit degrees of freedom of single photons [61]. The detection probabilities are proportional to the mean values of the intensity operator in each output port and they are easily calculated to be the same as the normalized intensity values shown in Eq. (4.32), obviously giving the same value $S = 2\sqrt{2}$.

4.5.3 Statistical Mixture

It is interesting to investigate the spin-orbit separability for a statistical mixture of two coherent states like

$$\rho = \frac{1}{2}(|\nu/2, 0\rangle\langle\nu/2, 0| + |0, \nu/2\rangle\langle 0, \nu/2|) \tag{4.34}$$

where the first and second slots in the kets correspond to the hH and vV mode respectively. Such statistical mixture can model two independent lasers (random relative phase) prepared in modes hH and vV, and combined in a beam splitter. The results for the intensity calculations of Eq. (4.29) are shown below:

$$\begin{aligned} I_1 = I_2 &= \frac{1}{2}(\cos^2\alpha\,\cos^2\beta + \sin^2\alpha\,\sin^2\beta)\,, \\ I_3 = I_4 &= \frac{1}{2}(\sin^2\alpha\,\cos^2\beta + \cos^2\alpha\,\sin^2\beta)\,. \end{aligned} \tag{4.35}$$

For the bases used in the experiment, they give $S = \sqrt{2}$ which does not violate the separability inequality. This shows that optical coherence plays an important role, so that no violation would be obtained if the modes were incoherently combined.

The notion of separable and non-separable spin-orbit modes in classical optics builds an useful analogy with entangled quantum states, allowing for the study of some of their important mathematical properties. This analogy has already been successfully exploited in our group to investigate the topological nature of the phase evolution of an entangled state under local unitary operations [25]. Many quantum computing tasks require entanglement but do not need nonlocality, so that using different degrees of freedom of single particles can be useful. This is the type of entanglement whose properties can be studied in the classical optical regime allowing one to replace time-consuming measurements based on photon count by the much more efficient measurement of photocurrents.

Although helpful, the notion of mode non-separability must not be confused with genuine quantum entanglement. The discussion around Eq. (4.31) is intended to avoid this confusion. On the other hand, its Fock state decomposition shows that the single photon component exhibits entanglement that can be accessed through post-selection.

5

Bell Inequality with Angular Correlations

As discussed in Section 4.1, the gedankenexperiment in the seminal EPR paper dealt with continuous variables (CV) q and p, but this original proposition was for some time neglected in favor of the discretized versions of the problem, such as the implementation with polarized photons, which benefitted from better detection efficiencies. In the realm of discrete variables several Bell-type inequalities have been proposed, studied and tested up to now. Each Bell-type inequality is suitable for revealing the non-local nature of quantum mechanics in a different type of quantum system: bipartite two-level systems [6, 62], bipartite discrete many level systems [63, 64, 65], multipartite systems [66, 67] and also CV systems [68, 69, 70, 71].

The first attempts to build CV non-locality tests consisted on finding ways to discretize the continuum to reuse concepts developed for the discrete case. It was shown in [69] that dichotomizing the phase space according to a state's parity and its displacement in phase space can lead to Bell type inequalities that can be violated by gaussian continuous variable entangled states. Other phase space dichotomizations are possible, as the one proposed in [72]. However, dichotomization does not correspond to a genuine CV measurement, since it provides an observable with a discrete, rather than a truly continuous spectrum. It is understood now that CV setups can provide advantages such as higher intensity signals, which could help to solve the detection loophole [73]. Most of these works are based on canonical unbounded variables, as (q, p). They can correspond, for instance, to the sum and the difference of two quadratures of the

electromagnetic field [45, 74, 75].

Sufficient inseparability criterion for CV based on variance inequalities, involving EPR–like operators pairs, have been proposed by L. Duan et al. [76] and experimentally tested [77].The Peres-Horodecki [78, 79] separability condition based on the positivity of the partial transpose of a separable density matrix has been applied to CV systems [80, 81]. Reid and co-workers [82] proposed variance based Bell-type inequalities which can be applied to discrete or continuous variables without demanding dichotomization. Their proposal is suitable for multipartite systems, and cannot be applied to bipartite ones. In order to derive their variance based inequalities, they ingeniously combine observables that can be easily measured for optical fields, for instance, to create other observables with mathematical properties revealing non-locality in a simple way. Other variance based inequalities can be found in [82, 83, 84]. Another possible approach are entropy based inequalities that may be advantageous to detect entanglement in non-gaussian states, since they go beyond the usual criteria that use second-order moments [85, 86].

In this chapter we will discuss a theoretical proposal for Bell inequalities in bipartite CV systems [87]. Up to now, most of the results on CV entanglement and non locality have been devoted to the case of canonical variables with an unbounded spectrum, as position and momentum. In this work, we consider a different type of CV. We deal with two quantum systems, A and B, characterized by angular variables $\theta_i \in [-\pi, \pi[$, $i = A, B$ on a circle, instead of a position q in the full real line. The variable θ can represent different things, as we can apply the resulting inequality for a variety of physical systems. For instance, θ can be the position of a particle on a circle, a rotator on a plane (for example, molecules confined to a plane [88]), or the polar angle locating the photon field in the plane transverse to its propagation, as illustrated in Fig. 5.1. Our ideas can also be applied to reveal non-locality in a system of particles diffusing on a one dimensional lattice (for example, an optical lattice) with period L. In that case, we can define an angular variable related to the particle position q as $\theta = \frac{2\pi q}{L}$, and the particle position could be the observable to be measured [89].

The main result presented here is the derivation of Bell-like inequalities which are genuinely continuous, and do not make use of dichotomization or phase space partitions. The particularity of the measured observables used here is that they present a

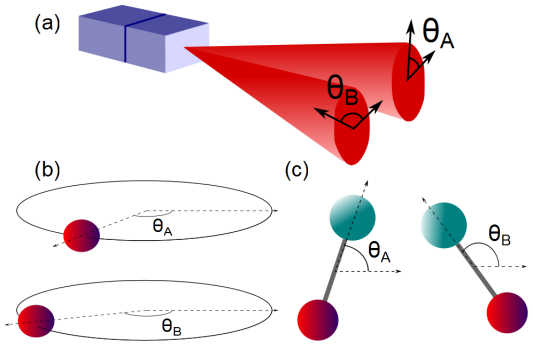

Figure 5.1: Examples of physical systems for which our results can be applied: (a) The transverse profile of a propagating light beam (b) Particles moving on a circle (as charged particles in an electromagnetic trap) (c) rigid rotators confined to two dimensional motion.

bounded spectrum, so that one can derive CHSH-type inequalities for them.The inequality consists on correlated measurements of continuous, real and periodic angular functions $f_i(\theta_i)$ $(i = A, B)$. As we will show, the derived inequalities share similarities to CHSH-like ones as their general form is given by a properly balanced continuous superposition of CHSH-type inequalities. Exploiting the possibility of revealing non locality using angular measurements is an approach that can be particularly useful and suitable for a number of physical systems in atomic and molecular physics, photonics and mesoscopic systems in condensed matter physics.

5.1 Theoretical model

As a starting point, we recall the CHSH inequalities for a bipartite two-level system presented in Section 4.1. We can write it in a simple form as $|\langle B(a, a', b, b')\rangle| \leq 2$, with:

$$B(a, a', b, b') = \sigma_a \otimes \sigma_b + \sigma_a \otimes \sigma_{b'} + \sigma_{a'} \otimes \sigma_b - \sigma_{a'} \otimes \sigma_{b'} \tag{5.1}$$

where σ_α is the Pauli matrix in the direction α of the tridimensional space. a and a' refer to different directions of the spin projection of subsystem A while b and b' are associated to subsystem B. The inequality $|\langle B(a, a', b, b')\rangle| \leq 2$ is fulfilled in the framework of local hidden variable (LHV) theories. The fact that there exist quantum states violating

these inequalities disproof quantum mechanics as a local or EPR realistic theory. For quantum mechanical systems, (5.1) is bounded by the Tsirelson bound of $2\sqrt{2}$ [90].

We now consider a different situation of measurement providing continuous and 2π-periodic outcomes. In other words, the underlying Hilbert space is the square integrable 2π-periodic functions space. Such functions can be spanned by the basis $\{|m_i\rangle; m_i \in \mathbb{Z}\}$, which are angular momentum eigenstates: $J_z|m_i\rangle = m_i|m_i\rangle$, where $J_z = -i\hbar\frac{\partial}{\partial\theta}$ is the operator that represents the z component of the total angular momentum of the beam, and $i = A, B$ indicates each of the two subsystems. An alternative continuous basis is $\{|\theta_i\rangle; \theta_i \in [-\pi, \pi[\}$, and it can be obtained from the $|m_i\rangle$ basis by Fourier transform:

$$\langle m_i|\theta_i\rangle = \frac{1}{\sqrt{2\pi}} e^{im_i\theta_i}. \tag{5.2}$$

In this representation, a local observable for each party can be written as

$$F_i = \int_{-\pi}^{\pi} d\theta_i f_i(\theta_i)|\theta_i\rangle\langle\theta_i|, \tag{5.3}$$

with $f_i(\theta_i)$ real, bounded and periodic.

Our guidelines to obtain continuous variables Bell inequalities is to build a CHSH [6] Bell–operator similar to the one given by (5.1), but based on the correlated measurements of an observable F_i for each particle. It is clear that, under the assumption that the spectra of F_i are bounded, this property is preserved by every unitary transformation $U_i(\phi_i)$ such that

$$F(\phi_i) = U_i(\phi_i)F_iU_i^{\dagger}(\phi_i). \tag{5.4}$$

It is also straightforward to show that, for an LHV theory, we have [91]:

$$\begin{aligned} \left|\langle\mathcal{B}(\phi_a, \phi'_a, \phi_b, \phi'_b)\rangle\right| &= \left|\big\langle F_A(\phi_a)\otimes F_B(\phi_b) + F_A(\phi'_a)\otimes F_B(\phi_b)\right. \\ &+ \left. F_A(\phi_a)\otimes F_B(\phi'_b) - F_A(\phi'_a)\otimes F_B(\phi'_b)\big\rangle\right| \leq 2, \end{aligned} \tag{5.5}$$

if the maximum value of $f_i(\theta_i)$ is normalized to 1. What are the conditions the functions $f_i(\theta_i)$ and the transformed operators $F_i(\phi_i)$ should satisfy to violate (5.5) and allow for non-locality and entanglement tests? In order to answer this question, we focus on $f_i(\theta_i) = \cos(\theta_i)$ which is a function that can be measured on a variety of physical systems. The results derived in the following can be straightforwardly generalized to all 2π periodic functions such that $f(\theta) = -f(\theta - \pi)\ \forall\theta \in [0, \pi]$.

5.2 Example of application: the cosine operator

The observables $C = F_i$ corresponding to $f_i(\theta_i) = \cos(\theta_i)$, can be expressed on the $|m\rangle$ basis as:

$$C = \sum_{m\in\mathbb{Z}} \frac{1}{2} \left(|m+1\rangle\langle m| + |m\rangle\langle m+1| \right). \tag{5.6}$$

Indeed,

$$\langle m'|C|m\rangle = \frac{1}{2\pi} \int_{-\pi}^{\pi} e^{-im'\theta} \frac{e^{i\theta} + e^{-i\theta}}{2} e^{im\theta} \mathrm{d}\theta = \frac{1}{2} \left[\delta_{m',m+1} + \delta_{m',m-1} \right]. \tag{5.7}$$

For a particle rotating on a circle in the xy plane, the operator C corresponds to the projection on the x axis of the particle position; it can also be related to the spatial orientation of a two dimensional rotor, or to the phase of a superconducting circuit. Operator C has a spectrum of doubly degenerated eigenstates $|\theta\rangle$ and $|-\theta\rangle$, both with eigenvalue $\cos\theta$. For this operator, we can define an equivalent to the rotation of a spin 1/2 system: it is the unitary operator $e^{iJ_z^2\phi}$, (that is, the free evolution operator during a time $t = 2\hbar\phi$, for a free particle with unit mass and angular momentum J_z, constrained to move on an unit circle). From C, we can define $C(\phi_i) \equiv F_i(\phi_i)$ as:

$$C(\phi) = e^{iJ_z^2\phi} C e^{-iJ_z^2\phi} = \frac{1}{2} \sum_{m\in\mathbb{Z}} e^{i(2m+1)\phi} |m\rangle\langle m+1| + e^{-i(2m+1)\phi} |m+1\rangle\langle m|, \tag{5.8}$$

and for a bipartite system (particles A and B) the Bell operator (5.5) reads:

$$\begin{aligned} \mathcal{B}(\phi_a, \phi'_a, \phi_b, \phi'_b) = {} & C_A(\phi_a) \otimes C_B(\phi_b) + C_A(\phi'_a) \otimes C_B(\phi_b) \\ & + C_A(\phi_a) \otimes C_B(\phi'_b) - C_A(\phi'_a) \otimes C_B(\phi'_b), \end{aligned} \tag{5.9}$$

where $C_{A(B)}(\phi)$ are operators defined as in Eq. (5.8) acting on the Hilbert space of particle $A(B)$. The spectrum of $C(\phi)$ does not depend on ϕ. Diagonalizing $C(\phi)$ shows that its spectrum is bounded, with $|\langle C\rangle| \leq 1$. Thus, for an LHV theory, $|\langle \mathcal{B}(\phi_a, \phi'_a, \phi_b, \phi'_b)\rangle| < 2$ holds. However, for some set of phases ϕ_is and some quantum states, this inequality is violated. In order to show that, we calculate the spectra of $\mathcal{B}(\phi_a, \phi'_a, \phi_b, \phi'_b)$ operators. Actually, such spectra depend only on the relative phases $\phi_a - \phi'_a$ and $\phi_b - \phi'_b$ [92, 93]. We can define

$$\begin{aligned} B(\xi_a, \xi_b) = B(\phi'_a - \phi_a, \phi'_b - \phi_b) \equiv \mathcal{B}(0, \phi'_a - \phi_a, 0, \phi'_b - \phi_b) = \\ e^{iJ_{Az}^2\phi_a} \otimes e^{iJ_{Bz}^2\phi_b} \mathcal{B}(\phi_a, \phi'_a, \phi_b, \phi'_b) e^{-iJ_{Az}^2\phi_a} \otimes e^{-iJ_{Bz}^2\phi_b}. \end{aligned} \tag{5.10}$$

$B(\xi_a, \xi_b)$ and $\mathcal{B}(\phi_a, \phi'_a, \phi_b, \phi'_b)$ are related by a unitary transformation. Therefore, the variation of only the two phases (ξ_a, ξ_b) is enough to explore the spectrum of all the $\mathcal{B}(\phi_a, \phi'_a, \phi_b, \phi'_b)$.

5.2.1 Finite dimension space

As a first approach to the study of the dependence of operators $B(\xi_a, \xi_b)$ with the phases ξ_i , we discretize the possible outcomes of the correlation measurements. This step gives us intuition on the properties of the Bell operator proposed because it allows numerical computations to be performed. For such, we consider that the measured quantum states lie on a $2M + 1$ finite dimension space generated by the basis set $\{|m\rangle; m \in \mathbb{Z}, |m| \leq M\}$. We thus define the projection $C^{(M)}(\xi)$ of the $C(\xi)$ operator on this reduced space as :

$$C^{(M)}(\xi) = \frac{1}{2} \sum_{|m| \leq M} e^{i(2m+1)\xi} |m\rangle\langle m+1| + e^{-i(2m+1)\xi} |m+1\rangle\langle m| \tag{5.11}$$

and $C^{(M)} = C^{(M)}(0)$.

Working in this reduced subspace gives insight on the continuous case that is explored later. The $2M + 1$ eigenstates $|\lambda_k\rangle$ of $C^{(M)}$ can be computed explicitly :

$$|\lambda_k\rangle = \sum_{m=-M}^{M} c_m^k |m\rangle, \tag{5.12}$$

with

$$c_m^k = \frac{\sin\left[\frac{(M-m+1)k\pi}{2(M+1)}\right]}{\sqrt{M+1}} \tag{5.13}$$

where each index $k = 1, 2, \cdots, 2M + 1$ refers to one of the eigenvectors of C, with eigenvalue $\lambda_k = \cos\left[\frac{k\pi}{2(M+1)}\right]$. We can see that $k = 1$ corresponds to the maximum eigenvalue and $k = 2M + 1$ to the minimum one. Also, the spectrum of C is anti-symmetric with respect to the middle eigenvalue ($\lambda_{M+1} = 0$), i.e. $\lambda_k = -\lambda_{2(M+1)-k}$.

We now make the correspondence $|\lambda_1\rangle \equiv |\lambda_{\max}\rangle$ and $|\lambda_{2M+1}\rangle = |-\lambda_{\max}\rangle \equiv |\lambda_{\min}\rangle$ and call these states *maximally oriented states*. The angular distribution $P_k(\theta) = |\langle\theta|\lambda_k\rangle|^2$ as a function of the polar angle θ for these two states are shown in Fig. 5.2 for $M = 2$ and $M = 5$. We can see that maximally oriented states, even for relatively low values of M, present an angular distribution in the transverse plane very concentrated in

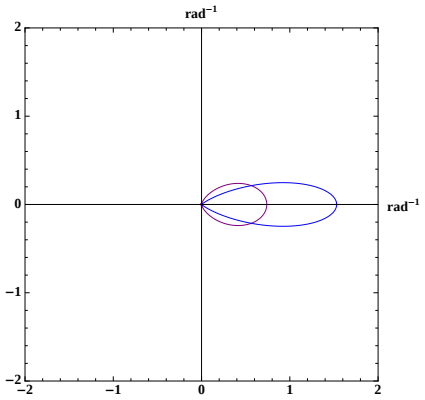

Figure 5.2: Plot of angular distribution $P_k(\theta) = |\langle\theta|\lambda_k\rangle|^2$ parameterized by the polar angle θ, for $M = 2$ in purple and $M = 5$ in blue.

one direction (around $\theta = 0$ for $|\lambda_{\max}\rangle$ and around $\theta = \pi$ for $|\lambda_{\min}\rangle$). These maximally oriented states are suitable for a semi-classical analogy with spin-states.

Using that $-\lambda_{\max} \leq \langle C_i^{(M)}(\xi_i)\rangle \leq \lambda_{\max}$ with $i = A, B$, it is easy to show that, for separable states,

$$|\langle B^{(M)}(\xi_A, \xi_B)\rangle_{\text{sep}}| \leq 2\lambda_{\max}^2, \tag{5.14}$$

which constitutes a Bell inequality with a threshold that depends on the dimension of the considered subspace (the value of M) and is equal to 2 in the continuous limit ($M \to \infty$). We have defined $B^{(M)}$ the discretized Bell operator defined as in Eq.(5.10) but with $C^{(M)}(\xi)$ instead of $C(\xi)$ operators.

Discretization allows to explicitly compute the $2M + 1$ eigenstates and corresponding eigenvalues of $C^{(M)}$, providing a more intuitive physical image of the considered operators. Also, it enables the numerical study of the spectrum of $B^{(M)}(\xi_a, \xi_b)$ and its phase dependence. Defining $b_{\max}^{(M)}(\xi_a, \xi_a)$ as the highest eigenvalue of $B^{(M)}(\xi_a, \xi_b)$ we see in Fig. 5.3 that, for $M = 2$ and $M = 5$, $b_{\max}^{(M)}(\xi_a, \xi_a)$ reaches its maximum at $\xi_a = \xi_b = \pi/2$. We verified numerically that this fact is independent of M for $1 \leq M \leq 20$. In addition, $|b(\pi/2, \pi/2)|$ increases as M increases, being already greater than 2 (i.e., enabling the Bell-type inequality violation) for $M = 2$. Thus, for all M, it is possible for non-separable and non-local states to violate the Bell inequality (5.9) in the restricted subspace. We thus conclude that our discretized Bell operator acts as an entanglement witness [94, 95] for bipartite $2M + 1$ levels systems, since

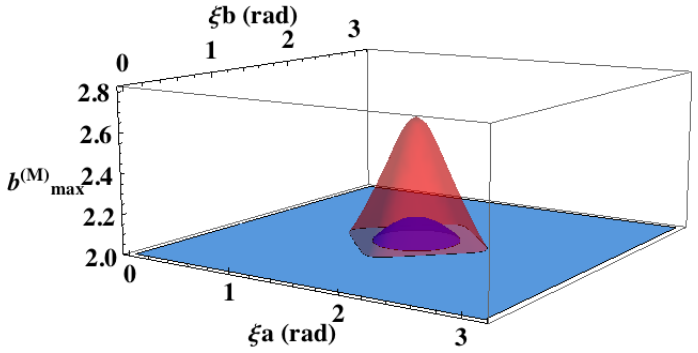

Figure 5.3: Plot of the maximum eigenvalue of $B^{(M)}(\xi_a, \xi_b)$, $b^{(M)}_{\max}$, in the region of violation ($b^{(M)}_{\max} > 2$) as a function of ξ_a and ξ_b for $M = 2$ (inner blue plot), and $M = 5$ (outer red plot).

$\mathrm{Tr}(B^{(M)}\rho_{AB}) > 2\lambda^2_{\max}$ only if ρ_{AB} is an entangled state.

The study of the discretized operators shows us that the point $\xi_a = \xi_b = \pi/2$ is the one that provides the highest contrast between $b_{\max}(\xi_a, \xi_a)$ and the violation threshold value of 2. This property is expected to be valid for all values of M and consequently, also in the continuous case.

5.2.2 Continuous variables

We now move to the study of the continuous variable case, where the operators have a continuous spectrum, which is our main purpose. We focus in the points $\xi_a = \xi_b = \pi/2$ to optimize the contrast of the violation and search for the corresponding non local states that violate the inequality for this choice of phases. It is now convenient to define the following operators :

$$\begin{aligned} \sigma^x(\theta) &= |\theta\rangle\langle\overline{\theta}| + |\overline{\theta}\rangle\langle\theta| \\ \sigma^y(\theta) &= i\left(|\overline{\theta}\rangle\langle\theta| - |\theta\rangle\langle\overline{\theta}|\right) \\ \sigma^z(\theta) &= |\theta\rangle\langle\theta| - |\overline{\theta}\rangle\langle\overline{\theta}|, \end{aligned} \tag{5.15}$$

for $\theta \in [0, \pi[$ and with $\overline{\theta} \equiv \theta - \pi$. These operators constitute an orthogonal continuous set of Pauli-like operators, and they fulfill relations analog to the usual Pauli matrices,

including orthogonality:

$$\sigma^j(\theta)\sigma^k(\theta') = i\sigma^l(\theta)\delta(\theta-\theta'), \tag{5.16}$$

$$\sigma^j(\theta)\sigma^j(\theta') = \delta(\theta-\theta')(|\theta\rangle\langle\theta| + |\overline{\theta}\rangle\langle\overline{\theta}|), \tag{5.17}$$

where (j,k,l) denotes circular permutations of (x,y,z).

With these definitions, we show in the Appendix A that the operators C and $C(\frac{\pi}{2})$, defined in Eqs. (5.6) and (5.8), can be simply written as:

$$C = \int_0^\pi \mathrm{d}\theta \cos\theta\, \sigma^z(\theta) \tag{5.18}$$

$$C\left(\frac{\pi}{2}\right) = -\int_0^\pi \mathrm{d}\theta \cos\theta \sigma^y(\theta). \tag{5.19}$$

Thus, the Bell operator $B_\mathrm{m} \equiv B(\frac{\pi}{2},\frac{\pi}{2})$ can be written as the following direct sum:

$$B_\mathrm{m} = \int_0^\pi \int_0^\pi \mathrm{d}\theta\mathrm{d}\theta' \cos\theta\cos\theta' X(\theta,\theta') \tag{5.20}$$

where

$$\begin{aligned} X(\theta,\theta') = \big[&\sigma_A^z(\theta)\otimes\sigma_B^z(\theta') - \sigma_A^y(\theta)\otimes\sigma_B^z(\theta') \\ &- \sigma_A^z(\theta)\otimes\sigma_B^y(\theta') - \sigma_A^y(\theta)\otimes\sigma_B^y(\theta')\big], \end{aligned} \tag{5.21}$$

and $\sigma_A^j(\theta)$ and $\sigma_B^j(\theta)$ $(j=x,y,z)$ are operators defined by Eqs. (5.15) on the Hilbert space of parties A and B respectively. The $X(\theta,\theta')$ operators are orthogonal:

$$\begin{aligned} &X(\theta_a,\theta_b)X(\theta'_a,\theta'_b) = 4\delta(\theta_a-\theta'_a)\delta(\theta_b-\theta'_b)\times \\ &(|\theta_a\rangle\langle\theta_a| + |\overline{\theta_a}\rangle\langle\overline{\theta_a}|)\otimes(|\theta_b\rangle\langle\theta_b| + |\overline{\theta_b}\rangle\langle\overline{\theta_b}|) \end{aligned} \tag{5.22}$$

and completely analog to the usual 2–qubits (4-dimensional) CHSH operators. We have thus the surprising result that the Bell operator B_m is the weighted continuous direct sum of 2–qubit-like CHSH Bell operators $X(\theta,\theta')$, with the weights being given by $\cos\theta\cos\theta'$. Thanks to the orthogonality property (5.22), finding the spectrum and eigenstates of B_m is a simple task, as shown in Appendix B. Indeed, for each θ and θ' it is enough to diagonalize the 4×4 matrix representing $X(\theta,\theta')$. We find that B_m can thus be written in diagonal form as:

$$B_\mathrm{m} = 2\sqrt{2}\sum_{n=\pm1} n\int_0^\pi\int_0^\pi \mathrm{d}\theta\mathrm{d}\theta' \cos\theta\cos\theta' \,|\chi^n(\theta,\theta')\rangle\langle\chi^n(\theta,\theta')| \tag{5.23}$$

where :

$$|\chi^{\pm 1}(\theta,\theta')\rangle = \frac{1}{N_\pm}[|\theta\rangle\otimes|\theta'\rangle + |\overline{\theta}\rangle\otimes|\overline{\theta'}\rangle \mp i(\sqrt{2}\mp 1)\left(|\theta\rangle\otimes|\overline{\theta'}\rangle + |\overline{\theta}\rangle\otimes|\theta'\rangle\right)] \quad (5.24)$$

are the eigenvectors of $X(\theta,\theta')$ and of $B_{\rm m}$ with non-zero eigenvalues and where $N_\pm = 2\left[(2\mp\sqrt{2})\right]^{1/2}$ is a normalization factor such that :

$$\langle\chi^{n'}(\theta'_a,\theta'_b)|\chi^{n}(\theta_a,\theta_b)\rangle = \delta_{nn'}\delta(\theta'_a-\theta_a)\delta(\theta'_b-\theta_b). \quad (5.25)$$

The same techniques could be employed for other observables connected to C and $C(\frac{\pi}{2})$ by a unitary transformation [92].

Therefore, the spectrum of $B_{\rm m}$ is continuous and equal to $[-2\sqrt{2},2\sqrt{2}]$. $|\langle B_{\rm m}\rangle|$ is thus bounded by $2\sqrt{2}$ as in the 2-qubit CHSH inequality. The extreme values $\pm 2\sqrt{2}$ cannot be exactly reached by physical states since they are composed of perfectly oriented states, namely $|0\rangle$ and $|\pi\rangle$, that correspond to delta functions in the angular representation ($\langle\theta|\theta'\rangle = \delta(\theta-\theta')$). However, they can be reached with arbitrary precision by considering localized wave packets. It is thus interesting to investigate the relation between the localization around $\theta = 0,\pi$ of the transverse profile and the violation of our Bell inequality, this is the subject of the next section.

5.2.3 States violating the Bell Inequality

In order to explicitly construct physically sound states violating our Bell inequality, we consider a continuous superposition of eigenstates $|\chi^{+1}(\theta,\theta')\rangle$, with θ and θ' localized around $\theta=\theta'=0$, the point of the maximum eigenvalue of $B_{\rm m}$. An example of such wave packet is given by:

$$|\Psi\rangle = \int_0^\pi {\rm d}\theta \int_0^\pi {\rm d}\theta' g_a(\theta)g_b(\theta')|\chi^{+1}(\theta,\theta')\rangle. \quad (5.26)$$

where $g_a(\theta)$ and $g_b(\theta)$ are normalized $L^2(]0,\pi[,d\theta)$ functions with support containing $\theta=0$. The expectation value of $B_{\rm m}$ for this state is

$$\langle B_{\rm m}\rangle_\Psi = 2\sqrt{2}\int_0^\pi {\rm d}\theta\int_0^\pi {\rm d}\theta' \cos\theta\cos\theta'|g_a(\theta)|^2|g_b(\theta')|^2 \quad (5.27)$$

The wave packet (5.26) can be produced making a linear combination of the one–particle wave packets

$$|g\rangle = \int_0^\pi {\rm d}\theta g(\theta)|\theta\rangle \text{ and } |\overline{g}\rangle = \int_0^\pi {\rm d}\theta g(\theta)|\overline{\theta}\rangle, \quad (5.28)$$

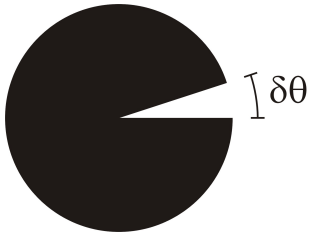

Figure 5.4: Amplitude mask with angular aperture $\delta\theta$.

taking the same coefficients of Eq. (5.24):

$$|\Psi\rangle = \frac{1}{\sqrt{2}N_+}[(|g_a\rangle \otimes |g_b\rangle + |\overline{g_a}\rangle \otimes |\overline{g_b}\rangle) - i(\sqrt{2}-1)\,(|g_a\rangle \otimes |\overline{g_b}\rangle + |\overline{g_a}\rangle \otimes |g_b\rangle)]. \quad (5.29)$$

It is useful now to obtain a simple relation between the wave packet localization and the violation of the Bell inequality. For such, we take for $g(\theta)$ the ideal case of an angular slit with aperture $\delta\theta$ as shown in Fig. 5.4, given by :

$$g_a(\theta) = g_b(\theta) = \begin{cases} \frac{1}{\sqrt{\delta\theta}} & \text{for } \theta < \delta\theta \\ 0 & \text{otherwise} \end{cases} \quad (5.30)$$

The mask can either be oriented with the slit between $\theta = 0$ and $\theta = \delta\theta$ or its symmetric with respect to the origin, between $\theta = -\pi$ and $\theta = -\pi+\delta\theta$, to create the superpositions $|g\rangle$ and $|\overline{g}\rangle$. Because of the mask shape and orientation, the sate $|\Psi\rangle$ given by Eq. (5.29), encompasses the eigenstates of $B_{\rm m}$ with eigenvalues close to $2\sqrt{2}$.

Using Eq. (5.27), the value of $\langle B_{\rm m}\rangle_\Psi$ can be written as function of the aperture $\delta\theta$ of the slit as follows:

$$\langle B_{\rm m}\rangle_\Psi = 2\sqrt{2}\left(\frac{\sin\delta\theta}{\delta\theta}\right)^2. \quad (5.31)$$

This equation above shows that we can obtain values of $\langle B_{\rm m}\rangle_\Psi > 2$, violating the Bell inequality, with an aperture of $\delta\theta < 18^\circ$ which is not a too restrictive condition. There is thus a relatively broad collection of simple two–particles non local pure states involving coherent superposition of one–particle wave packets localized around $\theta = 0$ and $\theta = \pi$ that violate the derived Bell inequality.

We now study the example of even more realistic states, which are non-pure ones, establishing some conditions for them to violate the derived Bell-type inequalities. We consider the analog of the Werner states [96, 97] :

$$\rho(\eta) = \eta\rho_A \otimes \rho_B + (1-\eta)\,|\Psi\rangle\,\langle\Psi|\,, \quad (5.32)$$

where

$$\rho_{A(B)} = \mathrm{Tr}_{B(A)}\left[|\Psi\rangle\langle\Psi|\right] = \frac{1}{2}\left(\left|g_{a(b)}\right\rangle\left\langle g_{a(b)}\right| + \left|\overline{g_{a(b)}}\right\rangle\left\langle\overline{g_{a(b)}}\right|\right), \tag{5.33}$$

with $|\Psi\rangle$ given by (5.29). As $\langle\chi^n(\theta_a,\theta_b)|\rho_A\otimes\rho_B|\chi^n(\theta_a,\theta_b)\rangle$ does not depend on $n=\pm1$ for all $\theta_a,\theta_b\in[0,\pi]$, then the contributions form $n=+1$ and $n=-1$ will cancel each other out in the sum, as we can see from the expression for B_{m} in (5.23). Consequently, $\mathrm{Tr}\left[B_{\mathrm{m}}\rho_A\otimes\rho_B\right]=0$ and the expectation of B_{m} for the state $\rho(\eta)$ is simply given by $(1-\eta)\langle B_{\mathrm{m}}\rangle_\Psi$. When g_a and g_b are given by (5.30), the maximal allowed value of the mixing coefficient η for the Bell equation to be violated is a simple function of the slit aperture :

$$\mathrm{Tr}\left[B_{\mathrm{m}}\rho(\eta)\right] > 2 \Rightarrow \eta < 1 - \frac{1}{\sqrt{2}}\left(\frac{\delta\theta}{\sin\delta\theta}\right)^2, \tag{5.34}$$

providing conditions for this type of mixed states to violate non-locality. In the next section we will give an example of how this kind of Werner state could be a source of noise in our proposed experimental setup.

5.3 Proposal of experimental implementation with photons

The inequalities derived in this chapter can be applied to measure the correlations between observables on the transverse profile of two photons. Significant experimental work has been made over spatial correlations of photons, from the first demonstrations of this kind of entanglement [98, 99], to the measurement of EPR correlations [84] between the angular position and orbital angular momentum. All of these experiments dealt with discrete variables.

In our proposal we measure the correlations between two observables with continuous spectrum, related to the azimuthal distribution of the wave front of two entangled photons. For the creation of the non local state we make use of the polarization entanglement generated in a spontaneous parametric down conversion process with two adjacent crystals, and we transfer it to the transverse profile degree of freedom.

5.3.1 Detection apparatus

To perform the measurement of the Bell operator we must be able to measure the operator $C(\phi)$ for each photon simultaneously. This can be achieved with two Mach-

Zender interferometers, one in each of the photons paths. The proposed interferometer is depicted in Figure (5.5) and consists of two Dove prisms (DP in the figure), one in each arm and one programmable spatial light modulator (SLM) in one arm. The effect of the two prisms over the state of the photon is a m dependent phase shift of $e^{i2m\phi}$ between the to arms of the interferometer, where m is the orbital angular momentum eigenvalue [35]. Another phase shift $e^{i\phi}$, independent of m, can be achieved by a simple imbalance of the lengths of the arms, controlled by a piezoelectric transducer (PZT) in one of the mirrors. The SLM is programmed to raise by one unity of angular momentum each OAM eigenstate, i.e., it acts as the operator $\sum_m |m+1\rangle\langle m| = e^{i\theta}$. This can be done using a "fork" pattern, already well explored in many experiments [31, 98].

The evolution of an input basis state $|m\rangle$ is described step by step below, where the lower path is denoted by a and the upper path by b. We also define the $|\text{vac}\rangle$ as being the vacuum state, as 1 and 2 as the output modes of the interferometer.

$$\begin{aligned}
|m\rangle \quad &\xrightarrow{\text{BS1}} \frac{1}{\sqrt{2}}\left[|m\rangle_a|\text{vac}\rangle_b + |\text{vac}\rangle_a|m\rangle_b\right] \\
&\xrightarrow{\text{DP}} \frac{1}{\sqrt{2}}\left[|m\rangle_a|\text{vac}\rangle_b + e^{i(2m+1)\phi}|\text{vac}\rangle_a|m\rangle_b\right] \\
&\xrightarrow{\text{SLM}} \frac{1}{\sqrt{2}}\left[e^{i\theta}|m\rangle_a|\text{vac}\rangle_b + e^{i(2m+1)\phi}|\text{vac}\rangle_a|m\rangle_b\right] \\
&\xrightarrow{\text{BS2}} = \frac{1}{2}[(e^{i\theta} - e^{i(2m+1)\phi})|m\rangle_1|\text{vac}\rangle_2 + (e^{i\theta} + e^{i(2m+1)\phi})|\text{vac}\rangle_1|m\rangle_2]
\end{aligned} \tag{5.35}$$

Calculating the intensities in the two output modes we get, for an arbitrary state:

$$I_1 = \frac{1}{4}\langle(e^{-i\theta} - e^{-i(2m+1)\phi})(e^{i\theta} - e^{i(2m+1)\phi})\rangle = \frac{1}{2}\langle 1 - C(\phi)\rangle \tag{5.36}$$

$$I_2 = \frac{1}{4}\langle(e^{-i\theta} + e^{-i(2m+1)\phi})(e^{i\theta} + e^{i(2m+1)\phi})\rangle = \frac{1}{2}\langle 1 + C(\phi)\rangle \tag{5.37}$$

So, the operators measured in the two planes of detection are:

$$\begin{aligned}
D_1 &= 1 + C(\phi) \\
D_2 &= 1 - C(\phi)
\end{aligned} \tag{5.38}$$

To measure the correlations $C(\phi_A, \phi_B) = \langle C_A(\phi_A) C_B(\phi_B)\rangle$ two interferometers as the one described above are needed, one for each photon. The orientation of the Dove

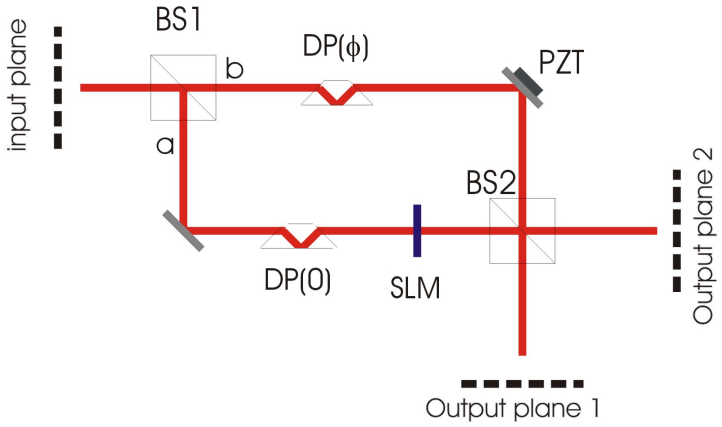

Figure 5.5: Mach-Zender interferometer designed to measure the operator $C(\phi)$. DP - Dove prism; BS - beam splitter; SLM - spatial light modulator.

prisms in each interferometer allows to change the values of the phases ϕ_A and ϕ_B. We have now four possible outputs from the pair of the interferometers, each one of them providing different intensities for the transverse plane. In order to obtain a measure of correlation between orientation operators with arbitrary values of ϕ_A and ϕ_B, such intensities must be combined as follows:

$$\langle C_A(\phi_A)C_B(\phi_B)\rangle = \frac{1}{4}\langle D_1^A D_1^B + D_2^A D_2^B - D_2^A D_1^B - D_1^A D_2^B\rangle \tag{5.39}$$

This shows that with the appropriate combinations of phases ϕ_A and ϕ_B we can perform the full measurement of the Bell operator.

5.3.2 Preparing entangled orientation states

To experimentally produce the entangled state $|\Psi\rangle$ given by Eq. (5.29), we propose a setup with non-linear crystals as a source of entangled photons, which can be manipulated afterwards to obtain the final desired state. In this subsection we explain in detail how this can be done.

Once we are able to create state $|g\rangle$ and $|\overline{g}\rangle$ using, for instance, a mask acting as suggested in Eq. 5.30, we must find a way to manipulate such states in a photon pair so as to create $|\Psi\rangle$. A reasonably simple way to manipulate photons and create entanglement is to use their polarization degree of freedom. The spontaneous parametric down

conversion process of two adjacent nonlinear crystals (type I) allows for the creation of a polarization entangled state of the form $\frac{1}{\sqrt{2}}\left[|H\rangle|H\rangle + |V\rangle|V\rangle\right]$ if they are pumped with a laser beam polarized at 45°[100]. Since entanglement in this case is created due to the ignorance regarding which crystal generated the photon pair, the other photonic degrees of freedom, as OAM, are unentangled. The total state of the photon pair, considering polarization and OAM degrees of freedom is thus

$$\frac{1}{\sqrt{2}}\left[|H\rangle_A|H\rangle_B + |V\rangle_A|V\rangle_B\right]|\Psi_o\rangle_A|\Psi_o\rangle_B, \tag{5.40}$$

where $|\Psi_o\rangle_i$, $i = A, B$ are gaussian states. We then use wave plates so as to create a polarization state that shares the same coefficients of state $|\Psi\rangle$, with the form:

$$\begin{aligned}&\frac{1}{N_+}\left[|H\rangle_A|H\rangle_B + |V\rangle_A|V\rangle_B + \right.\\ &\left.-i(\sqrt{2}-1)\left(|V\rangle_A|H\rangle_B + |H\rangle_A|V\rangle_B\right)\right]|\Psi_o\rangle_A|\Psi_o\rangle_B.\end{aligned} \tag{5.41}$$

The transition from (5.40) to (5.41) requires the application of local unitary transformations U_A and U_B performed by properly chosen wave plates, as shown in Fig. 5.6.

The next step is to transform the gaussian state into either $|g\rangle$ or $|\overline{g}\rangle$, the choice being controlled by the polarization. Both photons enter the same interferometer, as shown in Fig. 5.6, but each one in a different port. Since the interferometer uses a polarizing beam splitter, the path of the photon will be determined by its polarization. Because the photons enter in different ports, the polarization of photon labeled B is rotated before the PBS1. In that way, B photons that are initially H-polarized will go through the same path as the H-polarized A photons.

In one arm of the interferometer the photon goes through a mask with a slit oriented at $\theta = \pi$ with angular width of $\delta\theta$, and its transverse state undergoes the transformation $|\Psi_o\rangle \rightarrow |\overline{g}\rangle$. In the other arm the mask is oriented at $\theta = 0$ with the same angular width and performs the transformation $|\Psi_o\rangle \rightarrow |g\rangle$. Each photon has two possible evolutions,

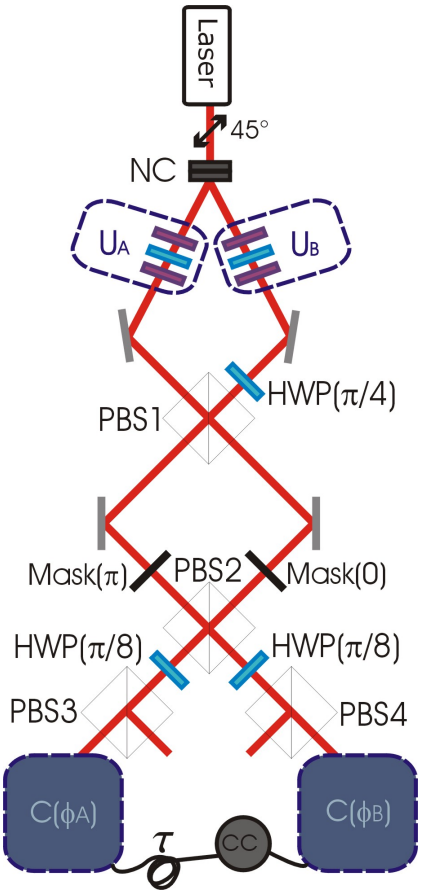

Figure 5.6: Proposed setup to create the state $|\Psi\rangle$ and measure the correlations $C_A(\phi_A)C_B(\phi_B)$; NC - nonlinear crystals type I; HWP - half-wave plate; PBS - polarizing beam splitter; CC - coincidence count.

summarized below:

$$
\begin{aligned}
&|H\rangle_A|\Psi_o\rangle_A \rightarrow |H\rangle_A|g\rangle_A \\
&|V\rangle_A|\Psi_o\rangle_A \rightarrow |V\rangle_A|\overline{g}\rangle_A \\
&|H\rangle_B|\Psi_o\rangle_B \rightarrow |V\rangle_B|g\rangle_B \\
&|V\rangle_B|\Psi_o\rangle_B \rightarrow |H\rangle_B|\overline{g}\rangle_B.
\end{aligned} \tag{5.42}
$$

It should be noted that, when presenting the final version of the experimental setup, a set of lenses to image the masks of the preparation step into the detection planes will be necessary. Our aim for the moment is to present a simple version of the experimental setup, focusing on more fundamental aspects.

After the transformations, a hyper-entangled state is formed:

$$
\begin{aligned}
&\frac{1}{N_+}\left[|H\rangle_A|g\rangle_A|V\rangle_B|g\rangle_B + |V\rangle_A|\overline{g}\rangle_A|H\rangle_B|\overline{g}\rangle_B + \right. \\
&\left. -i(\sqrt{2}-1)\left(|V\rangle_A|\overline{g}\rangle_A|V\rangle_B|g\rangle_B + |H\rangle_A|g\rangle_A|H\rangle_B|\overline{g}\rangle_B\right)\right].
\end{aligned} \tag{5.43}
$$

With the PBS2 in the end of the interferometer, all photons labeled A come out from the port on the left and photons labeled B from the right.

The final step is to transform polarization so as it becomes factorable, separable from the OAM degree of freedom. This can be done, for instance, by putting a half wavelength plate oriented at $\pi/8$ in the path of both photons and a PBS afterwards. Thus, all the photons will have a 50% chance of being transmitted by the PBS3 and PBS4, and once transmitted they will come out with the same polarization. We have thus the resulting state $|\Psi\rangle$ given by Eq. (5.29) and can, in principle, use it for testing the proposed Bell-type inequalities in a quantum optics set-up.

The detection of the two photons must be made in coincidence, in order to measure in each side photons that belong to the same pair, created together in one of the crystals. We can assume that there is a delay τ between the windows of detection of the two photons. If this delay increases, the probability of detecting photons from different pairs also increases. In that case, the final state measured is not $|\Psi\rangle$, but the mixed state $\rho_A \otimes \rho_B$ given by Eq. (5.33). We can see that this is the case because if we detect two photons created by two different processes, possibly in different crystals, the state of the system right after the crystals is the maximally mixed state $\frac{1}{4}(|HH\rangle\langle HH| + |HV\rangle\langle HV| + |VH\rangle\langle VH| + |VV\rangle\langle VV|)$. With the transformations described previously

in this section, this initial state becomes $\rho_A \otimes \rho_B$. So, with the variation of τ we can investigate the Werner states of Eq. (5.32) with varying η.

6

Conclusion

The work presented has its foundations on experiments in paraxial optics and the study of propagation modes that may carry orbital angular momentum. The experience that our research group has gained over the manipulation of such systems has allowed for applications on the fundamentals of quantum mechanics and quantum information. In particular we investigated two different approaches to Bell's inequalities, the first with a classical perspective of the problem and the last consisting on the development of an inequality that makes use of continuous variables, and a subsequent experimental proposal.

We presented the theoretical description of paraxial beams, showing two of the families of propagation modes that arise from the solution of the paraxial equation in free space, namely the Hermite-Gaussian and the Laguerre-Gaussian modes. We discussed the angular momentum carried by light beams, and we presented its decomposition in spin and orbital components.

We showed that, analogously to polarization, the first-order transverse modes of a beam can encode one qubit of information. These two degrees of freedom are combined when we define the Spin-Orbit modes, forming a basis to a 4-dimensional subspace. We showed how to experimentally produce such modes through the use of holographic masks and interferometers.

The Spin-Orbit modes allow the encoding of two-qubits in one photon, and with this extra resource we were able to perform a BB84 quantum key distribution protocol without a shared reference frame.

6. CONCLUSION

We have proposed a Bell-like inequality criterion as a sufficient condition for the spin-orbit non-separability of a classical laser beam. The inequality was measured with the apparatus we designed, and the violation was obtained. The notion of separable and non-separable spin-orbit modes in classical optics builds a useful analogy with entangled quantum states, allowing for the study of some of their important mathematical properties. Many quantum computing tasks require entanglement but do not need non-locality, so that using different degrees of freedom of single particles can be useful. This is the type of entanglement whose properties can be studied in the classical optical regime allowing one to replace time-consuming measurements based on single photon detection by the much more efficient measurement of photocurrents. We have presented a detailed quantum optical description of the experiment, analyzing the case of measuring a coherent state, a Fock state and a mixed state, and we showed that coherence was key to obtain our violation.

Following the study of Bell's inequalities we considered bipartite quantum systems characterized by a continuous angular variable θ. We showed how to reveal non-locality on this type of system using inequalities similar to CHSH ones, originally derived for bipartite spin 1/2 like systems. Such inequalities involve correlated measurement of continuous angular functions. We discussed in detail the case of measuring orientation correlations on the transverse profile of entangled photons, using the cosine as the periodic function. We showed that our Bell inequality is equivalent to the continuous superposition of CHSH inequalities acting on two-dimensional subspaces of the infinite dimensional Hilbert space. The introduced Bell-type inequalities open the perspective of new and simpler experiments to test non-locality on a variety of quantum systems described by continuous variables.

We have worked in the frontier between the experiments and their theoretical developments and background, and hopefully we have built a more complete understanding of the physical system we have in hands.

Appendix A

C and $C(\frac{\pi}{2})$ operators

To write the operators C and $C(\frac{\pi}{2})$ in terms of the Pauli operators $\sigma^z(\theta)$ and $\sigma^y(\theta)$ defined in (5.15), we use the states:

$$|\theta\rangle = \sum_{m=-\infty}^{\infty} \frac{1}{\sqrt{2\pi}} e^{im\theta}|m\rangle \tag{A.1}$$

$$|\overline{\theta}\rangle = \sum_{m=-\infty}^{\infty} \frac{(-1)^m}{\sqrt{2\pi}} e^{im\theta}|m\rangle \tag{A.2}$$

We start by calculating $U(\frac{\pi}{2})|\theta\rangle$, which can be obtained in the following way

$$\begin{aligned} e^{i\frac{\pi}{2}J_z^2}|\theta\rangle &= \sum_{m=-\infty}^{\infty} \frac{(i)^{m^2}}{\sqrt{2\pi}} e^{im\theta}|m\rangle \\ &= \frac{1}{\sqrt{2}}\left[e^{i\frac{\pi}{4}} \sum_{m=-\infty}^{\infty} \frac{1}{\sqrt{2\pi}} e^{im\theta}|m\rangle \right. \\ &\left. + e^{-i\frac{\pi}{4}} \sum_{m=-\infty}^{\infty} \frac{(-1)^m}{\sqrt{2\pi}} e^{im\theta}|m\rangle\right] \\ &= \frac{1}{\sqrt{2}}\left[e^{i\frac{\pi}{4}}|\theta\rangle + e^{-i\frac{\pi}{4}}|\overline{\theta}\rangle\right], \end{aligned} \tag{A.3}$$

where we have used $(i)^{m^2} = \frac{1}{\sqrt{2}}\left[e^{i\frac{\pi}{4}} + (-1)^m e^{-i\frac{\pi}{4}}\right]$. The same can be done for $U(\frac{\pi}{2})|\overline{\theta}\rangle$ and we obtain:

$$e^{i\frac{\pi}{2}J_z^2}|\overline{\theta}\rangle = \frac{1}{\sqrt{2}}\left[e^{i\frac{\pi}{4}}|\overline{\theta}\rangle + e^{-i\frac{\pi}{4}}|\theta\rangle\right] \tag{A.4}$$

Using the antisymmetry property of the spectrum of C and Eqs. (A.3) and (A.4),

the following decompositions for C and $C(\frac{\pi}{2})$ can be obtained:

$$\begin{aligned} C &= \int_{-\pi}^{\pi} d\theta \cos\theta \left|\theta\right\rangle \left\langle\theta\right| \\ &= \int_{0}^{\pi} d\theta \cos\theta \left\{\left|\theta\right\rangle \left\langle\theta\right| - \left|\overline{\theta}\right\rangle \left\langle\overline{\theta}\right|\right\} \\ &= \int_{0}^{\pi} d\theta \cos\theta \sigma^{z}(\theta) \end{aligned} \tag{A.5}$$

$$\begin{aligned} C(\frac{\pi}{2}) &= U(\frac{\pi}{2}) C U^{\dagger}(\frac{\pi}{2}) \\ &= i \int_{0}^{\pi} d\theta \cos\theta \left\{\left|\theta\right\rangle \left\langle\overline{\theta}\right| - \left|\overline{\theta}\right\rangle \left\langle\theta\right|\right\} \\ &= -\int_{0}^{\pi} d\theta \cos\theta \sigma^{y}(\theta). \end{aligned} \tag{A.6}$$

Appendix B

Eigenvalues of $B_{\mathbf{m}}$

For each θ and θ' the operator $X(\theta,\theta')$ defined in Eq. ((5.21)) can be represented in the basis formed by the 4 orthonormal states: $|\theta\rangle\otimes|\theta'\rangle$, $|\theta\rangle\otimes|\overline{\theta'}\rangle$, $|\overline{\theta}\rangle\otimes|\theta'\rangle$, $|\overline{\theta}\rangle\otimes|\overline{\theta'}\rangle$ as the following 4×4 matrix:

$$X(\theta,\theta') = \begin{bmatrix} 1 & i & i & 1 \\ -i & -1 & -1 & -i \\ -i & -1 & -1 & -i \\ 1 & i & i & 1 \end{bmatrix} \tag{B.1}$$

To justify this operation we can also decompose $X(\theta,\theta')$ in an arbitrary basis:

$$\begin{aligned} X(\theta,\theta') = \int_0^\pi \int_0^\pi \int_0^\pi \int_0^\pi d\theta_a d\theta_b d\theta'_a d\theta'_b \\ \langle\theta'_a,\theta'_b|X(\theta,\theta')|\theta_a,\theta_b\rangle \left|\theta'_a,\theta'_b\right\rangle \langle\theta_a,\theta_b| \end{aligned} \tag{B.2}$$

Calculating the matrix element $\langle\theta'_a,\theta'_b|X(\theta,\theta')|\theta_a,\theta_b\rangle$ we obtain a set of 16 products of delta functions, and upon integration they select the 16 operators represented by the 4×4 matrix of Eq. (B.1).

Now we can easily obtain the eigenvalues and eigenstates of the above operator. Because of the symmetry of $X(\theta,\theta')$ under the swap of A and B (equivalent to swapping θ with θ'), the following antisymmetric states correspond to zero eigenvalues :

$$\begin{aligned} |\psi^{a++}(\theta,\theta')\rangle &= \frac{1}{\sqrt{2}}[|\theta\rangle\otimes|\theta'\rangle - |\overline{\theta}\rangle\otimes|\overline{\theta'}\rangle] \\ |\psi^{a+-}(\theta,\theta')\rangle &= \frac{1}{\sqrt{2}}[|\theta\rangle\otimes|\overline{\theta'}\rangle - |\overline{\theta}\rangle\otimes|\theta'\rangle] \end{aligned} \tag{B.3}$$

The two remaining symmetric eigenstates correspond to eigenvalues $\pm 2\sqrt{2}$. They can be written as:

$$
\begin{aligned}
&|\chi^{\pm 1}(\theta, \theta')\rangle = \\
&\frac{1}{N_{\pm}}[|\theta\rangle \otimes |\theta'\rangle + |\overline{\theta}\rangle \otimes |\overline{\theta'}\rangle \\
&\mp i(\sqrt{2} \mp 1)\left(|\theta\rangle \otimes |\overline{\theta'}\rangle + |\overline{\theta}\rangle \otimes |\theta'\rangle\right)]
\end{aligned}
\tag{B.4}
$$

where $N_{\pm} = \left[2(2 \mp \sqrt{2})\right]^{1/2}$ is a normalization factor such that $\langle \chi^{n'}(\theta'_A, \theta'_B)|\chi^{n}(\theta_A, \theta_B)\rangle = \delta_{nn'}\delta(\theta'_A - \theta_A)\delta(\theta'_B - \theta_B)$.

References

[1] [link]. 1

[2] [link]. 1

[3] H. Moysés Nussenzveig. *Curso de Física Básica 4 - Ótica, Relatividade e Física Quântica*. Editora Edgard Blücher, 1998. 1

[4] A. Einstein, B. Podolsky, and N. Rosen. **Can Quantum-Mechanical Description of Physical Reality Be Considered Complete?** *Phys. Rev.*, **47**:777–780, May 1935. 2, 39

[5] J S Bell. **On the Einstein Podolsky Rosen paradox**. *Physics*, **1**:195 – 200, 1964. 2, 40

[6] J F Clauser, M A Horne, A Shimony, and R A Holt. **Proposed Experiment to Test Local Hidden-Variable Theories**. *Phys. Rev. Lett.*, **23**:880, 1969. 2, 40, 42, 44, 55, 58

[7] A Aspect, P Grangier, and G Roger. **Experimental Realization of Einstein-Podolsky-Rosen-Bohm Gedankenexperiment: A New Violation of Bell's Inequalities**. *Phys. Rev. Lett.*, **49**(2):91–94, 1982. 2, 39, 42

[8] C. H. Bennett, F. Bessette, G. Brassard, L. Salvail, and J. Smolin. **Experimental quantum cryptography**. *J. Cryptology*, **5**:3 – 28, 1992. 2

[9] Max Born and Emil Wolf. *Principles of Optics: Electromagnetic Theory of Propagation Interference and Diffraction of light*. Pergamon Press, sixth edition, 1985. 3, 16

[10] David J. Griffiths. *Introduction to Electrodynamics*. Prentice Hall, third edition, 1999. 3

[11] Leonard Mandel and Emil Wolf. *Optical Coherence and Quantum Optics*. Cambridge University Press, first edition, 1995. 4, 8, 10, 11

[12] Anthony E. Siegman. *Lasers*. University Science Books, first edition, 1986. 4

[13] Frank W. J. Olver, Daniel W. Lozier, Ronald F. Boisvert, and Charles W. Clark, editors. *NIST Handbook of Mathematical Functions*. National Institute of Standards and Technology and Cambridge University Press, first edition, 2010. 6

[14] G. Nienhuis and L. Allen. **Paraxial wave optics and harmonic oscillators**. *Phys. Rev. A*, **48**:656, 1993. 6

[15] S.J. van Enk and G. Nienhuis. **Eigenfunction description of laser beams and orbital angular momentum of light**. *Optics Communications*, **94**:147, 1992. 6

[16] Amnon Yariv. *Quantum Electronics*. John Wiley & Sons, 3rd edition, 1989. 7

[17] John David Jackson. *Classical Electrodynamics*. John Wiley & Sons, 1962. 8

[18] Stephen M. Barnett aand L. Allen. **Orbital angular momentum and nonparaxial light beams**. *Optics Communications*, **110**:670–678, 1994. 8

[19] Michael Berry. *Singular Optics*, pages 6–11. SPIE 3487, 1998. 9

[20] A. T. O'Neil, I. MacVicar, L. Allen, and M. J. Padgett. **Intrinsic and Extrinsic Nature of the Orbital Angular Momentum of a Light Beam**. *Phys. Rev. Lett.*, **88**:053601, 2002. 10

[21] L. Allen, MW Beijersbergen, RJC Spreeuw, and JP Woerdman. **Orbital angular momentum of light and the transformation of Laguerre-Gaussian modes**. *Phys. Rev. A*, **45**:8185–8189, 1992. 10, 21

[22] J. W. Simmons and M. J. Guttmann. *States, Waves and Photons*. Acfdison-Wesley, Reading, MA, 1970. 13

[23] Michael A. Nielsen and Isaac L. Chuang. *Quantum Computation and Quantum Information*. Cambridge University Press, 2000. 15, 18, 29, 30

[24] M. J. Padgett and J. Courtial. **Poincaré-sphere equivalent for light beams containing orbital angular momentum**. *Optics Letters*, **24**:430–432, 1999. 16

[25] C. E. R. Souza, J. A. O. Huguenin, P. Milman, and A. Z. Khoury. **Topological Phase for Spin-Orbit Transformations on a Laser Beam**. *Physical Review Letters*, **99**:160401, 2007. 17, 18, 20, 43, 53

[26] Amiel A. Ishaaya, Luat T. Vuong, Taylor D. Grow, and Alexander L. Gaeta. **Self-focusing dynamics of polarization vortices in Kerr media**. *Optics Letters*, **33**:13–15, 2008. 18

[27] William K. Wootters. **Entanglement of Formation of an Arbitrary State of Two Qubits**. *Phys. Rev. Lett.*, **80**:2245, 1998. 18

[28] P. Milman. **Phase dynamics of entangled qubits**. *Phys. Rev. A*, **73**:062118, 2006. 18

[29] W. LiMing, Z. L. Tang, and C. J. Liao. **Representation of the** SO(3) **group by a maximally entangled state**. *Phys. Rev. A*, **69**:064301, 2004. 18

[30] Berthold-Georg Englert, Christian Kurtsiefer, and Harald Weinfurter. **Universal unitary gate for single-photon two-qubit states**. *Phys. Rev. A*, **63**:032303, 2001. 19

[31] N. R. Heckenberg, R. McDuff, C. P. Smith, and A. G. White. **Generation of optical phase singularities by computer-generated holograms**. *Optics Letters*, **17**(3):221, 1992. 19, 47, 67

[32] Miles Padgett and L. Allen. **Light with a twist in its tail**. *Contemporary Phisics*, **41**(5):275–285, 2000. 19

[33] C. E. R. Souza. *Aplicações do Momento Angular Orbital da luz à Computação e Informação Quântica*. PhD thesis, Instituto de Física - UFF, 2010. 20

[34] Eugene Hecht. *Optics*. Addison Wesley, 2002. 20

[35] Jonathan Leach, Miles J. Padgett, Stephen M. Barnett, Sonja Franke-Arnold, and Johannes Courtial. **Measuring the Orbital Angular Momentum of a Single Photon**. *Physical Review Letters*, **88**:257901, 2002. 21, 67

[36] M.W. Beijersbergen, R.P.C. Coerwinkel, M. Kristensen, and J.P. Woerdman. **Helical-wavefront laser beams produced with a spiral phaseplate**. *Optics Communications*, **112**:321, 1994. 21

[37] Lorenzo Marrucci, Ebrahim Karimi, Sergei Slussarenko, Bruno Piccirillo, Enrico Santamato, Eleonora Nagali, and Fabio Sciarrino. **Spin-to-orbital conversion of the angular momentum of light and its classical and quantum applications**. *Journal of Optics*, **13**:064001, 2011. 21

[38] L. Aolita and S. P. Walborn. **Quantum Communication without Alignment using Multiple-Qubit Single-Photon States**. *Physical Review Letters*, **98**:100501, 2007. 29, 31, 33

[39] C. E. R. Souza, C. V. S. Borges, A. Z. Khoury, J. A. O. Huguenin, L. Aolita, and S. P. Walborn. **Quantum key distribution without a shared reference frame**. *Physical Review A*, **77**:032345, 2008. 29, 43

[40] C. H. Bennett and G. Brassard. **Proceedings of IEEE International Conference on Computer, Systems, and Signal Processing**. page 175. IEEE, New York, 1984. 30

[41] Asher Peres and Petra F. Scudo. **Entangled Quantum States as Direction Indicators**. *Physical Review Letters*, **86**:4160, 2001. 33

[42] Asher Peres and Petra F. Scudo. **Transmission of a Cartesian frame by a quantum system**. *Physical Review Letters*, **87**:167901, 2001. 33

[43] Nicolas Gisin, Grégoire Ribordy, Wolfgang Tittel, and Hugo Zbinden. **Quantum cryptography**. *Reviews of Modern Physics*, **74**:145, 2002. 38

[44] C. V. S. Borges, M. Hor-Meyll, J. A. O. Huguenin, and A. Z. Khoury. **Bell-like inequality for the spin-orbit separability of a laser beam**. *Phys. Rev. A*, **82**:033833, 2010. 39, 43

[45] M. D. Reid, P. D. Drummond, E. G. Cavalcanti, P. K. Lam, H. a. Bachor, U. L. Andersen, and G. Leuchs. **Colloquium: The Einstein-Podolsky-Rosen paradox: From concepts to applications**. *Reviews of Modern Physics*, **81**(4):1727–1751, December 2009. 39, 56

[46] Gregor Weihs, Thomas Jennewein, Christoph Simon, Harald Weinfurter, and Anton Zeilinger. **Violation of Bell's Inequality under Strict Einstein Locality Conditions**. *Phys. Rev. Lett.*, **81**:5039 – 5043, 1998. 39

[47] M. A. Rowe, D. Kielpinski, V. Meyer, C. A. Sackett, W. M. Itano, C. Monroe, and D. J. Wineland. **Experimental violation of a Bell's inequality with efficient detection**. *Nature*, **409**:791 – 794, 2001. 39

[48] Paul G. Kwiat, Philippe H. Eberhard, Aephraim M. Steinberg, and Raymond Y. Chiao. **Proposal for a loophole-free Bell inequality experiment**. *Phys. Rev. A*, **49**:3209 — 3220, 1994. 39

[49] A. Aspect. *Quantum [Un]speakables – From Bell to Quantum information*, chapter 9, pages 119–153. Springer, 2002. 40

[50] D. Bohm. *Quantum Theory*. Constable, London, 1951. 40

[51] Daniel Salart, Augustin Baas, Cyril Branciard, Nicolas Gisin, and Hugo Zbinden. **Testing the speed of 'spooky action at a distance'**. *Nature*, **454**:861–864, 2008. 43

[52] D. N. Matsukevich, P. Maunz, D. L. Moehring, S. Olmschenk, and C. Monroe. **Bell Inequality Violation with Two Remote Atomic Qubits**. *Phys. Rev. Lett.*, **100**:150404, 2008. 43

[53] Yuji Hasegawa, Rudolf Loidl, Gerald Badurek, Matthias Baron, and Helmut Rauch. **Violation of a Bell-like inequality in single-neutron interferometry**. *Nature*, **425**:45, 2003. 43

[54] Lixiang Chen and Weilong She. **Single-photon spin-orbit entanglement violating a Bell-like inequality**. arXiv:0911.0544v2, 2009. 43

[55] Jian Fu, Zhijian Si, Shaofang Tang, and Jian Deng. **Classical simulation of quantum entanglement using optical transverse modes in multimode waveguides**. *Phys. Rev. A*, **70**:042313, 2004. 43

[56] M. Goldin, D. Francisco, and S. Ledesma. **Simulating Bell inequalities violation with classical optics encoded qbits**. arXiv:0904.3286v1. 43

[57] C. E. R. Souza and A. Z. Khoury. **A Michelson controlled-not gate with a single-lens astigmatic mode converter**. *Optics Express*, **18**:9207–9212, 2010. 43

[58] Hiroyuki Sasada and Megumi Okamoto. **Transverse-mode beam splitter of a light beam and its application to quantum cryptography**. *Phys. Rev. A*, **68**:012323, 2003. 45, 47

[59] J. A. O. Huguenin, B. Coutinho dos Santos, P. A. M. dos Santos, and A. Z. Khoury. **Topological defects in moiré fringes with spiral zone plates**. *JOSA A*, **20**:1883, 2003. 47

[60] N. K. Langford, R. B. Dalton, M. D. Harvey, J. L. O'Brien, G. J. Pryde, A. Gilchrist, S. D. Bartlett, and A. G. White. **Measuring Entangled Qutrits and Their Use for Quantum Bit Commitment**. *Phys. Rev. Lett.*, **93**:053601, 2004. 47

[61] L. Chen and W. She. **Single-photon spin-orbit entanglement violating a Bell-like inequality**. *J. Opt. Soc. Am. B*, **27**:A7, 2010. 52

[62] B Jack, A. M. Yao, J. Leach, J. Romero, S. Franke-Arnold, D.G. Ireland, S. M. Barnett, and M.J. Padgett. **Entanglement of arbitrary superpositions of modes within two-dimensional orbital angular momentum state spaces**. *Phys. Rev. A*, **81**:043844, 2010. 55

[63] J F Clauser, M A Horne, A Shimony, and R A Holt. **Bell Inequalities for Arbitrarily High-Dimensional Systems**. *Phys. Rev. Lett.*, **88**:040404, 2002. 55

[64] A Vaziri, G Weihs, and A Zeilinger. **Experimental Two-Photon, Three-Dimensional Entanglement for Quantum Communication**. *Phys. Rev. Lett.*, **89**:240401, 2002. 55

[65] A. Aiello, S.S.R. Oemrawsingh, E.R. Eliel, and J.P. Woerdman. **Nonlocality of high-dimensional two-photon orbital angular momentum states**. *Phys. Rev. A*, **72**:052114, 2005. 55

[66] N D Mermin. **Extreme quantum entanglement in a superposition of macroscopically distinct states**. *Phys. Rev. Lett.*, **65**:1838, 1990. 55

[67] M. Li and S M Fei. **Gisin's Theorem for Arbitrary Dimensional Multipartite States**. *Phys. Rev. Lett.*, **104**:240502, 2010. 55

[68] K. Banaszek and K. Wodkiewicz. **Nonlocality of the Einstein-Podolsky-Rosen state in the Wigner representation**. *Phys. Rev. A*, **58**:4345, 1998. 55

[69] K. Banaszek and K. Wodkiewicz. **Testing Quantum Nonlocality in Phase Space**. *Phys. Rev. Lett.*, **82**:2009, 1999. 55

[70] P. Grangier, M.J. Potasek, and B. Yurke. **Probing the phase coherence of parametrically generated photon pairs: A new test of Bell's inequalities**. *Phys. Rev. A*, **38**:3132, 1988. 55

[71] Z.B. Chen, J.W. Pan, G. Hou, and Y.-D. Zhang. **Maximal Violation of Bell's Inequalities for Continuous Variable Systems**. *Phys. Rev. Lett.*, **88**:040406, 2002. 55

[72] J. Wenger, M. Hafezi, F. Grosshans, R. Tualle-Brouri, and P. Grangier. **Maximal violation of Bell inequalities using continuous-variable measurements**. *Phys. Rev. A*, **67**:012105, 2003. 55

[73] A. Gilchrist, P. Deuar, and M. D. Reid. **Contradiction of Quantum Mechanics with Local Hidden Variables for Quadrature Phase Amplitude Measurements**. *Phys. Rev. Lett.*, **80**:3169–3172, Apr 1998. 55

[74] Z. Y. Ou, S. F. Pereira, H. J. Kimble, and K. C. Peng. **Realization of the Einstein-Podolsky-Rosen paradox for continuous variables**. *Phys. Rev. Lett.*, **68**:3663–3666, 1992. 56

[75] SL Braunstein. **Quantum information with continuous variables**. *Reviews of Modern Physics*, **77**:513, 2005. 56

[76] Lm Duan, G Giedke, Ji Cirac, and P Zoller. **Inseparability criterion for continuous variable systems**. *Phys. Rev. Lett.*, **84**(12):2722–5, March 2000. 56

[77] W. P. Bowen, R. Schnabel, and P. K. Lam. **Experimental Investigation of Criteria for Continuous Variable Entanglement**. *Physical Review Letters*, **90**:4–7, 2003. 56

[78] Asher Peres. **Separability Criterion for Density Matrices**. *Phys. Rev. Lett.*, **77**(8):1413–1415, Aug 1996. 56

[79] P Horodecki. **Separability criterion and inseparable mixed states with positive partial transposition**. *Phys. Lett. A*, **232**(5):333–339, 1997. 56

[80] R Simon. **Peres-horodecki separability criterion for continuous variable systems**. *Phys. Rev. Lett.*, **84**(12):2726–9, March 2000. 56

[81] E. Shchukin and W. Vogel. **Inseparability Criteria for Continuous Bipartite Quantum States**. *Phys. Rev. Lett.*, **95**(23):1–4, November 2005. 56

[82] E G Cavalcanti, C J Foster, M D Reid, and P D Drummond. **Bell Inequalities for Continuous-Variable Correlations**. *Phys. Rev. Lett.*, **99**:210405, 2007. 56

[83] Q. Y. He, E. G. Cavalcanti, M. D. Reid, and P. D. Drummond. **Bell inequalities for continuous-variable measurements**. *Phys. Rev. A*, **81**:062106, 2010. 56

[84] J. Leach, B. Jack, J. Romero, A.K. Jha, A.M. Yao, S. Franke-Arnold, D.G. Ireland, R.W. Boyd, S.M. Barnett, and M.J. Padgett. **Quantum Correlations in Optical Angle–Orbital Angular Momentum Variables**. *Science*, **329**:662, 2010. 56, 66

[85] S. P. Walborn, B. G. Taketani, A. Salles, F. Toscano, and R. L. de Matos Filho. **Entropic Entanglement Criteria for Continuous Variables**. *Phys. Rev. Lett.*, **103**:160505, Oct 2009. 56

[86] A. Rojas-Gonzales, J. A. Vaccaro, and S. M. Barnett. **Entropic uncertainty relations for canonically conjugate operators**. *Phys. Lett. A*, **205**:247, 1995. 56

[87] C. V. S. Borges, A. Z. Khoury, S. P. Walborn, P. H. S. Ribeiro, P. Milman, and A. Keller. **Bell inequalities with continuous angular variables**. *Phys. Rev. A*, 2012. Accepted, in production. 56

[88] K. Svensson, L. Bengtsson, J. Bellman, M. Hassel, M. Persson, and S. Andersson. **Two-Dimensional Quantum Rotation of Adsorbed H_2**. *Phys. Rev. Lett.*, **83**:124, 1999. 56

[89] T. Yu. Ivanova and D. A. Ivanov. **Quantum measurement of collective atomic position in optical lattice**. *Optics Communications*, **272**:148 — 153, 2007. 56

[90] Tsirelson. **Quantum generalizations of Bell's inequality**. *Lett. Math. Phys.*, **4**:93, 1980. 58

[91] J. F. Clauser and A. Shimony. **Bell's theorem. Experimental tests and implications**. *Rep. Prog. Phys.*, **41**:1881, 1978. 58

[92] P Milman, A Keller, E Charron, and O Atabek. **Molecular orientation entanglement and temporal Bell-type inequalities**. *Eur. Phys. J. D*, **53**:383, 2009. 59, 64

[93] P Milman, A Keller, E Charron, and O Atabek. **Bell-Type Inequalities for Cold Heteronuclear Molecules**. *Phys. Rev. Lett.*, **99**:130405, 2007. 59

[94] M. Horodecki, P. Horodecki, and R. Horodecki. **Separability of mixed states: necessary and sufficient conditions**. *Phys. Lett. A*, **223**:1–8, 1996. 61

[95] Barbara M Terhal. **Bell inequalities and the separability criterion**. *Phys. Lett. A*, **271**(5-6):319–326, 2000. 61

[96] Reinhard F. Werner. **Quantum states with Einstein-Podolsky-Rosen correlations admitting a hidden-variable model**. *Phys. Rev. A*, **40**:4277–4281, Oct 1989. 65

[97] Ladislav Mista, Radim Filip, and Jaromir Fiurasek. **Continuous-variable Werner state: Separability, nonlocality, squeezing, and teleportation**. *Phys. Rev. A*, **65**:062315, Jun 2002. 65

[98] A Mair, A Vaziri, G Weihs, and A Zeilinger. **Entanglement of the orbital angular momentum states of photons**. *Nature*, **412**:313, 2001. 66, 67

[99] P H Souto Ribeiro, M França Santos, P Milman, and A Z Khoury. **Entanglement of the transverse degrees of freedom of the photon**. *J. Opt. B*, **4**:S437, 2002. 66

[100] P G Kwiat, E Waks, A G White, I Appelbaum, and P H Eberhard. **Ultrabright source of polarization-entangled photons**. *Phys. Rev. A*, **60**:R773, 1999. 69